Czech Technical University in Prague

Faculty of Electrical Engineering

Doctoral Thesis

July 2021

Ing. Tomáš Košťál

Czech Technical University in Prague
Faculty of Electrical Engineering
Department of Electric Drives and Traction

ON-LINE IDENTIFICATION METHODS OF INDUCTION MACHINES PARAMETERS

Doctoral Thesis

Ing. Tomáš Košťál

Prague, July 2021

Ph.D. Programme: Electrical Engineering and Information Technology, P2612
Branch of study: Electric Machines, Apparatus and Drives, 2642V004

Supervisor: ***doc. Ing. Pavel Mindl, CSc.***
Supervisor-Specialist: ***prof. Ing. Jiří Pavelka, DrSc.***

Declaration

Hereby I declare that I have written my doctoral thesis on my own and I have used only the literature listed at the end of the doctoral thesis in the references.

Tomáš Košťál

Abstract

This thesis deals with parameter identification of induction machines and proposes a novel method for on-line identification suitable for electric drives with resource-constraint microcontrollers.

Modern control strategies of induction machines usually utilize some form of mathematical model of the machine, that is characterized by a set of parameters. Different control strategies stress importance of different parameters, but the most common set of parameters that describe the machine consist of the following five: a stator resistance R_s, a rotor resistance R_r, a stator leakage inductance $L_{\sigma s}$, a rotor leakage inductance $L_{\sigma r}$, and a magnetizing inductance L_m.

Out of these parameters, only stator resistance R_s is directly measurable and therefore a necessity of usage of some indirect methods to identify these parameters arose. This topic is further complicated by the fact, that some of these parameters change during operation of the drive due to influences of temperature, frequency, and saturation of the magnetic circuit. Tracking of changes of parameters important to a particular control strategy can improve performance of the drive. As a representative control strategy, indirect field oriented control was chosen for its widespread usage both in industry and transportation. This control strategy is sensitive to inaccuracies of R_r and L_m.

A number of so-called on-line identification methods based on various principles was proposed, but most of them are computationally or memory intensive. However a number of cases in transportation or industry can be found where the existing older control hardware or components in new cost-sensitive applications cannot cope with demanding algorithms. Therefore a novel on-line identification method of R_r and L_m was developed and tested that is suitable for drives with IFOC control strategy that has a resource-constraint control hardware. The method is based on a steady-state voltage model and uses only standard equipment of a common electrical drive to obtain input quantities.

The thesis presents an overview of the equipment of a common electric drive with induction machine to state the default hardware conditions. Further it describes a derivation of the mathematical model of the machine that serves as a starting point for the derivation of the proposed method. A summary of the conventional, off-line and on-line identification methods is presented with their advantages and disadvantages to show ideas that the identification of parameters can be based on. A thorough analysis of the mechanisms of parameter changes is showed being followed by a derivation of the method and a description of the final algorithm for the microcontroller. The method has been tested within four different drives with rated powers ranging from 3,5 kW to 1,6 MW, some of them being traction drives of railway vehicles. Experimental tests and the achieved results are presented and discussed in final chapters of this thesis.

Keywords: induction motor drives; rotor resistance; magnetizing inductance; on-line parameter identification; resource-constrained microcontrollers

Abstrakt

Tato práce se zabývá identifikací parametrů asynchronních motorů a návrhem nové identifikační metody, má nízké nároky na výpočetní prostředky řídicího mikropočítače elektrického pohonu.

Moderní metody řízení elektrických pohonů s asynchronními motory využívají pro svou funkci matematický model řízeného stroje (motoru). Tento model je popsán mimo soustavy rovnic také sadou parametrů stroje, která se může lišit podle užití nebo podle zohlední některých přídavných parazitních jevů. V technické praxi je ovšem nejčastější sadou parametrů, popisujících asynchronní motor, následujících pět: odpor statorového vinutí R_s, odpor rotorového vinutí R_r, statorová rozptylová indukčnost $L_{\sigma s}$, rotorová rozptylová indukčnost $L_{\sigma r}$ a magnetizační indukčnost L_m.

U asynchronních motorů s kotvou na krátko (klecovou kotvou), které jsou v technické praxi nejběžnější, lze z uvedených parametrů přímým měřením určit pouze odpor statorového vinutí R_s. Z tohoto důvodu byla vyvinuta řada nepřímých metod pro určování ostatních parametrů stroje. Během provozu stroje navíc dochází ke změnám některých parametrů v důsledku vlivů teploty, kmitočtu a nasycení magnetického obvodu stroje. Různé řídící metody pohonů s asynchronními motory jsou citlivé na rozdílné parametry. Jako zástupce řídících metod bylo pro svou širokou rozšířenost zvoleno tzv. nepřímé vektorové řízení (IFOC), pro které byla vyvíjena navržená metoda identifikace. Tento způsob řízení asynchronního motoru je citlivý na přesnost určení R_r a L_m.

Za účelem zjišťování parametrů stroje během provozu byla vyvinuta řada tzv. on-line identifikačních metod, z nichž většina je ovšem charakterizována mimo jiné i vysokými nároky na výpočetní prostředky nebo paměť řídícího mikropočítače pohonu. I přes průběžně se zdokonalující vlastnosti řídících mikropočítačů je stále možné najít řadu případů v trakčních i průmyslových pohonech, kde použitý mikropočítač nemá dostatek prostředků k vykonávání dalšího složitého algoritmu. Takovými pohony mohou být jednak stávající instalace, kde dosud identifikace parametrů nebyla použita a zároveň není žádoucí provádět výměnu řídícího systému za výkonnější nebo aplikace kde je snaha dosáhnout finanční úspory a tedy použít co nejlevnější, výpočetním výkonem neoplývající komponenty. Navržená identifikační metoda pokrývá právě tyto případy. Je určena pro pohony s nepřímým vektorovým řízením a proto určuje rotorový odpor R_r a magnetizační indukčnost L_m. Je založena na napěťovém modelu stroje v ustáleném stavu a pro získávání vstupních veličin využívá pouze prostředky dostupné v běžných pohonech.

V úvodu práce jsou popsány součásti elektrického pohonu, které jsou uvažovány jako výchozí podmínky pro návrh i realizaci identifikační metody. Následuje odvození a popis matematického modelu, ze kterého navržená metoda vychází. Pro porovnání různých možností identifikace parametrů je uveden přehled laboratorních, off-line i on-line metod včetně jejich výhod a nevýhod, následovaný přehledem principů změn uvedených parametrů stroje. V další části je popsáno odvození navržené on-line identifikační metody včetně výsledného algoritmu pro řídící mikropočítač. V závěru práce jsou ukázány výsledky experimentálního ověření metody na pohonech s asynchronními motory s výkonem od 3,5 kW do 1,6 MW, z nichž některé jsou skutečnými pohony kolejových vozidel.

Klíčová slova: asynchronní motor, rotorový odpor, magnetizační indukčnost, on-line identifikace parametrů, mikropočítač s omezenými prostředky

Acknowledgements

This thesis is the result of my Ph.D. studies at the Department of Electric Drives and Traction, Faculty of Electrical Engineering, Czech Technical University in Prague which I would like to give thanks for support and help. My special gratitudes belong to Ing. Bc. Pavel Kobrle, Ph.D., Ing. Pavel Karlovský, Ph. D., Ing. Jan Bauer, Ph.D., Ing. Jakub Zedník, Ing. Ondřej Lipčák and Ing. Petr Pichlík, Ph.D. for creating an inspirational and friendly as well as motivation atmosphere.

Further I would like to express my acknowledgements for the possibility of taking part in a research project in a Joint Research Centre CRRC-CTU related with this topic, to the team members of the Joint Research Centre, for possibility of usage of equipment of the JRC and last but not least the possibility to carry out experiments in the laboratory test room of the CRRC.

I would like to express my gratitude to my parents, my family and friends for their care and support, especially to my brother for advices concerning academic issues. Further, I would like to thank to Matěj Peterka and Iva Jakubíková for motivation.

Special gratitude belongs to Hana Bartůňková not only for language consultancy but for overall mental support.

Finally, I would like to thank my supervisor doc. Ing. Pavel Mindl, CSc. and my supervisor-specialist prof. Ing. Jiří Pavelka, DrSc. for leadership, advices, patience and inspiration.

This thesis is devoted to prof. Ing. Jiří Pavelka, DrSc. who passed away before the theses has been finished.

Table of Contents

1 Introduction

Electrical energy accompanies humans in present-day society in almost every field of life. One of the most common manners of its usage is its conversion into mechanical movement. The most common type of electromechanical converter that can be found in present electric drives is the induction machine. Among the factors that lead to its widespread usage are robustness, low cost, reliability and low maintenance requirements that are all based on a simplicity of construction.

However, induction machines have suffered for a long time with non-existence of a comfortable and effective way of controlling their speed. Therefore their usage was limited to drives with no or very low demands of speed control or dynamic properties. This has been changed with the continuous evolution of power electronic switching devices. Decreasing of their price and increasing of their power and dynamic properties allowed for construction of reliable and economically viable frequency converters that enabled usage of the induction machines also in the field of variable speed drives.

There are many types of applications of electric drives, that require variable speed and demanding dynamic properties. Therefore various methods of control of the drives with induction machines have been developed. Nowadays most of the modern control strategies of the drives with induction machines rely on some form of mathematical model of the machine. The model of the induction machine is characterized by a set of parameters. This set of parameters can vary based on the complexity of the mathematical model needed for the control strategy, the purpose of the model or the phenomena of the machine that are being studied. Precision of knowledge of the machine parameters can have a great influence on the performance of the control algorithm.

There are two significant difficulties with the parameters of induction machines. Firstly, majority of parameters of the induction machine are not directly measurable and therefore complicated to obtain their values. There are only two exceptions: first is the resistance of stator winding by all types of machines and second is by induction machines with wound rotor where also the rotor resistance measurement is accessible via slip rings. However, machines with rotors without terminals conducted outside of the machine (squirrel cage rotors) make up the vast majority of the all induction machines. Secondly the parameters of the machine vary during the operation of the machine due to effects of temperature, saturation or frequency.

Various methods for obtaining the machine parameters before the start of operation (off-line) or during operation of the drive (on-line) have been already developed, but majority of them is computationally or memory intensive. This can be a hurdle in case of older existing hardware or a low-cost control hardware which could otherwise benefit from parameter identification. Therefore a niche for a computationally modest on-line identification method exists.

1.1 Current State of Art

There are numbers of parameter identification methods of induction machines. Although not all of the authors use the same nomenclature, which is a typical situation for research fields that are under excessive research, some main directions of division can be found across literature. In general, these

are methods used for obtaining the required parameters before the start of the drive or monitoring of changes of parameters during operation. The methods used before the start of the drive can be further divided into conventional/laboratory/standard which use laboratory equipment and are usually carried out on a test bench in a testing room [1]–[4]. However a common situation on the field of electric drives is that particular components of the electric drive comes from different producers and meet not until then on a place of installation. Therefore so called off-line identification methods or commissioning methods were developed to be used in these situations [1], [2], [5], [6]. For such methods should be ideally enough to use only the equipment of the drive to minimize organizational and logistic cost. These off-line methods can be further divided into methods that requires to rotate with the machine (commissioning methods) or that manage the required tasks in standstill (self-commissioning methods). All these already mentioned methods are good for obtaining initial parameter values.

However the parameters vary also during the operation of the drive. Resistances of both stator and rotor windings rise with the temperature as the machine warms up [1], [2], [7]. Windings made up of thicker solid conductors are further influenced by skin effect [7]–[9]. The effects of skin effect can be detected also in case of inductances yet being usually neglected [7], [9]. Lastly, inductance is known to change its value due to saturation [2], [7]. These variations can deteriorate the performance of the control strategies and therefore a vast effort of researchers has been invested also in the development of the so called on-line methods that are able to monitor changes of the parameters also during the operation of the drive [1], [5], [10].

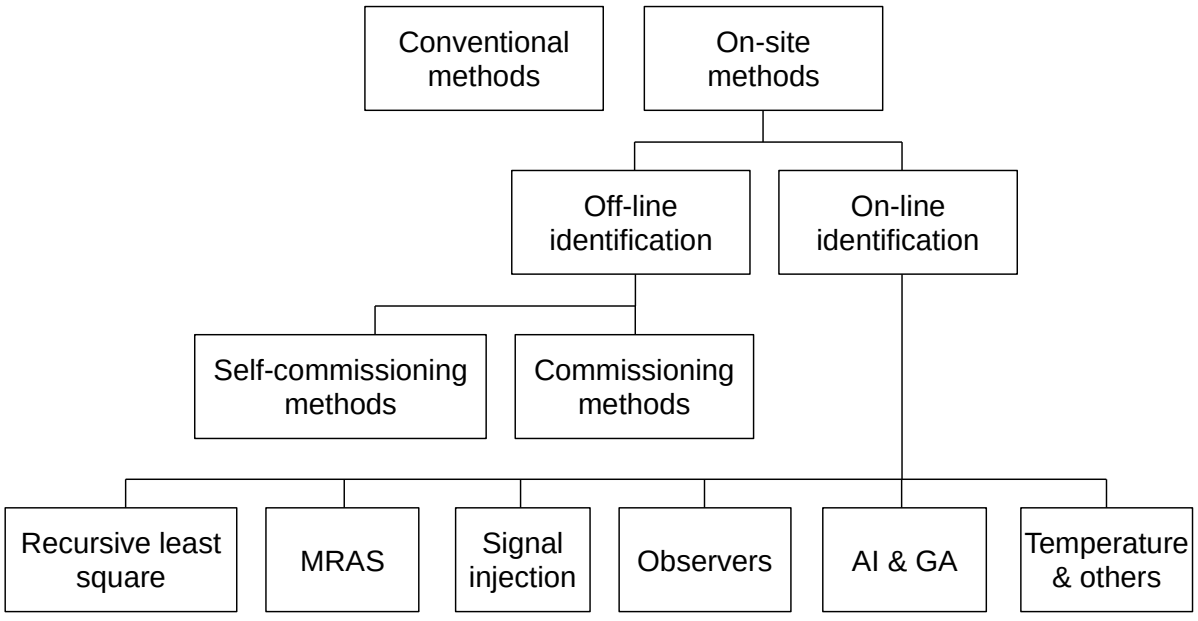

Fig. 1: Classification of parameter identification methods.

Searched parameters depend on the purpose, which usually means the demands of the particular control strategy. They usually involve a stator resistance R_s, a rotor resistance R_r, a stator leakage inductance $L_{s\sigma}$, a rotor leakage inductance $L_{r\sigma}$ and a magnetizing inductance L_m [1], [2], [11]–[13]. Further, iron losses represented by R_{Fe} can be demanded [14].

A number of different so-called on-line methods was developed for monitoring machine parameters during operation [1], [5], [10]. However, a lot of them are computationally or memory demanding and thus are not suitable for microcontrollers with limited resources. This is caused probably by continually increasing capabilities and computational power of the microcontrollers which attract attention of researcher with the possibility to implement even more complex algorithm.

Among the most demanding algorithms for parameter identification are those based on Artificial Neural Networks (ANN), Genetic Algorithms (GA) and Optimization Algorithms (OA) [1]. Extra time and resources are needed for ANNs as they need to have training samples or training algorithm. A real-time control accelerator may be needed adjacent to a microcontroller to implement ANN as presented in [15]. Large number of calculations is needed by OAs such as Particle Swarm Optimization. On the contrary, GAs have demanding requirements on storage of historical data [16].

Another vast group of methods used for parameter identification are those with different types of observers. They offer a variety of usage but need often comparatively complex matrix calculations in their algorithms which can be a limiting point for their deployment in resource-constrained control hardware. Many examples of usage of different types of observers can be found in literature. For example, adaptive observer for stator and rotor resistance was utilised in [17] while sliding mode observer usage for stator resistance estimation has been proposed in [18] and [19]. Luenberger observer was used for flux estimation with a following calculation of stator and rotor resistances in [20] or for a stator resistance estimation in [18] and [21]. Extended Kalman Filter (EKF) has been also widely studied for parameter identification [14], [22], [23] but this method is also characterized by its excessive computational demands [1].

Recursive Least Square (RLS) [12], [24], [25] lie between complicated and modest methods. On one hand, it is easy to implement it and it is not so computationally intensive. On the other hand, it usually needs to implement more sophisticated filters as it is very sensitive to noise [26]. Also tuning of the forgetting factor of RLS can be tricky [1] and can lead to error accumulation. To overcome this a time-varying forgetting factor has been proposed [27] which however makes the RLS more complex.

Signal injection is generally not demanding on the microcontroller, but brings other related difficulties with its implementation. DC signal injection is more favourable that usage of high-frequency signal because as the high frequency is more demanding on the speed of switching devices of the converter [1]. On the other hand, injected DC signal can cause unwanted additional torque pulsations. These pulsations could be avoided for instance by introducing second-order harmonics [28] but this leads to more complicated structures in the microcontroller. To avoid unnecessary additional power losses caused by the DC test signal, it should be used only in specified time spans [29].

Among computationally undemanding techniques with simple structure and implementation can be counted also Model Reference Adaptive System (MRAS) based methods [30]–[33]. Adaptation, or better to say *adaptive law*, is often implemented by PI or I controller which can be seen as a burden from the point of view of limited-resources hardware, because it needs an additional controller(s) in

the control structure. MRAS based methods are usually used to identify one or two parameters because it is difficult to find a stable adaptive law [1].

Other group of methods that do not require excessive microcontroller resources are those based on voltage model calculation. Calculation of rotor resistance and magnetizing inductance by means of voltage-model-derived differential equations were presented in [34]. A great simplification can be achieved if at least a part of the working cycle of the drive can be considered as steady-state. Under such condition, a steady-state model of the machine can be used, which enables usage of algebraic equations instead of differential ones, which are far less complex to solve [31].

Temperature measurements based compensations of machine resistances are another area of computationally modest approaches. Temperature sensor mounted to the stator winding of the machine was used in [7]. Based on the temperature change, the authors calculated the values of both stator and rotor resistances assuming the same temperature through the whole machine volume. In [35], the authors equipped also the rotor of a machine with a wireless temperature sensor besides the wired one attached to the stator winding. A temperature sensor is however usually not standard equipment of a machine and has to be mounted additionally. Considering for example embedding the temperature sensor directly into the machine stator winding means at least to decompose the end bells which is a task for motor repair workshop. Rotor temperature sensor would be even more complicated to maintain in the longer period of time due to its power supply requirements.

Among the sensors that are far more common in electric drives is a speed sensor. A combination of information from a mechanical speed sensor and a steady-state voltage model was used in [13] to calculate rotor resistance which change was used to obtain the temperature change of the rotor of the induction machine in a battery electric vehicle drive. In [31], the same combination of speed sensor and steady-state voltage model was used for estimation of rotor magnetic flux and its angle. Such methods, that can use an additional independent value in a form of speed information seem to represent a promising niche for modest identification method for drives with resource-constrained microcontrollers.

Research on the parameter identification is presently conducted mostly by academic institutions as the industrial environment is not inclined towards publishing results of their findings which are normally carried out with a potential of commercialization. Exceptions exist and the majority of them are the companies providing variable speed drives for industry such as Siemens, Rockwell, Grundfos, Yaskawa or ABB [36]–[40] both alone or more often in a collaboration with a university. It can be expected that also automotive industry will get into this field with the advent of electrification. As an example is the carmaker Renault [13] can be noted.

There are various academic workplaces where parameters of induction machines and their identification is being studied e.g. Aalto university [6], [41]–[43], Beijing Jiaotong University [1], [7] or University of Manchester [5], [44], [45].

1.2 Objectives Formulation

The doctoral thesis objectives are:

1. **Summarize the current state of knowledge on mechanisms that cause changes of the parameters.** Parameters of the machine vary during operation of the machine due to various effects. Quantities that contribute to these changes and behaviour of the parameters related to particular machine construction are identified. Detailed knowledge of parameter behaviour is essential not only for the design of the method, but also for interpreting the results obtained by experiments.
2. **Summarize the current state of knowledge on parameter identification methods and their principles and evaluate their requirements and effectiveness.** Analysis of knowledge is the first step towards designing a new parameter identification method. There is a large number of publications about various principles and available methods as the research and development in this area started decades ago. Every method has some specific properties which can be classified as strengths or weaknesses. As the parameters of an induction machine are strongly associated with its construction, geometry and mathematical model, these topics are also covered.
3. **Design an on-line identification method of selected parameters for resource-constrained microcontrollers.** The design of the method is based only on quantities available in an ordinary industrial or traction drive without any need for special hardware or sensors. The method is meant for a new low-cost hardware or existing older hardware that can be upgraded. The design is based on a voltage model of a machine which has been identified as a computationally modest option.
4. **Implement and test the designed method on induction machine drives with various rated power.** The designed method has been implemented on four variable speed drives to evaluate its applicability and relevance of its results. The drives were laboratory drives and traction drives used in real railway vehicles.

2 Variable Speed Drives with Induction Machines

An electric drive is a system consisting of a suitable set of electrical devices for a conversion of electrical to mechanical energy. They can be found in a variety of applications. Whether in home appliances, transportation, manufacturing or computer equipment, our present way of life would be impossible without them. The wide range of applications of course requires adaptations of the drive for specific purposes. Because of this, an electric drive is nowadays not only the electric motor itself, as the basic element of transformation of electric to mechanical energy, but it also contains a power converter and control devices. The evolution of power electronics and control microcomputers has affected the construction of electric drives so much, that the converter and control part reach sometimes an even higher level of complexity than the motor itself.

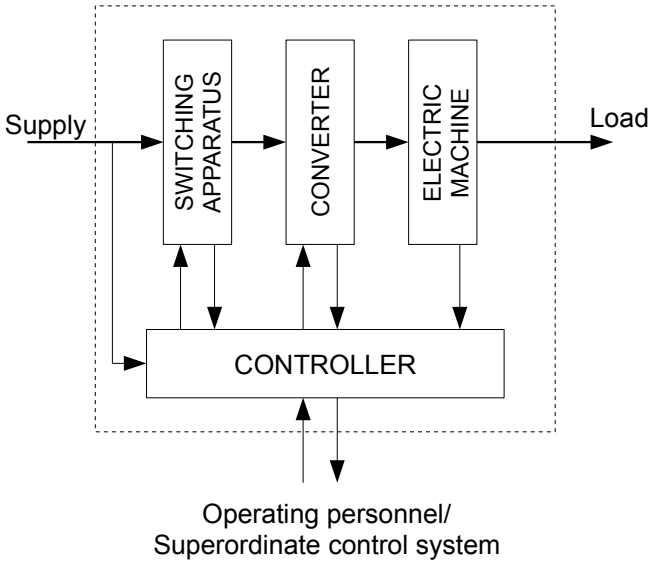

Fig. 2: General structure of an electric drive.

Many different types of categorization of electric drives can be created. When speed control is the criterion we can divide electric drives into groups of drives with a single speed, with two or more discrete degrees of speed and variable-speed drives with fully continuously controllable speed [46], [47].

While single speed drives and drives with multiple degrees of speed require no or very simple control, variable-speed drives need more complex solutions. Variable speed drives with induction machines belong to a comparatively complex group. However, their other advantages prevail this complexity and thus they can bes used in almost all kind of industrial applications where a variable speed drive is needed. Exceptions are a limited space for a motor in the installation or fractional horsepower applications. Their power can rise up to megawatts, so there are no obstacles to use them in high power railway traction vehicles (locomotives, high speed train units, commuter electrical multiple units [7], [48]), as ship propellers or in mining equipment. Other examples in the field of transportation are electric vehicles, elevators or rope-ways. In manufacturing, we can find them as different types of manipulators and robots as well as machining tools and other production engines or as drives for pumps and compressors [49]. On the contrary, they are sparsely used in

household appliances where the required power is comparatively small (even horsepower fractions) due to higher cost or lower efficiency in comparison with other types of motors.

Fig. 3 shows a typical scheme of a variable-speed industrial drive with induction machine common in industry or traction. Presence of the speed sensor can be questionable with the advent and popularity of various speed-sensorless control methods, however, a number of drives are still equipped with a speed sensor. Such examples can be found in the manufacturing industry [49]–[51] or railway traction vehicles [48].

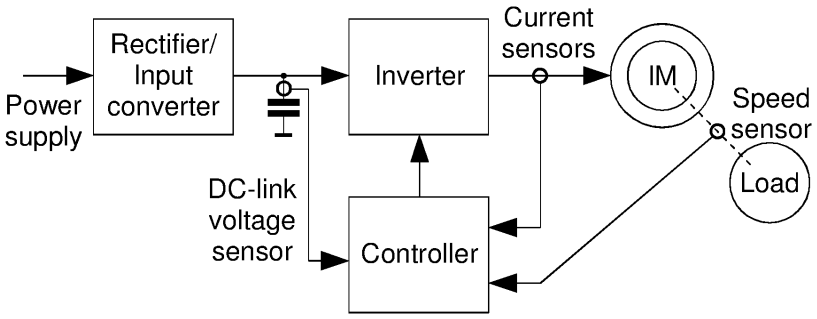

Fig. 3: Structure of a common drive with induction machine.

Other sensors used in industrial or traction electric drives are current sensors on machine terminals and voltage sensors in the DC-links of power converters [51], [52]. As the voltage measurement of the switched voltage at the output of the inverter is complicated due to its rectangular nature with steep rising and falling edges, voltage is usually reconstructed from the switching pattern and the measured DC-link voltage that has normally far slower changes [6]. Nonlinearity of the inverter is also taken into account in most cases [13], [52]. With the help of this procedure, stator voltage and frequency (or angular speed of stator magnetic field) are obtained. Current sensors for measuring the machine stator current are placed on the inverter output, normally on two phases while the third current is calculated from the other two [51]. A speed sensor is mounted on the shaft of the machine or on the gearbox giving the information about mechanical speed of the machine [48], [53].

The controller of such a drive is thus enabled to acquire stator current components I_{sd}, I_{sq}, stator voltage components U_{sd}, U_{sq}, stator angular frequency ω_s and rotor angular frequency ω_m.

2.1 Converters Used in Variable Speed Drives

Switching apparatus could have only minimal interactions with parameter identification so it will not be discussed in this work. On the contrary, converters are very often engaged in parameter identification e.g. by modulating waveforms supplied to the machine or by using the converter's sensors. This will be discussed in detail in chapter 5. Main requirements of the converter for variable speed drive is the possibility of variable output frequency and variable output voltage. Converters with the capability of changing frequency can be divided into two main groups: rotational and electronic (solid-state). The first group is nowadays obsolete and had never been widely used with induction motors, so only the second group will be considered. This second group can be further divided into two subcategories – direct and indirect frequency converters. The main

difference between these two groups is the presence of a DC link which the former does not have while the latter converts the current at first into DC current and then back into AC with different parameters.

Among the direct frequency converters, we can find the so called cycloconverters [54] and matrix converters [55]–[57]. The first consists of two anti-parallel thyristor (three-phase) rectifier bridges. Matrix converters use mostly switching devices with a capability of switching on and off. Their principle lies in the possibility of connecting every output phase to any of the input phases – they are limited to multiple phase supply only (however the output can be single or any desired number of phases).

As mentioned before, the indirect frequency converters work on a principle of rectifying and then again “alternating” the electrical energy. Output phase (or phases) can be connected to a positive or negative terminal of the so called DC link. If this DC link consists of a capacity it behaves as a voltage source (voltage type DC link). We call the converter a Voltage Source Inverter (VSI, Fig. 4). If it consists of an inductance (current type of DC link), it is named Current Source Inverter (CSI).

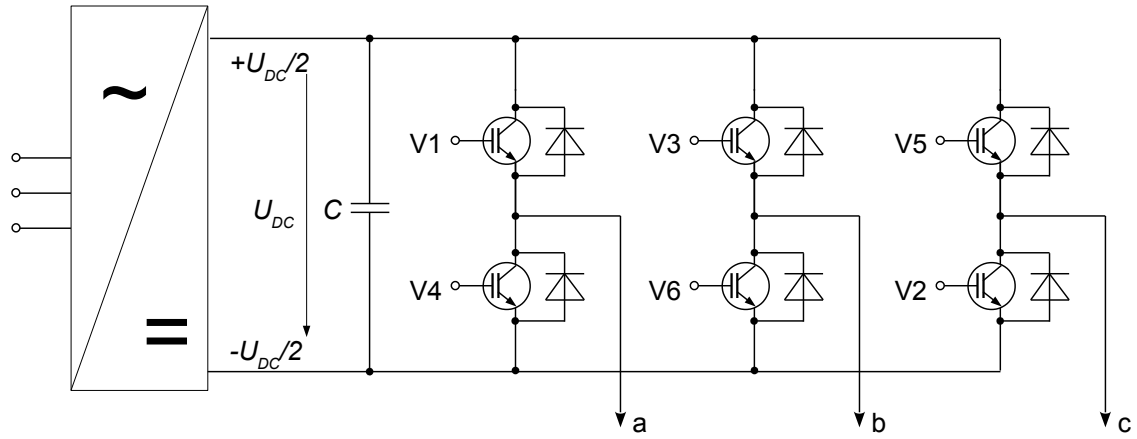

Fig. 4: Topology of a voltage source inverter.

The presented topology enables connection of a positive or negative voltage to the load which are two voltage levels and thus it is in general called a two level inverter. If more than two voltage levels can be connected to the load, we speak of a multilevel converter [58]. The main advantages of such a topology are better harmonic indicators (e.g. THD) and lower voltage stress of the switching devices, so it is suitable for high voltage applications. As drawbacks an increased number of components and a more complex control can be seen. Main types of topologies of multilevel converters are Flying Capacitor Multilevel Inverter, Diode Clamped Inverter, H-Bridge Cascaded Inverter and Modular Multilevel Converter (M^2C or MMC) [59]. If the Diode Clamped Converter is carried out as a three-level, it is often called a Neutral Point Connected (NPC) [60]. All of them are carried out as VSIs. More about different types of converters and their classification can be found in [61], [62].

We can see that there is a plethora of different inverter topologies that could be potentially used for a drive with an induction machine. However, the three-phase two level voltage source inverter

(Fig. 4) is nowadays the first choice in most cases and is therefore the most common one in drives with induction machines. Among the reasons simplicity, comparatively low number of switching devices and thus reliability, lower costs and simpler implementation of control strategies can be mentioned.

2.2 Control System of a Drive

Controllers and control systems of the drives have been evolving for more than a century. From electromechanical and relay based controllers that could automate not only speed or current loop but run-up, brake or cycling as well [63], [64] through controllers built from analogue devices [65] to first microprocessor [66] the demands made on them were continually rising. Nowadays the controller should not only carry out the control strategy, but should be able to communicate with sensors, and converter bi-directionally and also provide some human-machine interface and/or communicate with some superordinate control system (see Fig. 2). Controller can also have embedded a diagnostic system or protections against damage in case of failure of the mechanism or some component of the drive. There can be further other special algorithms such a for minimizing losses [67] or a slip control algorithm in case of railway traction [48]. Buses like CAN, Modbus, IO-Link or serial interface require processor time even in case that have usually a dedicated peripherals in the controller. Regarding all the mentioned tasks, the controller can reach its limits with the processor time or with the memory. Despite the microcontrollers are still evolving into faster ones with more capabilities, the tasks that they need to carry out are also getting more and more complex. When a question of financial cost of the hardware comes to the scene, it can imply that a modest controller should be used. Therefore it is not a problem to reach limits of the controller. This can of course happen also in case when some existing control hardware which should be enriched by some new software functions.

Authors in [68] carried a study on requirements of different modern control methods of drives with induction machines on a microcontroller TMS320F28035 (Texas Instruments) which application field involves also a control of AC drives, according to the manufacturer. This microcontroller has 20 kilobits of memory and a clock frequency of 60 MHz. Tab. 1 shows memory usage and execution times of six different control strategies. Compared strategies included Indirect Field Oriented Control (IFOC), Fuzzy Indirect Field Oriented Control (FIFOC), Predictive Current Control (PCC), Direct Torque Control (DTC), Fuzzy Direct Torque Control (FDTC), Predictive Torque Control (PTC) which will be in brief described in a following subchapter.

Tab. 1: Comparison of memory usage and execution time of different control strategies on TMS320F28035 microcontroller [68].

	IFOC	**FIFOC**	**PCC**	**DTC**	**FDTC**	**PTC**
Memory usage (%)	37,8	52,5	37,8	36,5	46,9	36,8
Execution time (μs)	16	28	25	15	31	42
Clock cycles (-)	911	1700	1497	879	1855	2494

In case of execution time there is reserve for probably most types of other tasks as it is usually sufficient to carry out the control algorithm loop in hundreds of microseconds. But in case of memory, control strategies with fuzzy controllers reached 50% of the available memory. If these parameters would be projected to some existing, older control hardware or low-cost devices with slower clock frequency or smaller memory, it is clear that the limits can be easily. Therefore there is a field for computationally modest method of induction machine parameter identification.

2.3 Control Strategies of Dynamic Drives

Demands in the dynamic properties of drive systems are constantly rising in some fields. In manufacturing this is due to even faster machining processes, increases in automation cycles and an overall effort to increase efficiency of the equipment which is driven by economical needs – the manufacturing equipment should carry out the manufacturing operations in the shortest possible time as no customer would pay for a standstill. In electric traction, demands on acceleration and deceleration are driven by competition with other means of transport with the aim of shortening travel times.

A dynamic drive can be characterized by a demand for comparatively fast changes in speed and braking. Such a drive has to accelerate fast and brake to a halt in the shortest possible time and there are also demands on the accuracy of positioning.

Among the drives with the highest dynamic requirements are those employed in manufacturing. These are the drives of robots and manipulators that should not slow down the processing so they should move in the time given by capabilities of the previous and following machining tool in the production line. Their acceleration is limited only by values that the transported goods can withstand. Drives with demanding dynamic properties are also to be found within machining tools e.g. flying shears. In electric traction on railway, fast acceleration can cut down travel times significantly especially in case of commuter systems with comparatively large number of stops in short distances. Drives of electric vehicles should be regarded as dynamic ones as well [69]. With an accurate estimation of position, drives with induction machines can be used in general as servodrives.

Modern control strategies includes Indirect Field Oriented Control (IFOC), Fuzzy Indirect Field Oriented Control (FIFOC), Predictive Current Control (PCC), Direct Torque Control (DTC), Fuzzy Direct Torque Control (FDTC), Predictive Torque Control (PTC). All these control strategies rely on some form of a mathematical model and thus a proper knowledge of the model – and therefore machine – parameters can improve the performance of the control strategy.

3 Mathematical Model of an Induction Machine

As mentioned before, most of the modern methods of control of a variable speed drive with an induction machine rely on some form of a mathematical model of the controlled machine. Deriving of the mathematical model is based on its construction and principles of working which are briefly described in following chapters.

3.1 Construction of a Machine

An induction motor consists of motor frame with a stator packet and rotor packet of the sheets from electric steel on a shaft that is placed axially through the motor being attached by bearings in end bells (also called end shields). There is often an axial fan on one end of the shaft, covered by an end bell serving for cooling the engine. This type of construction is widely known as Totally Enclosed Fan Cooled (TEFC) motor. However, high power motors have normally a separate cooling (air or water). Types of cooling of motor are standardised and their types and designations are given by [70], type of mounting by [71].

Magnetic circuit of an induction machine consists of isolated steel sheets composed together and pressed into the frame. In these sheets, holes are stamped that form slots along the longitudinal axis (see Fig. 5). Various shapes of the slots exist and their geometry can influence the properties of the machine, e.g. the division of the leakage inductance (see chapter 5.1.3) especially in case of rotor bars (Fig. 36). Neglecting the actual shape of the slot, slot construction can be divided into fourmain categories: semi-closed slot, open slot, open slot to be closed with wedge and closed slot (Fig. 5). Construction from insulated sheets should minimize the eddy currents. Magnetic circuit is divided into stator and rotor with an air gap between them that allows rotation. In stator slots, stator winding is placed that is usually wounded with an insulated copper wire. This winding can be carried out by multiple parallel strands to mitigate the skin effect (more about skin effect and its influence in chapter 4.1.2). Rotor winding is placed in rotor slots and can be wounded as well (so called slip ring motor) or formed by die-casting from aluminium or copper in the form of rods and rings (squirrel cage) or assembled from rods also from special materials like bronze [9].

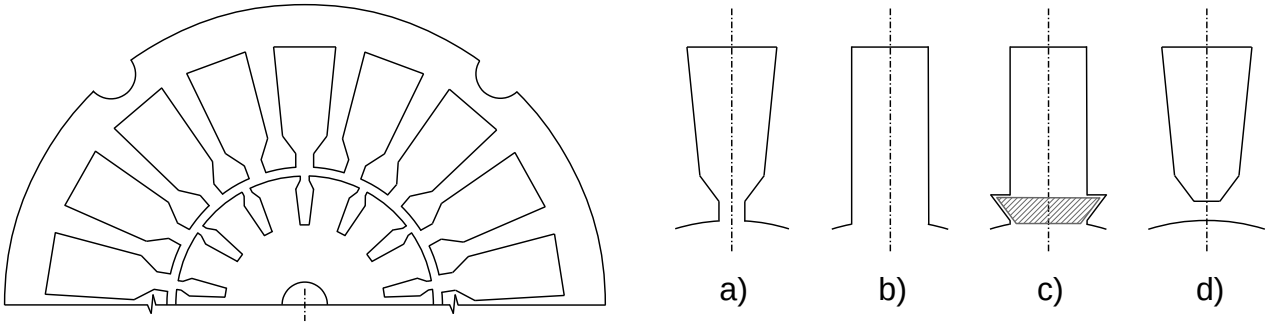

Fig. 5: Left: Cutaway of rotor and stator sheets that constitute a magnetic circuit; Right: Main types of slot shapes: a) semi-closed slot, b) open slot, c) open slot to be closed with wedge, d) closed slot.

Stator winding is multiphase (except single phase induction machines that requires additional technical means to start), the most frequent case is still a three phase machine. This winding generates a rotating magnetic field. According to the number of phases, the wires of the winding are divided into equal groups placed symmetrically along the circumference. Each phase consists of a separate electrical circuit, which can be divided into several parallel branches for large values of current and to mitigate skin effect. The basic element is a winding thread, i.e. the connection of two conductors deposited in the slots of the distant pole pitch at full step or a small step in the shortened distance. Several wires involved in the series comprise a coil provided with a total isolation (wires are insulated themselves as mentioned before) from the slot.

When rotor winding is wound, it is usually made as three phase with the ends of the coils conducted to so called slip rings. With brushes sliding on these moving rings it can be conducted out of the motor. In case of bare bars, each bar represents one phase, so it is a multiphase winding.

Fig. 6: Cutaway of small squirrel cage induction motor.

3.2 Magnetic Field and the Principle of Working

The principle of the induction machine operation is based on the mutual interaction of the magnetic field of the stator and rotor. Stator magnetic field is produced by currents supplied to the stator winding by power supply through the machine terminals, while the rotor currents that form a magnetic field of a rotor are induced by variable magnetic field of stator. We can imagine the rotating magnetic field inside the machine as a field of a rotating permanent magnet.

The simplest three phase winding of a two pole machine $2p = 2$ ($2p$ being number of poles) is with one slot per pole and phase $q_w = 1$ as depicted in Fig. 7. The number of turns in one slot and also in the phase is equal to $N = 1$. Coils of phases are shifted mutually by the angle $2\pi/3 = 120°$.

This three phase winding is supplied from a source of sinusoidal symmetrical three phase current. Phase current is then responsible for creation of a magneto-motive force (MMF).

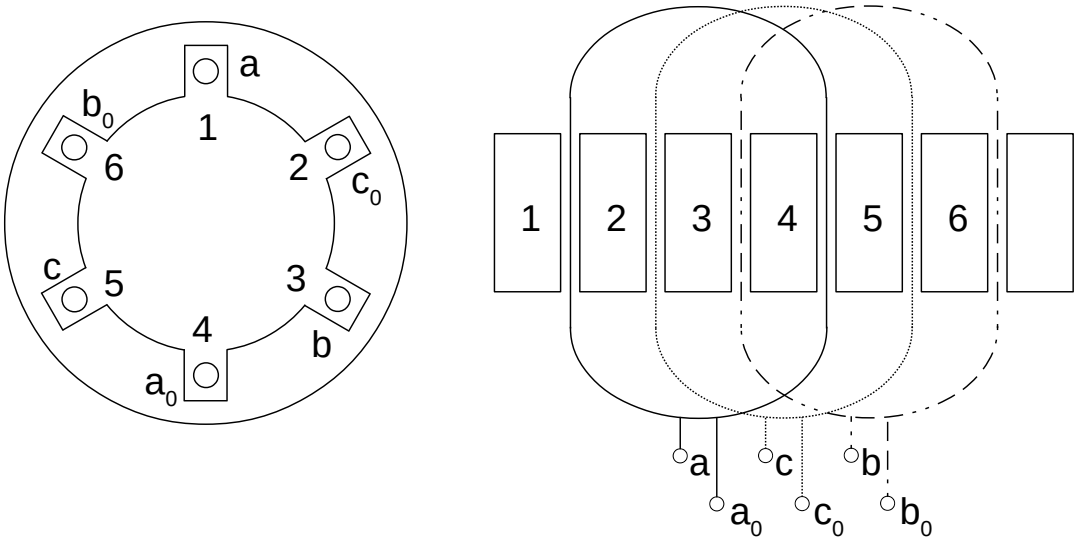

Fig. 7: The simplest three phase winding, $p_p = 1$ and $q_w = 1$.

The amplitude of the fundamental component of MMF is given by:

$$F_a = F_b = F_c = \frac{3}{2}\frac{2\sqrt{2}}{\pi}\frac{N I_s k_w}{p_p} , \tag{1}$$

where N is number of turns of the winding per phase, I_s is stator current, k_w is winding constant (based on implementation of the winding) and p_p ($p_p = 2p/2$) is winding pole-pair number.

The resulting amplitude of the first harmonic MMF is equal to a vector sum of first the harmonic instantaneous values of all three phases (F_a, F_b, F_c). This sum can be expressed as

$$F_1 = F_a + \frac{1}{2}F_b\cos\frac{\pi}{3} + \frac{1}{2}F_c\cos\left(-\frac{\pi}{3}\right) = \frac{3}{2}F_a . \tag{2}$$

The resultant amplitude of MMF is constant and it changes its position only with the space angle $\Omega_s t$ (Ω_s given by (3), t is time). The resultant magnetic field has the constant amplitude and it rotates in the air gap with the constant angular speed.

The angular speed of this rotation is

$$\Omega_s = \frac{2\pi f_s}{2p} , \tag{3}$$

where $2p$ is a number of poles of the machine and f_s is a frequency of the stator current (voltage). It is called a synchronous speed. At this point, a difference between electrical and mechanical angular frequencies should be mentioned. If the machine is a two-pole ($2p = 2$; $p_p = 1$) than electrical and mechanical angular speeds are equal. In other cases, the mechanical angular frequency is different, proportional to the number of pole-pairs of the machine.

If a machine has $p_p > 1$, than the magnetic field amplitude travels only from one pole-pair to the next pole-pair within one cycle of the electrical angular frequency. This means

$$\Omega_s = \frac{\omega_s}{p_p} , \tag{4}$$

where Ω_s is the angular frequency of the stator magnetic field and ω_s is the electrical angular speed of the stator supply current I_s.

The relation between MMF and stator current can be simplified with introducing an effective stator turns per pole N_{l1}. With an RMS value of stator phase current I_1, it yields:

$$F_1 = N_{l1} I_1 . \tag{5}$$

The effects caused by stator currents result in a voltage being induced in the rotor winding (at the beginning of standstill). This voltage causes currents to flow in the closed rotor circuit. By effect of these currents, torque arises and according to Lenz's law it works against the cause of its formation and thus prevents rising up of currents in the rotor. Due to the rotation of the rotor, torque reduces the rate of crossings of the rotating field and stator wires and therefore reduces the magnitude of the induced voltage and current in the rotor as well.

When the motor works with no-load on its shaft, it is loaded only by its mechanical losses, which means a very small torque. Therefore the rotor does not reach synchronous speed, because the synchronous speed would mean no crossings of the rotating field and rotor wires resulting in zero torque. This fact is responsible for the other commonly used name of the induction motor, which is asynchronous motor. The rotor speed at normal operation always stabilizes at a value somewhat smaller than the field speed, because as the motor slows down, the rotor conductors cross the rotating field faster, greater voltages are induced in the rotor circuits, heavier currents flow in them, stronger magnetic poles are produced on the rotor surface, and greater torque is developed.

For describing the relation between rotating stator magnetic field and the rotor, quantity called *slip* was introduced, defined as:

$$s = \frac{\omega_s - \omega_m}{\omega_s} \quad \text{or} \quad s = \frac{\Omega_s - \Omega_m}{\Omega_s} , \tag{6}$$

where ω_m is the electrical angular frequency the rotor and Ω_m is the mechanical angular frequency the rotor. Relation between Ω_m and ω_m is the same as shown in (4) for stator angular frequencies.

The frequency of the rotor voltages and currents is given by the difference of the stator and mechanical frequencies (or angular frequencies). For electrical angular frequencies, the rotor frequency f_r is given by equation (7):

$$f_r = \frac{\omega_s - \omega_m}{2\pi} . \tag{7}$$

If equations (6) and (7)are combined properly, we can describe the rotor frequency f_r using slip s by relation:

$$f_r = s f_s . \tag{8}$$

When a heavy mechanical load is connected to the induction motor, the rotor slows down and the slip increases. For most of the motors, the full-load slip is around 0,03. The frequency of rotor voltages and currents will still be quite small (units of Hertz).

As in every other physical system, there are also mostly unwanted parasitic effects that cause losses in the transformation of electrical to mechanical energy.

In a direction of energy flow stator winding losses (P_s) come at first. These are considered as ohmic losses (called also Joule losses) as they are caused by resistivity of the winding material across which the stator currents flow. These are followed up by iron losses P_{Fe} which represent losses in the magnetic circuit and can be generally iron divided into hysteresis losses and eddy current losses. Both components vary with the square of the magnetic induction. Hysteresis losses vary linearly with frequency, eddy current losses with the square of frequency. Iron losses come partially from both the stator and the rotor, but since the induction motor normally operates at a speed close to synchronous speed, the rotor frequency is comparatively low and thus iron losses caused by rotor are negligible. Further there are additional losses P_{ad} caused by additional stray of magnetic field.

In rotor there are also ohmic (Joule) losses in the rotor winding (P_r) and further losses caused by friction of the rotating mass of the rotor in bearings (P_{fric}). In case of own cooling of the machine (e.g. TEFC, see chapter 3.1) there are ventilation losses caused by cooling fan (P_{vent}). As these coud be present or not based on construction of the machine, P_{fric} and P_{vent} are often expressed together as mechanical losses P_{mech}.

3.3 Equivalent Circuits of the Induction Machine

The mathematical model of an induction machine is a system of equations that describe its behaviour. Complexity of these equations and number of parameters needed for their constitution may differ based on the complexity of the mathematical model, the purpose of the model or the phenomena of the machine that are being studied. This system of equations can be represented by an equivalent circuit (equivalent scheme; e.g. Fig. 11, Fig. 13 or Fig. 14). Following chapter shows the derivation of a model that leads to probably the most common representation of an induction machine in technical praxis, which is a five parameter so called “T” equivalent circuit (Fig. 11).

From the point of view of creation of a mathematical model, the motor has three main components, illustrated on left side of Fig. 8 including their configuration. These are:

- three electric circuits of three stator windings that are located in three axes a, b, c
- three or more electric circuits of three or more rotor windings that are located in three or more axes A, B, C. Even if there are more than three phases (e.g. squirrel cage motor), three phase system is considered.
- one common magnetic circuit with an air gap, teeth and slots

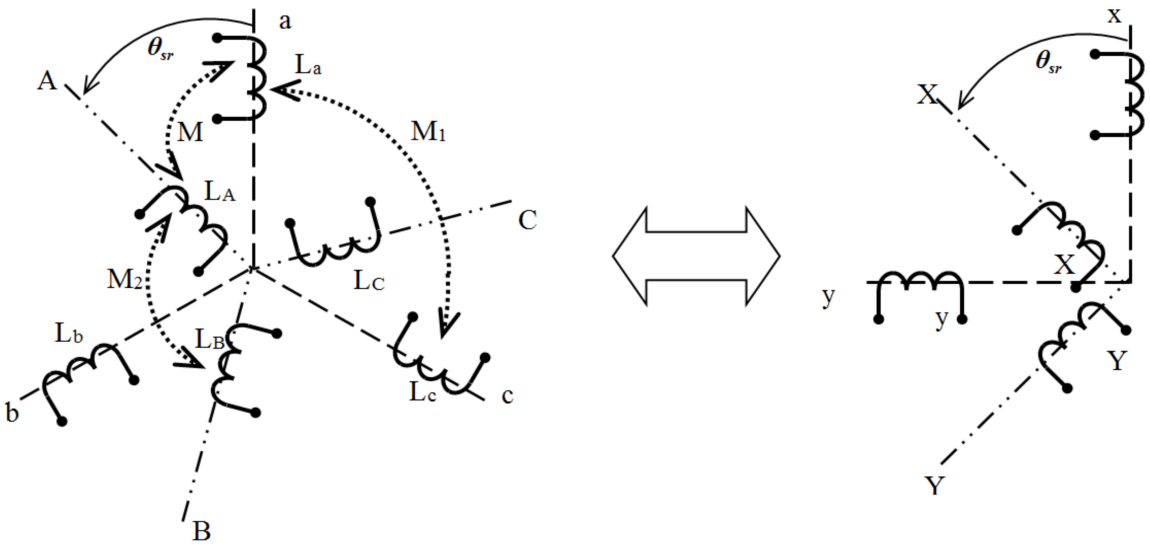

Fig. 8: Left: Schematic depiction of induction machine windings and relations between them in three phase system; Right: Transformed into two axis, two phase system.

For each separate winding (a, b, c for stator and A, B, C for rotor) voltage equation for the voltage of the terminals of the winding (a general induction machine with terminal also on rotor is supposed, special cases such as squirrel cage will be covered later in the text) can be written in the form

$$u_p = R_w i_p + \frac{\mathrm{d}\,\Psi_p}{\mathrm{d}\,t}\ , \tag{9}$$

where index *p* stands for the respective phases (a, b, c for stator and A. B, C for rotor), *i* being the current flowing through the respective phase, R_w is the stator or rotor resistance R_s or R_r and Ψ is magnetic flux. Each phase winding has then a magnetic coupling with all other phase windings both on rotor and on stator as depicted in Fig. 8 left. It supposes a symmetrical construction of the machine so that all stator winding self inductances $L_a = L_b = L_c$ are equal, as well as all rotor winding self inductances $L_A = L_B = L_C$. In Fig. 8 further symbols mean: *M* the mutual inductance between corresponding stator and rotor phase winding – it depends on a rotor and stator mutual angle θ_{sr}, thus a notation $M(\theta_{sr})$ is used. M_1 is being a mutual inductance of between two phases of stator winding and M_2 being a mutual inductance of between two phases of rotor winding – under symmetrical construction of a machine, these are independent on stator and rotor mutual angle. For phase *a* as an example, the relation between currents, mutual inductances and resulting magnetic flux can be written as

$$\Psi_a = L_a i_a + M_1 i_b \cos 2\frac{\pi}{3} + M_1 i_c \cos 4\frac{\pi}{3} + M(\theta_{sr}) i_A + M(\theta_{sr}) i_B \cos 2\frac{\pi}{3} + M(\theta_{sr}) i_C \cos 4\frac{\pi}{3}\ . \tag{10}$$

If star (wye, Y) connection of stator and rotor windings is supposed with an identical configuration, the following relations are valid:

$$i_b + i_c = -i_a \quad i_B + i_C = -i_A\ . \tag{11}$$

This enables to simplify (10) into form of (12):

$$\begin{gathered}\Psi_{\mathrm{a}}=L_{\mathrm{a}}\, i_{\mathrm{a}}+M_{1}(-0{,}5)(i_{\mathrm{b}}+i_{\mathrm{c}})+M(\theta_{\mathrm{sr}})\, i_{\mathrm{A}}+M(\theta_{\mathrm{sr}})(-0{,}5)(i_{\mathrm{B}}+i_{\mathrm{C}})= \\ (L_{\mathrm{a}}+0{,}5\,M_{1})\, i_{\mathrm{a}}+1{,}5\,M(\theta_{\mathrm{sr}})\, i_{\mathrm{A}}=L_{\mathrm{s}} i_{\mathrm{a}}+L_{\mathrm{m}} i_{\mathrm{A}}\end{gathered}\quad , \tag{12}$$

where $L_{\mathrm{s}} = (L_{\mathrm{a}} + 0{,}5\, M_1)$ is the resulting inductance of one stator phase and $L_{\mathrm{m}} = 1{,}5\, M(\theta_{\mathrm{sr}})$ is for the mutual inductivity between one stator phase and all rotor windings. For an initial position of a rotor when $\theta_{\mathrm{sr}} = 0°$, $L_{\mathrm{m}} = 1{,}5\, M$. Because of this dependence on mutual angle between rotor and stator, the rotor and stator flux per phase are usually expressed separately and then transformed to a common system of axes, as described further.

Space configuration of stator windings lets us define space vectors for the stator variables u_p, i_p and Ψ_p (p being the index of particular phase – a, b, c). A general space vector $\hat{G}_{\mathrm{s}}$ of an exemplary stator variable g is defined:

$$\begin{gathered}\hat{G}_{\mathrm{s}}=K\left(g_{\mathrm{a}}+g_{\mathrm{b}}\left(\cos 2\frac{\pi}{3}+\mathrm{j}\sin 2\frac{\pi}{3}\right)+g_{\mathrm{c}}\left(\cos 4\frac{\pi}{3}+\mathrm{j}\sin 4\frac{\pi}{3}\right)\right)= \\ K\left[g_{\mathrm{a}}+g_{\mathrm{b}}\left((-0{,}5)+0{,}866\,\mathrm{j}\right)+g_{\mathrm{c}}\left((-0{,}5)-0{,}866\,\mathrm{j}\right)\right]= \\ g_{\alpha}+\mathrm{j}\, g_{\beta}\end{gathered}\quad . \tag{13}$$

This general variable's vector $\hat{G}_{\mathrm{s}}$ can be written also in a form of two components (according to Clarke transformation) in a two axis plane, like in a complex plane, according to real and imaginary part:

$$\begin{gathered}g_{\mathrm{x}}=K\left(g_{\mathrm{a}}-0{,}5\, g_{\mathrm{b}}-0{,}5\, g_{\mathrm{c}}\right)=1{,}5\, K g_{\mathrm{a}} \\ g_{\mathrm{y}}=K\left(0{,}866\, g_{\mathrm{b}}-0{,}866\, g_{\mathrm{c}}\right)=0{,}866\, K\left(g_{\mathrm{b}}-g_{\mathrm{c}}\right)\end{gathered}\quad . \tag{14}$$

Constant K that appears in the equations can be chosen arbitrarily, but selecting some certain values of K lead to useful relations:

If $K=\sqrt{\frac{2}{3}}$ then the power is identical in both systems.

If $K=1$ then the vector in α, β system is 1,5 time larger than in a,b,c system.

If $K=\frac{2}{3}$ then the instantaneous value of variable g is identical in both systems. This value of K is used most often.

Three equations of stator phase voltage shown in (9) for phases a, b and c can be simplified into one equation using of vectors:

$$\hat{U}_{\mathrm{s}}=R_{\mathrm{s}}\,\hat{I}_{\mathrm{s}}+\frac{\mathrm{d}\,\hat{\Psi}_{\mathrm{s}}}{\mathrm{d}\,t}\ . \tag{15}$$

The equation for magnetic fluxes shown in (10) can be simplified into one vector equation

$$\hat{\Psi}_{\mathrm{s}}=L_{\mathrm{s}}\,\hat{I}_{\mathrm{s}}+L_{\mathrm{m}}\,\hat{I}_{\mathrm{r}}\, e^{\mathrm{j}\theta_{\mathrm{sr}}}\ . \tag{16}$$

Rotor windings normally rotate against stator windings with an angular speed ω_m and therefore the angle θ_{sr} between rotor real axis and stator real axis changes according to the relation

$$\theta_{sr} = \omega_m t \ . \tag{17}$$

The same transformations from a three phase system to a two phase system (Clarke transformation) as for stator can be applied to a rotor system. Even if there are more than three phases (e.g. squirrel cage motor), a three phase system is considered. Resulting equations for voltage and flux are:

$$\hat{U}_r = R_r \hat{I}_r + \frac{\mathrm{d}\hat{\Psi}_r}{\mathrm{d}t} \tag{18}$$

and

$$\hat{\Psi}_r = L_r \hat{I}_r + L_m \hat{I}_s e^{j\theta_{sr}} \ . \tag{19}$$

Vectors in axes that do not turn relative to the stator (α, β) can be transformed to another axes (x, y) that turn relative to the stator with an angular speed ω_k (Park transformation). An angle between axes (α, β) and (x, y) is usually marked θ_k and is equal to $\theta_k = (\omega_k t + \theta_{k0})$ where θ_{k0} is the mutual angle in the time $t = 0$.

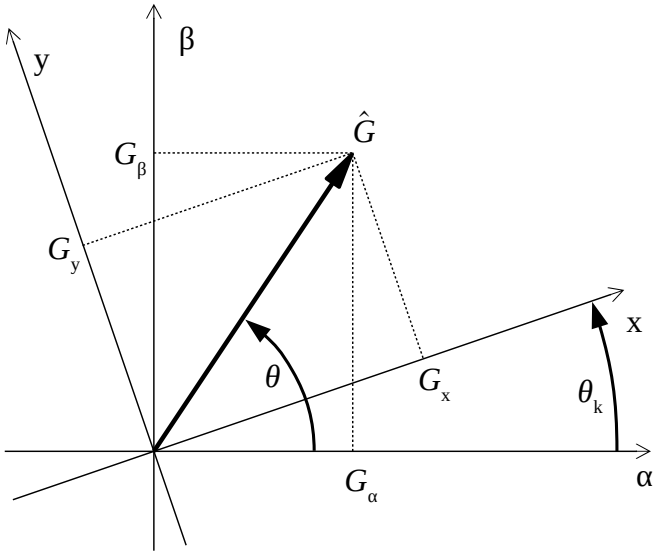

Fig. 9: Transformation of axes systems (α,β) and (x, y).

Forward transformation from (α, β) to (x, y) for vector components of a general vector $\hat{G}$:

$$\begin{aligned} G_x &= G_\alpha \cos\theta_k + G_\beta \sin\theta_k \\ G_y &= G_\beta \cos\theta_k - G_\alpha \sin\theta_k \end{aligned} \ . \tag{20}$$

And a reverse transformation:

$$\begin{aligned} G_\alpha &= G_x \cos\theta_k - G_y \sin\theta_k \\ G_\beta &= G_y \cos\theta_k + G_x \sin\theta_k \end{aligned} \ . \tag{21}$$

In a form of vector equations it would be written as

$$\begin{aligned} \hat{G}^{xy} &= \hat{G}^{\alpha\beta} e^{j\theta_k} \\ \hat{G}^{\alpha\beta} &= \hat{G}^{xy} e^{-j\theta_k} \end{aligned} \ . \tag{22}$$

We use general relation (22) for particular stator and rotor voltage equations (15) and (18) to transform them to a common general axis system k, l. This axis system turns with the angular speed ω_k relative to the stator axes system and with the angular speed (ω_k - ω_m) relative to the rotor axes system. It yields

$$\begin{aligned} \hat{U}_s^k e^{j\theta_k} &= R_s \hat{I}_s^k e^{j\theta_k} + \frac{d\left(\hat{\Psi}_s^k e^{j\theta_k}\right)}{dt} \\ \hat{U}_r^k e^{j(\theta_k-\theta)} &= R_r \hat{I}_r^k e^{j(\theta_k-\theta)} + \frac{d\left(\hat{\Psi}_r^k e^{j(\theta_k-\theta)}\right)}{dt} \end{aligned} . \tag{23}$$

Further rearranged, we get

$$\begin{aligned} \hat{U}_s^k &= R_s \hat{I}_s^k + \frac{d\hat{\Psi}_s^k}{dt} + j\omega_k \Psi_s^k \\ \hat{U}_r^k &= R_r \hat{I}_r^k + \frac{d\hat{\Psi}_r^k}{dt} + j(\omega_k - \omega_m)\Psi_r^k \end{aligned} . \tag{24}$$

Relations in (24) contain three important components:

- voltage drops across the resistances R_s and R_r respectively
- voltages proportional to derivation of the magnetic flux that are called *transformation voltages*
- voltages that are proportional to product of the magnetic flux and the angular speed called *rotational voltages.* In a steady state these voltages disappear.

We further rearrange equations (16) and (19) in a manner that MMF of both windings in the same axis subtracts from positive currents:

$$\begin{aligned} \hat{\Psi}_s^k &= L_s \hat{I}_s^k - L_m \hat{I}_r^k \\ \hat{\Psi}_r^k &= L_r \hat{I}_r^k - L_m \hat{I}_s^k \end{aligned} . \tag{25}$$

Relations in (24) and (25) can be rewritten into a commonly presented system of algebraic equations for respective vector components representing the induction machine's behaviour:

$$\begin{aligned} u_{sx} &= R_s i_{sx} + \frac{d\Psi_{sx}}{dt} - \omega_k \Psi_{sy} \\ u_{sy} &= R_s i_{sy} + \frac{d\Psi_{sy}}{dt} + \omega_k \Psi_{sx} \\ u_{rx} &= R_r i_{rx} + \frac{d\Psi_{rx}}{dt} - (\omega_k - \omega_m)\Psi_{ry} \\ u_{ry} &= R_r i_{ry} + \frac{d\Psi_{ry}}{dt} + (\omega_k - \omega_m)\Psi_{rx} \\ \Psi_{sx} &= L_s i_{sx} - L_m i_{rx} \\ \Psi_{sy} &= L_s i_{sy} - L_m i_{ry} \\ \Psi_{rx} &= L_r i_{rx} - L_m i_{sx} \\ \Psi_{ry} &= L_r i_{ry} - L_m i_{sy} \end{aligned} . \tag{26}$$

This system of equations can be represented as two equivalent circuits (Fig. 10) representing *x* and *y* axis respectively. The two circuits are coupled to each other through induced "rotational" voltages that are exited from coupled magnetic fluxes from the other axis.

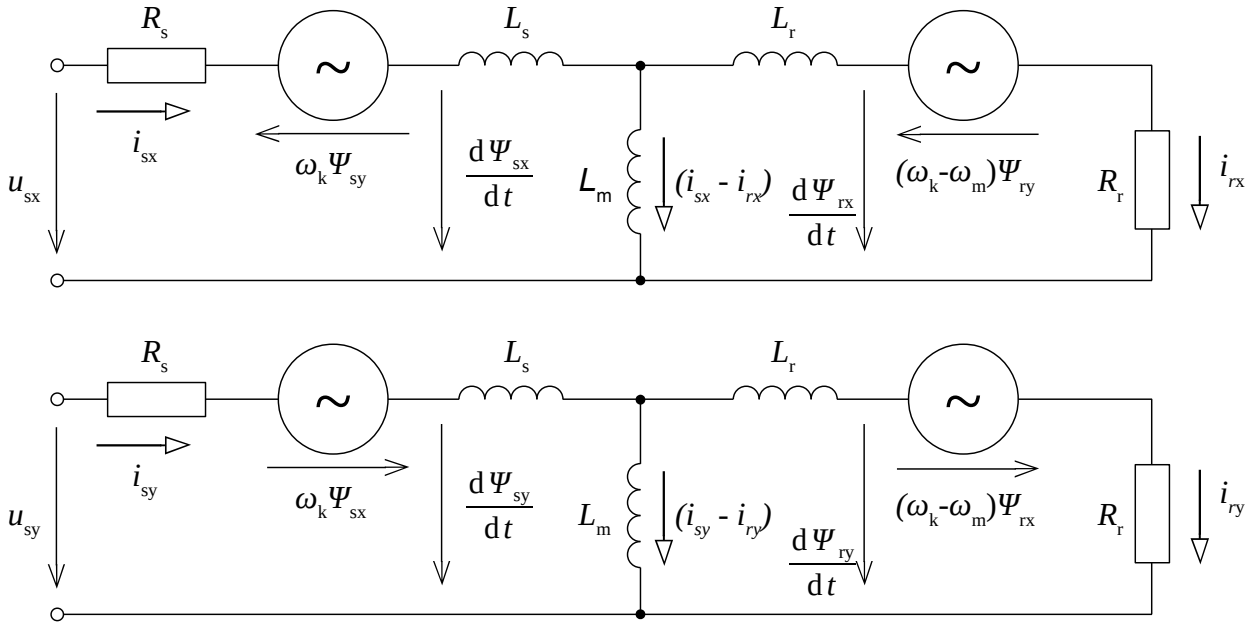

Fig. 10: Equivalent circuits of a squirrel cage induction motor according to (26).

Other systems of axes are used as well. The (α, β) system is one of them. It is fixed to the stator, so it does not rotate against the stator and therefore $\omega_k = 0$. The position of axis α is mostly located in the position of the winding axis *a*. Corresponding system of equations (27) is similar to (26):

$$\begin{aligned}
u_{s\alpha} &= R_s i_{s\alpha} + \frac{d\Psi_{s\alpha}}{dt} \\
u_{s\beta} &= R_s i_{s\beta} + \frac{d\Psi_{s\beta}}{dt} \\
u_{r\alpha} &= R_r i_{r\alpha} + \frac{d\Psi_{r\alpha}}{dt} + \omega_m \Psi_{r\beta} \\
u_{r\beta} &= R_r i_{r\beta} + \frac{d\Psi_{r\beta}}{dt} - \omega_m \Psi_{r\alpha} \\
\Psi_{s\alpha} &= L_s i_{s\alpha} - L_m i_{r\alpha} \\
\Psi_{s\beta} &= L_s i_{s\beta} - L_m i_{r\beta} \\
\Psi_{r\alpha} &= L_r i_{r\alpha} - L_m i_{s\alpha} \\
\Psi_{r\beta} &= L_r i_{r\beta} - L_m i_{s\beta}
\end{aligned} \quad . \qquad (27)$$

It is a system of 8 equations with 13 variables ($u_{s\alpha}$, $u_{s\beta}$, $u_{r\alpha}$, $u_{r\beta}$, $i_{s\alpha}$, $i_{s\beta}$, $i_{r\alpha}$, $i_{r\beta}$, $\Psi_{s\alpha}$, $\Psi_{s\beta}$, $\Psi_{r\alpha}$, $\Psi_{r\beta}$, ω_m) and 5 parameters. These parameters are namely a stator resistance R_s, a rotor resistance R_r, a stator inductance L_s, a rotor inductance L_r and a magnetizing inductance L_m. For an explicit solution, 5 variables out of these 13 have to be defined as we have only 8 equations.Most frequently, $u_{s\alpha}$, $u_{s\beta}$, $u_{r\alpha}$, $u_{r\beta}$ and ω_m are chosen as these independent variables. In case of a squirrel cage motor it simplifies as $u_{r\alpha} = u_{r\beta} = 0$.

Another system of axes that is widely used is marked as (d, q). It rotates with the angular speed of the motor magnetic field which means that it rotates against the stator with the angular speed $\omega_k = \omega_s$. Position of axis *d* is mostly situated to the position of the coupled magnetic flux Ψ. Equations for this system are in following form:

$$\begin{aligned} u_{sd} &= R_s i_{sd} + \frac{d\Psi_{sd}}{dt} - \omega_s \Psi_{sq} \\ u_{sq} &= R_s i_{sq} + \frac{d\Psi_{sq}}{dt} + \omega_s \Psi_{sd} \\ u_{rd} &= R_r i_{rd} + \frac{d\Psi_{rd}}{dt} - (\omega_s - \omega_m)\Psi_{rq} \\ u_{rq} &= R_r i_{rq} + \frac{d\Psi_{rq}}{dt} + (\omega_s - \omega_m)\Psi_{rd} \\ \Psi_{sd} &= L_s i_{sd} - L_m i_{rd} \\ \Psi_{sq} &= L_s i_{sq} - L_m i_{rq} \\ \Psi_{rd} &= L_r i_{rd} - L_m i_{sd} \\ \Psi_{rq} &= L_r i_{rq} - L_m i_{sq} \end{aligned} \tag{28}$$

Unlike in the previous case, we have 14 variables (u_{sd}, u_{sq}, u_{rd}, u_{rq}, i_{sd}, i_{sq}, i_{rd}, i_{rq}, Ψ_{sd}, Ψ_{sq}, Ψ_{rd}, Ψ_{rq}, ω_m, ω_s) and 5 parameters (R_s, R_r, L_s, L_r, L_m), so we need to define 6 variables as independent for an explicit solution. Most often u_{sd}, u_{sq}, u_{rd}, u_{rq}, ω_m and ω_s are chosen. Again as in previous case, when a squirrel cage motor is considered $u_{rd} = u_{rq} = 0$.

To derive the frequently used equivalent circuit, we rewrite (24) and (25) for harmonic waveforms in a way that (25) is substituted into (24) and $\omega_k = \omega_s$. With further help of slip *s* defined in (6), when the second equation is divided by *s* to eliminate the difference $\omega_k - \omega_m$ or better to say $\omega_s - \omega_m$ in (24), we get:

$$\begin{aligned} \hat{U}_s &= R_s \hat{I}_s + j\omega_s L_s \hat{I}_s - j\omega_s L_m \hat{I}_r \\ \frac{\hat{U}_r}{s} &= \frac{R_r}{s}\hat{I}_r + j\omega_s L_r \hat{I}_r - j\omega_s L_m \hat{I}_s \end{aligned} . \tag{29}$$

This could be expressed also with reactances as $X_i = \omega_s \cdot L_i$ while *i* stands for an index *r, s* or *m.* Rotor voltage, current and resistance as well as rotor reactance are recalculated to the stator side and so, stator angular frequency ω_s could be used in all places in the equations.

Further we define a stator leakage inductance $L_{\sigma s}$ and rotor leakage inductance $L_{\sigma r}$ as

$$\begin{aligned} L_{\sigma s} &= L_s - L_m \\ L_{\sigma r} &= L_r - L_m \end{aligned} \tag{30}$$

and then we can rewrite (29) as

$$\begin{aligned} \hat{U}_s &= R_s \hat{I}_s + j\omega_s L_{s\sigma} \hat{I}_s + j\omega_s L_m (\hat{I}_s - \hat{I}_r) \\ j\omega_s L_m (\hat{I}_s - \hat{I}_r) &= \frac{R_r}{s}\hat{I}_r + j\omega_s L_{r\sigma} \hat{I}_r - \frac{\hat{U}_r}{s} \end{aligned} . \tag{31}$$

The purpose of these two equations can be seen on Fig. 11.

In addition we define

$$\hat{U}_\mathrm{i} = \mathrm{j}\omega_\mathrm{s} L_\mathrm{m} (\hat{I}_\mathrm{s} - \hat{I}_\mathrm{r}) \tag{32}$$

and

$$\hat{I}_\mathrm{m} = \hat{I}_\mathrm{s} - \hat{I}_\mathrm{r} \,. \tag{33}$$

In case of a squirrel cage motor, rotor voltage $\hat{U}_\mathrm{r} = 0$ so we finally obtain

$$\begin{aligned} \hat{U}_\mathrm{s} &= R_\mathrm{s}\hat{I}_\mathrm{s} + \mathrm{j}\omega_\mathrm{s} L_{\mathrm{s}\sigma}\hat{I}_\mathrm{s} + \mathrm{j}\omega_\mathrm{s} L_\mathrm{m}\hat{I}_\mathrm{m} = R_\mathrm{s}\hat{I}_\mathrm{s} + \mathrm{j}\omega_\mathrm{s} L_{\mathrm{s}\sigma}\hat{I}_\mathrm{s} + \hat{U}_\mathrm{i} \\ \mathrm{j}\omega_\mathrm{s} L_\mathrm{m}\hat{I}_\mathrm{m} &= \hat{U}_\mathrm{i} = \frac{R_\mathrm{r}}{s}\hat{I}_\mathrm{r} + \mathrm{j}\omega_\mathrm{s} L_{\mathrm{r}\sigma}\hat{I}_\mathrm{r} \end{aligned} \tag{34}$$

For these two electrical equations, an equivalent circuit can be drawn as shown on Fig. 11, called a “T equivalent circuit”. It is a basic representation of a model of an induction machine. This mathematical model neglects some phenomena, to enable its effective calculation and solution e.g. by a motor controller. In a large number of applications it is suitable for all operational conditions.

Five parameters occur in this model: a stator resistance R_s, a rotor resistance R_r, (referred to a stator) a stator leakage inductance $L_{s\sigma}$, a rotor leakage inductance $L_{r\sigma}$ and a magnetizing inductance L_m. This five parameter model occur in vast amount of publications [1], [2], [11]–[13], [72].

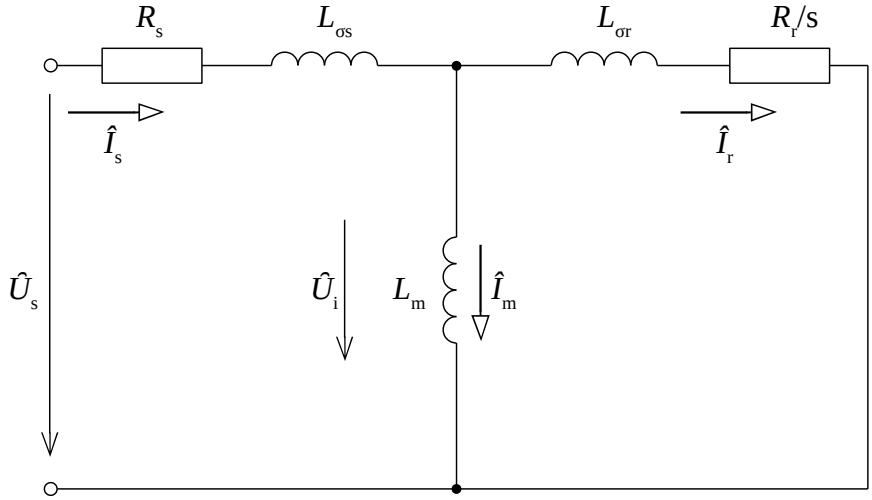

Fig. 11: “T” equivalent circuit of an induction machine.

Some deviations in this equivalent scheme depiction can be found across various sources. Most apparent is the marking of the rotor branch values by an apostrophe to explicitly show that they are recalculated values referred to the stator. Then, the stator and rotor inductances are sometimes presented instead of the leakage inductances (marked with the lower index of Greek letter σ). Difference between these two is given by relation (30). In some cases, reactances are marked instead of inductances as well.

A vector diagram in the d,q plane that corresponds to the T equivalent circuit in Fig. 11 should not be omitted as it gives a valuable overview of the conditions in the machine from other point of view.

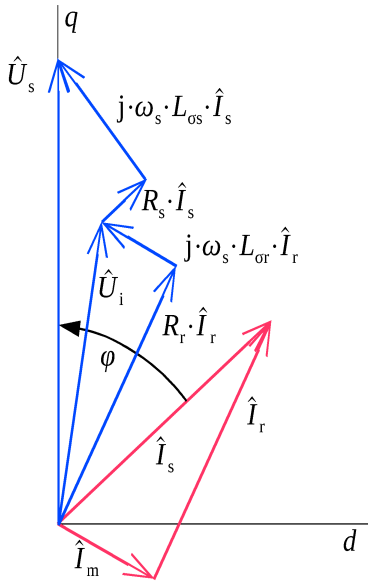

Fig. 12: Vector diagram of the induction machine corresponding to the T equivalent circuit.

If the model should be even more precise, we must admit that its parameters are not constants and that they can vary as described in chapter 4. Among other simplifications is for example a consideration, that the magnetic flux Ψ is a constant. If we assume that it is a function of current Ψ = *f*(i), equations became non-linear which makes the calculations more difficult.

Further, not all of the losses that occur in the machine are expressed in Fig. 11. Losses P_s and P_r (see 3.2) are represented by R_s and R_r. Losses P_{fric}, P_{vent}, and P_{LL} must be respected only by more accurate calculations. If there is a demand for expressing the iron losses in the model of an induction machine, model that contains six parameters instead of five is carried out. Iron losses are represented there by a resistance R_{Fe} connected in parallel to the inductance L_m [14], [33], [61], [73]–[75]. Sometimes it is called a Π equivalent circuit [76]. Copper losses and stray losses can be also included to the model parameters [77], [78] or parameters reflecting the deep bar effect can be added [79]–[81].

In many cases, the classical T-scheme is transformed into so called *Γ equivalent circuit* or *inverse Γ equivalent circuit* depicted in Fig. 13 and Fig. 14 respectively. These two schemes can be considered as closer to the nature of the induction machine as the division of leakage reactance into $L_{s\sigma}$, $L_{r\sigma}$ has only a little physical justification. Further, unequivocal identifiability of this four parameter equivalent circuit is cited [82], [83] compared to five parameter T equivalent circuit which has one more degree of freedom. Therefore, these four parameter equivalent circuits are used in identification methods, e.g. in [84]. Especially useful for some control strategies, mainly rotor flux FOC is the inverse Γ (also marked as Γ^{-1}) circuit, because in this scheme, the stator current divides into the currents I_0 and I_2 which correspond to flux- and torque- component respectively [46], [47], [85]. Therefore some authors call it a “reduced model for rotor flux oriented control” [2].

In case of Γ equivalent circuit, star or "T" connection of $L_{\sigma s}$, $L_{\sigma r}$ and L_m is replaced by a Γ shaped connection of two inductances $L_{\sigma\Gamma}$ and $L_{\mu\Gamma}$. Stator resistance R_s remains the same. These new parameters are recalculated as follows [82]:

$$\begin{aligned} L_{\sigma\Gamma} &= \frac{L_{\sigma r}\left(L_{\sigma s}+L_m\right)^2 + L_{\sigma s} L_m \left(L_{\sigma s}+L_m\right)}{L_m^2} \\ L_{\mu\Gamma} &= L_{\sigma s} + L_m \\ R_{r\Gamma} &= R_r \frac{\left(L_{\sigma s}+L_m\right)^2}{L_m^2} \end{aligned} \quad . \tag{35}$$

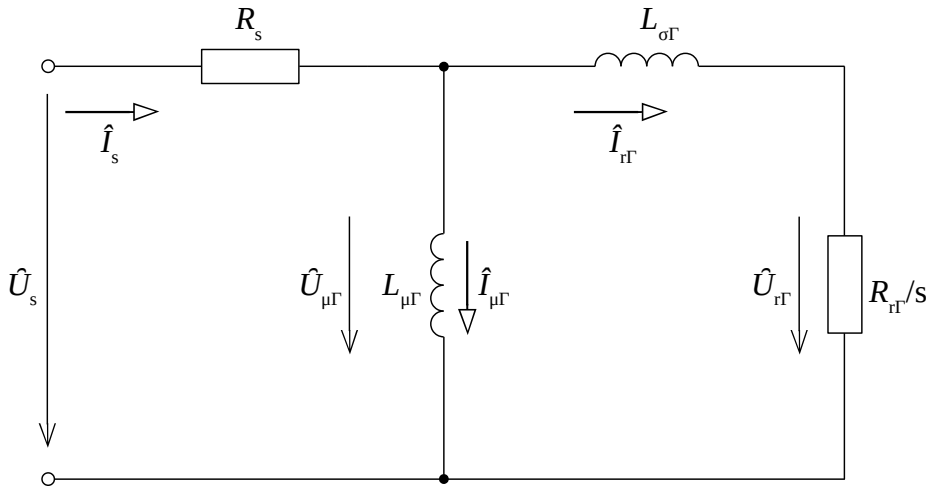

Fig. 13: "Γ"equivalent circuit an induction machine.

The backward calculation is more tricky as it could have an infinite number of solutions as it transforms four parameters into five. For a unique solution, one parameter need to be chosen, which is often the stator leakage inductance $L_{\sigma s}$ of the T equivalent circuit. Then the other parameters will be according to (36):

$$\begin{aligned} L_m &= L_{\mu\Gamma} - L_{\sigma s} \\ L_{\sigma r} &= \frac{L_{\sigma\Gamma}\left(L_{\mu\Gamma}-L_{\sigma s}\right)^2 - L_{\mu\Gamma} L_{\sigma s}}{L_{\mu\Gamma}^2} \\ R_r &= R_\Gamma \frac{\left(L_{\mu\Gamma}+L_{\sigma s}\right)^2}{L_{\mu\Gamma}^2} \end{aligned} \quad . \tag{36}$$

If the ration between leakage inductances in the T equivalent is one ($L_{\sigma s} = L_{\sigma r}$) then the solution is also unambiguous and the transformation equations can be rewritten as:

$$\begin{aligned} L_m &= \sqrt{\frac{L_{\mu\Gamma}^3}{L_{\sigma\Gamma}+L_{\mu\Gamma}}} \\ L_{\sigma s} = L_{\sigma r} &= L_{\mu\Gamma} - \sqrt{\frac{L_{\mu\Gamma}^3}{L_{\sigma\Gamma}+L_{\mu\Gamma}}} \\ R_r &= R_\Gamma \frac{L_{\mu\Gamma}}{L_{\sigma\Gamma}+L_{\mu\Gamma}} \end{aligned} \quad . \tag{37}$$

Transition from Γ to inverse Γ equivalent circuit is based on following relations:

$$\begin{aligned} L_{\mu I\Gamma} &= \frac{L_{\mu\Gamma}}{L_{\mu\Gamma}+L_{\sigma\Gamma}} \\ L_{\sigma I\Gamma} &= \frac{L_{\sigma\Gamma}L_{\mu\Gamma}}{L_{\mu\Gamma}+L_{\sigma\Gamma}} \\ R_{I\Gamma} &= R_{\Gamma}\frac{L_{\mu\Gamma}^2}{\left(L_{\mu\Gamma}+L_{\sigma\Gamma}\right)^2} \end{aligned} \quad . \tag{38}$$

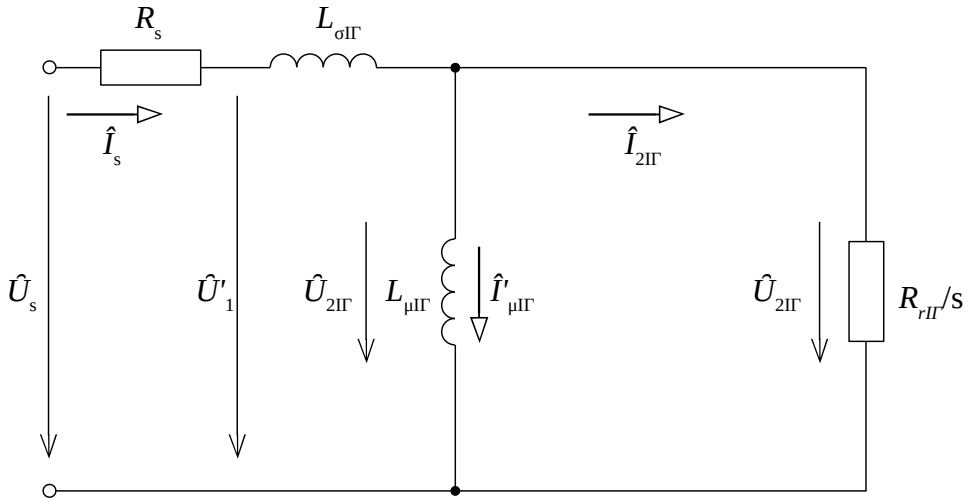

Fig. 14: "Inverse Γ"equivalent circuit an induction machine.

The backwards calculation from inverse Γ to Γ:

$$\begin{aligned} L_{\sigma\Gamma} &= \frac{L_{\sigma I\Gamma}\left(L_{\sigma I\Gamma}+L_{\mu I\Gamma}\right)}{L_{\mu I\Gamma}} \\ L_{\mu\Gamma} &= L_{\sigma I\Gamma}+L_{\mu I\Gamma} \\ R_{r\Gamma} &= R_{rI\Gamma}\frac{\left(L_{\sigma I\Gamma}+L_{\mu I\Gamma}\right)^2}{L_{\mu I\Gamma}^2} \end{aligned} \quad . \tag{39}$$

As the number of parameters is the same in both equivalent circuits, the solution is unambiguous.

Despite the advantages mentioned above, the five parameter T equivalent circuit still remains as a first choice for induction machine description in majority of cases.

4 Parameters of the Induction Machine, Their Changes and Quantities That Influence Them

Previous chapter showed a derivation of a mathematical model of induction machine. Such a model is represented by a set of parameters. However these parameters are not constant in a real world. As by other physical systems, various parasitic effects occurs also in case of induction machine that react to other physical quantities. Various quantities can be thought of such as air humidity but temperature, frequency and saturation are considered as to have the most significant effects to the parameter values [1], [2], [7], [86].

If the error in parameter values are to high, it can lead to decrease of efficiency, or dynamic properties or even total detune of the drive operation, so respecting changes of parameters can improve performance of the drive. Fig. 15 shows the situation of rotor flux oriented FOC if the controller of the drive uses different parameter values than the actual ones in the machine. The rotor flux assumed by the controller (d_{con}, q_{con}) differs from the actual one (d_{act}, q_{act}) which leads to a loss of flux and torque control.

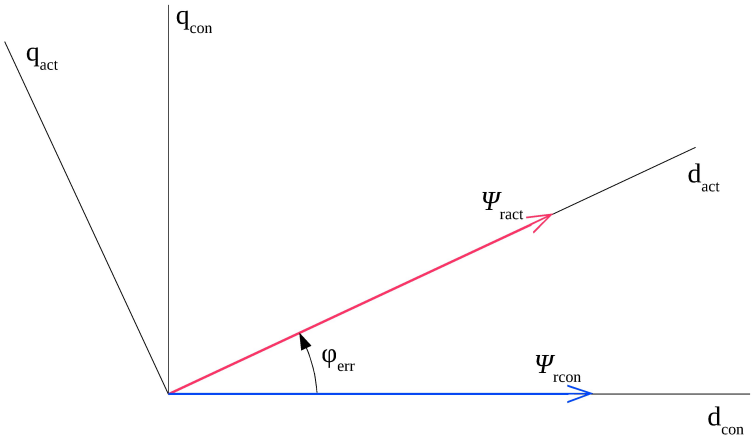

Fig. 15: Difference between actual rotor flux (d_{act}, q_{act}) and rotor flux estimated by controller (d_{con}, q_{con}).

Temperature directly affects the resistance of metal conductors thus the increasing temperature of the machine leads to increase of stator and rotor resistance [1], [2]. Temperature dependence of inductances is not observable under normal operational conditions of the machine [2], because the magnetic properties of the materials are unchanged in this range [87]. Frequency can affect the value of resistances due to skin effect. Stator winding of the machine is usually made out of more parallel branches to prevent skin effect caused by supply frequency. However, skin effect can be observed in rotor cage conductors as they have a larger cross section, despite most control strategies maintain low rotor frequency. As the slip of the machine rises, the rotor frequency rises as well, increasing the value of the rotor resistance [1], [2]. Saturation influences the magnetizing inductance, which is decreasing with the rising magnetic flux (or stator current magnetizing component) [1], [2]. Fluxes of leakage inductances represents mainly the magnetic field that closes

through the air which cannot saturate so their values are considered as stable in most of cases [2]. In following chapters, these dependencies will be described in more detail.

4.1 Influence of Various Quantities on Parameter Values

4.1.1 Inductances and the Influence of Frequency

Frequency influence on impedance of a coil is a well known phenomenon from the theory of electric circuits. However there is an influence of frequency not only to the impedance but directly to the inductance itself mainly due to skin effect. Therefore a construction of a conductor is responsible for inductance behaviour related to frequency. In case of induction machines this applies mainly to the construction of the rotor but it can extent also to the stator winding of the large power machines which has large cross sections of conductors.

In wound rotor the skin effect influence is far smaller than in a squirrel cage rotor bar where similar cross-section constitutes of single massive wire. This is nicely illustrated by authors in [72] where they studied the influence of high frequency switching to inductances of the induction machines. Instead of dealing with the particular inductances, they introduced an equivalent inductance for the whole machine as

$$L_{\mathrm{eq}} = \frac{L'\left(1-\omega_{\mathrm{s}}^2 L' C_{\mathrm{s}}\right) - C_{\mathrm{s}} R'^2}{\left(1-\omega^2 L' C_{\mathrm{s}}\right)^2 + \left(\omega_{\mathrm{s}} C_{\mathrm{s}} R'\right)^2} \,. \tag{40}$$

Assumptions for (40) are that R_{s} and R_{r} can be neglected for higher frequencies compared to voltage drops on inductances. A parasitic capacity C_{s} is connected in parallel to middle branch of the T equivalent circuit. Further L’ in (40) is an equivalent series inductance of a machine defined as

$$L' = L_{\sigma\mathrm{s}} + \frac{L_{\sigma\mathrm{s}} R_{\mathrm{Fe}}^2}{R_{\mathrm{Fe}}^2 + \omega_{\mathrm{s}}^2 L_{\sigma\mathrm{s}}^2} \,, \tag{41}$$

(with simplification, that value of $L_{\sigma\mathrm{r}}$ is almost equal to value of parallel connected L_{m} and $L_{\sigma\mathrm{r}}$: $L_{\sigma\mathrm{r}} \sim L_{\sigma\mathrm{r}} \,||\, L_{\mathrm{m}}$) and R’ is an equivalent series resistance of a machine defined as

$$R' = \frac{\omega_{\mathrm{s}}^2 L_{\sigma\mathrm{r}}^2 R_{\mathrm{Fe}}}{R_{\mathrm{Fe}}^2 + \omega_{\mathrm{s}}^2 L_{\sigma\mathrm{s}}^2} \,. \tag{42}$$

Observed behaviour of inductances in a manner of dependence of this equivalent inductance L_{eq} on stator switching frequency f_{sw} as $L_{\mathrm{eq}} = \mathrm{f}(f_{\mathrm{sw}})$ is presented in Fig. 16 for three different types of induction machines with squirrel cage rotor (different in their rated power which is written by their respective waveforms in the figure) and in Fig. 63 for a machine with wound rotor.

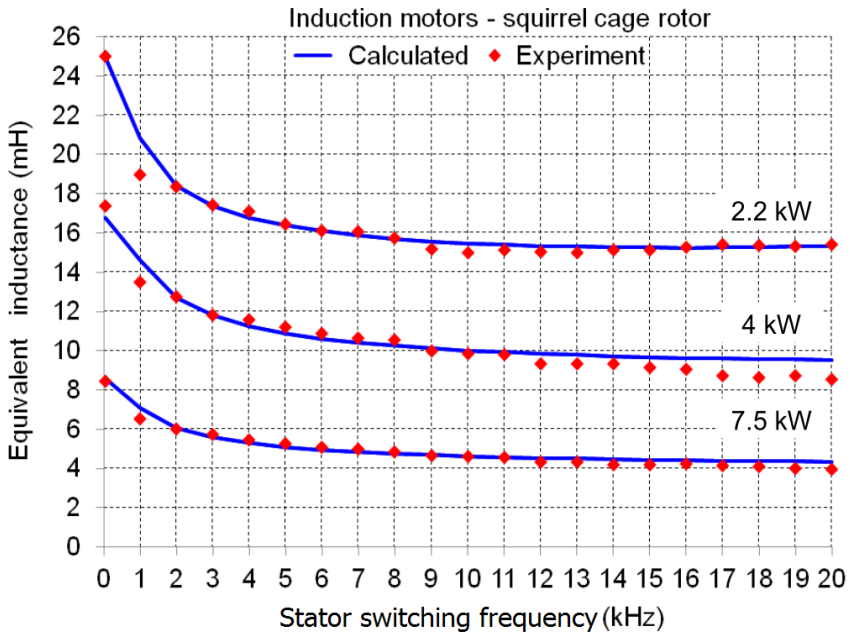

Fig. 16: Equivalent inductance L_{eq} of IM as function of stator switching frequency f_{sw} – squirrel cage rotors [72].

It is clear that the wound rotor has considerable smaller "inductance drop" with switching frequency compared to squirrel cage rotors which is approximately 11 % in case of wound rotor compared to around 40 % drop in case of solid bars.

Another fact that can be pointed out from Fig. 16 is that the behaviour depends also on the particular construction of the machine as the waveforms of squirrel cage motors looks similar but their shape is not the same.

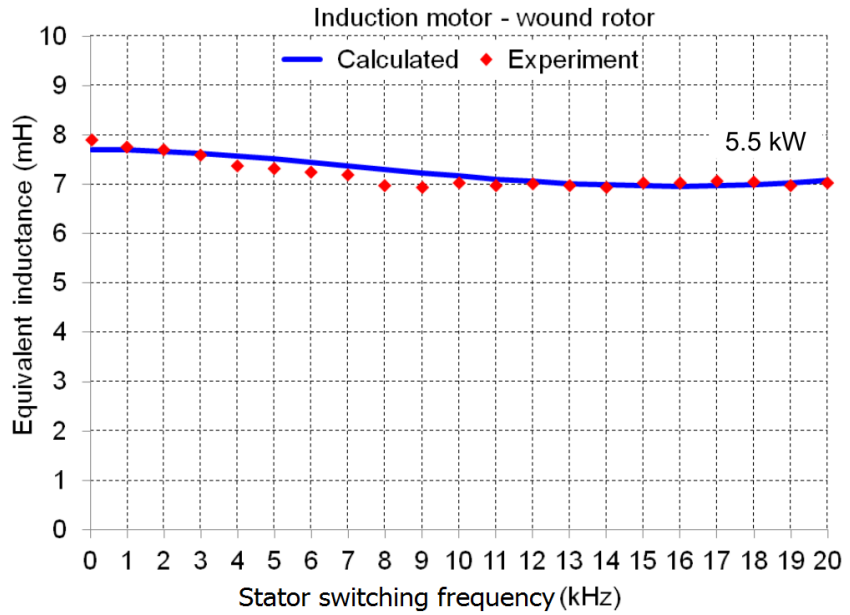

Fig. 17: Equivalent inductance L_{eq} of IM as function of stator switching frequency f_{sw} – wound rotor [72].

Analytic description of the skin effect to inductance of rectangular bar is presented in various publications [7], [9], [72]. [9] defines a coefficient of inductance lowering k_{lskin} as:

$$k_{lskin} = \frac{3 \cdot (\sinh(2 \cdot \zeta) - \sin(2 \cdot \zeta))}{2 \cdot \zeta \cdot (\cosh(2 \cdot \zeta) - \cos(2 \cdot \zeta))} , \tag{43}$$

with ζ according to (44) as

$$\zeta = \alpha_{skin} \cdot h_v , \tag{44}$$

h_v (cm) being height of the rectangular rotor bar. Coefficient α_{skin} is defined according to (45) as

$$\alpha_{skin} = \sqrt{\frac{b_v \cdot f \cdot \gamma}{b_d \cdot 50 \cdot 50}} , \tag{45}$$

with b_v (mm) being width of the bar self and b_d (mm) width of the slot where the bar is placed, f (Hz) is the frequency of the flowing current and γ a conductivity of the bar's material.

Fig. 18 shows a waveform of this k_{lskin} coefficient as a function of ζ, which has a meaning of geometry. Parameters of the bar were set as h_v = 6 cm, b_v = 9 mm, b_d = 10mm and γ = 56,2 S·m·mm^2 for copper. Fig. 19 shows a dependence of k_{lskin} as a function of frequency. From these figures, it is obvious that both construction (geometry) and frequency can have significant effect on the inductances. Usage of this relation is however limited as the real rotor bar cross section usually have different cross section profiles than rectangle as can be seen on Fig. 5, Fig. 6 and Fig. 36.

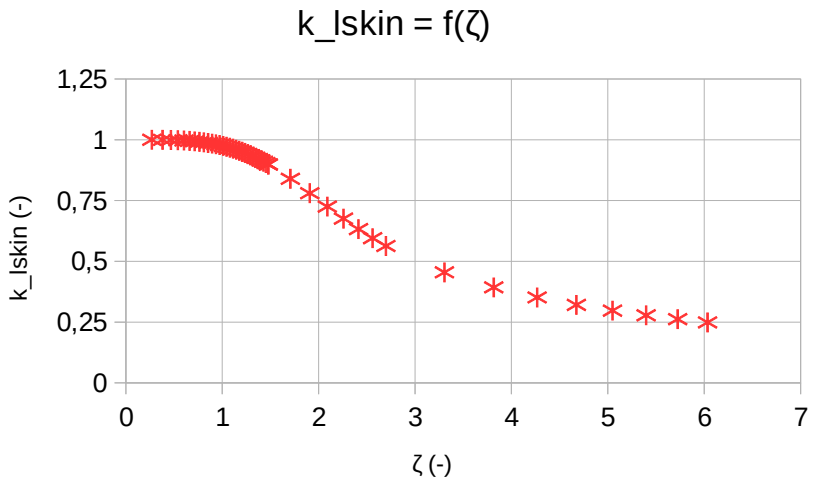

Fig. 18: Inductance lowering coefficient k_{lskin} as a function of ζ.

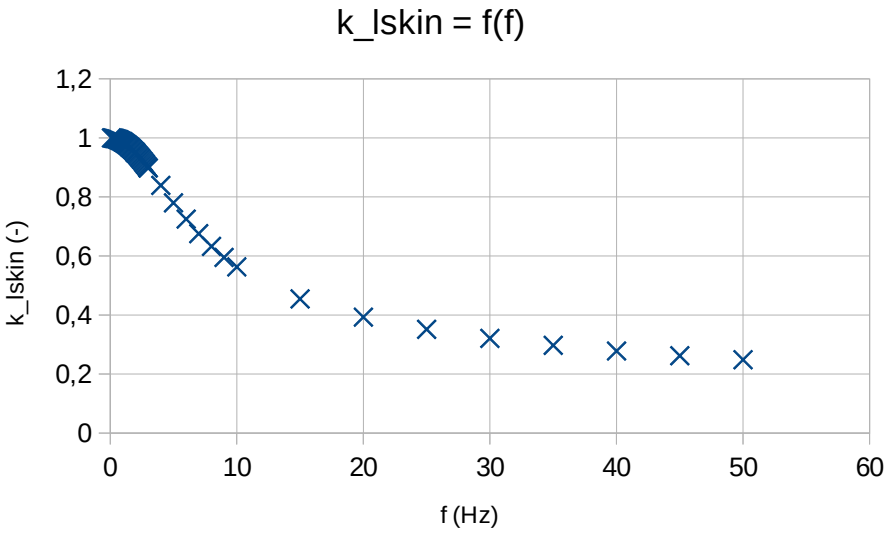

Fig. 19: Inductance lowering coefficient k_{lskin} as a function of frequency f.

The general cause of these phenomena is the skin effect.

4.1.2 Skin Effect

Skin effect is caused by eddy currents opposite to the main current. These eddy currents are induced by the alternating current itself due to its alternating nature. The result is a deformation of a uniform distribution of current density in the cross section of the conductor, pushing the current towards the surface.

Skin effect is generally increasing the effective resistance of the conductor and decreasing part of its inductance. Impedance of the rounded solid conductor can be described as

$$Z = \frac{k_{\mathrm{wn}}\rho}{2\pi\frac{d}{2}} \cdot \frac{J_0\left(k\frac{d}{2}\right)}{J_1\left(k\frac{d}{2}\right)}\ , \tag{46}$$

where J_0 and J_1 are Bessel functions of the first kind of order 0 and 1 respectively, d being the diameter of the wire, ρ being the resistivity of the wire's material, and k_{wn} a constant called wave number defined as:

$$k_{\mathrm{wn}} = \sqrt{\frac{1-\mathrm{j}}{\delta}}\ , \tag{47}$$

where δ is the skin depth defined as:

$$\delta = \sqrt{\frac{2\gamma}{\omega\,\mu_{\mathrm{r}}\,\mu_0}}\ . \tag{48}$$

In (48), γ is the electrical conductivity, ω the angular frequency, μ_{r} the relative magnetic permeability of the conductor and μ_0 the permeability of vacuum.

Sin effect can have an influence to inductance as a part of the inductance of a contactor is given by a magnetic field inside the conductor. This is called internal inductance [88]. This part is thus lowered by lowering the effective conductor's cross section and also the cross section of the magnetic field in the conductor. This happens when the skin depth is no longer large compared to the conductor's size. As this internal inductance is only a small part of the overall inductance and thus the neglecting the influence of frequency to inductance in most of cases [2].

The influence to resistances is more significant as the resistance of conductor depends on its cross section surface as shown in (49):

$$R = \rho \frac{l}{S} , \tag{49}$$

where l is the length of the conductor, ρ resistivity of the conductor's material and S surface of the cross section of the conductor. Therefore, with lowering the effective cross section by skin effect, the resistance increases.

A coefficient of resistance increase k_{rskin} is defined by [9] as:

$$k_{rskin} = \zeta \cdot \frac{\sinh(2\cdot\zeta) + \sin(2\cdot\zeta)}{\cosh(2\cdot\zeta) - \cos(2\cdot\zeta)} , \tag{50}$$

where $\zeta = \alpha \cdot h_v$ is the same as in previous chapter 4.1.1 - h_v being height of the rectangular rotor bar and α according to (45). With the same configuration as in case of inductance in chapter 4.1.1 (h_v = 6 cm, b_v = 9 mm, b_d = 10mm and γ = 56,2 S·m·mm^2 for copper), the course of k_{rskin} as a function of frequency is shown in Fig. 20 for a range from 1 to 50 Hz and in Fig. 21 from 0,1 to 3 Hz.

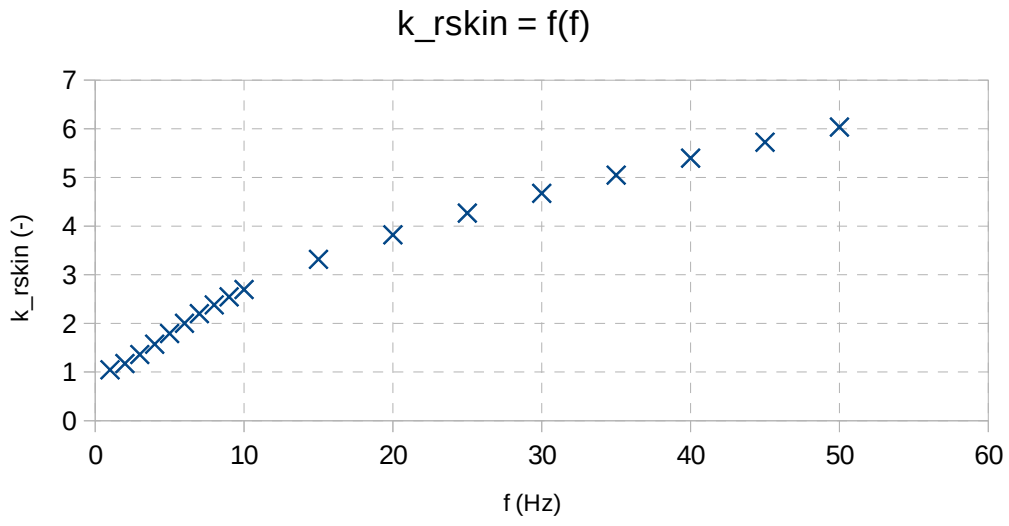

Fig. 20: Coefficient of resistance increase k_{rskin} as a function of frequency 1÷50 Hz.

We can see that the influence can be significant even in range of dozens of hertz and therefore the value of rotor resistance obtained by no-load test (chapter 5.1.2) can be very different from the value during operation with low slip frequency.

Even within the low slip frequency, increase of the rotor resistance can be expected (Fig. 21) which was confirmed by experimental tests presented in chapter 7 e.g. in Fig. 50.

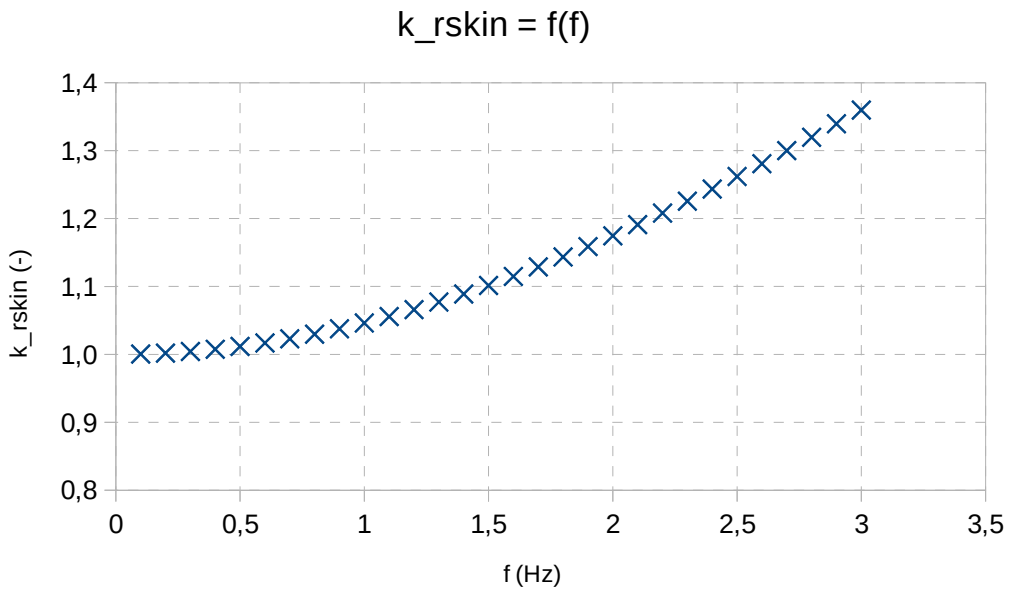

Fig. 21: Coefficient of resistance increase k_{rskin} as a function of frequency 0,1÷3 Hz.

4.1.3 Leakage Inductances

Leakage inductances in the T equivalent circuit of the induction machine (Fig. 11) represent part of the magnetic flux that flows only through particular winding (stator or rotor). The flux that they represent flows mainly through the air and thus the effects of temperature change or saturation are usually negligible or being consciously neglected [2], [43], [89], [90]. However they are related with the winding which itself is sensitive to some phenomena. Therefore the behaviour of the leakage inductances depends also on the construction of the machine. The actual attitude to the leakage inductances depends on application and level of accuracy that is needed [90]. Chapter 4.1.1 showed that when the inductance is associated with a solid wire, the influence of frequency can be significant.

Despite the statement that the changes of leakage inductances are usually neglected, [2] presents a graph where leakage inductance of a four parameter inverse Γ equivalent circuit $L_{\sigma I\Gamma}$ depends on stator current magnitude I_s (Fig. 22).

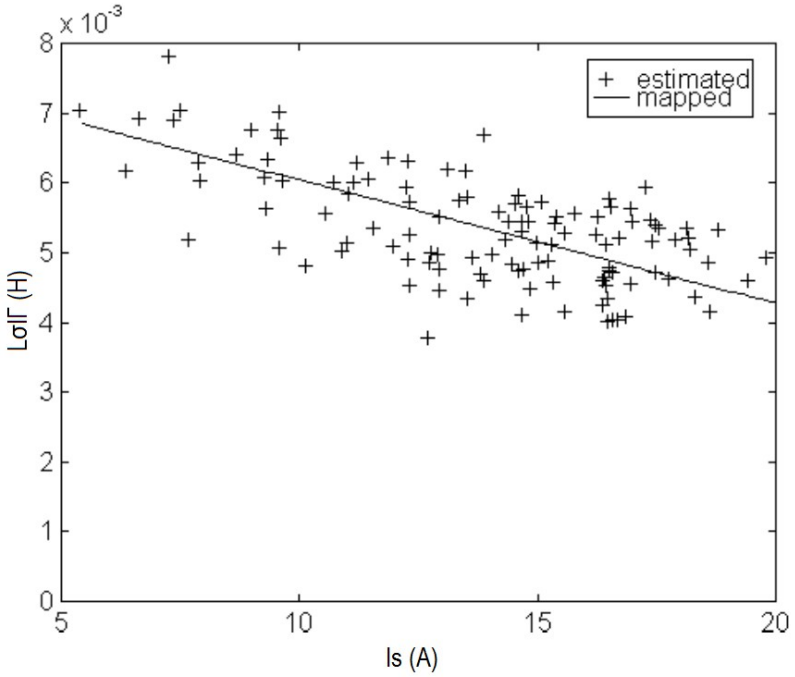

Fig. 22: $L_{\sigma I\Gamma}$ as function stator current magnitude I_s [2].

However, closer details such as geometry or at least some rated values of a tested machine are not provided so closer analysis of this saturation is not possible. As the saturation of leakage inductance is described by some authors [90]–[92], this phenomenon should be addressed to saturation effect. Saturation of leakage inductance paths depends on geometry of the machine i.e. whether slots are closed, open or semi-closed [92] (Fig. 5) as the slot bridges can saturate [79]. Effects of saturation from the main magnetic flux are also reported [90]. None of the authors report influence of temperature to leakage inductance as the magnetic properties of the steel sheets that the machine consist of are unchanged in the whole possible operating temperature range [87].

4.1.4 Rotor Leakage Inductance

Based on the application and level of detail, the rotor leakage inductance can be considered as stable or as variable. Construction of the rotor have a great influence on actual behaviour of the $L_{\sigma r}$, because skin effect is considered to be the main reason of $L_{\sigma r}$ change. In wound rotor the skin effect influence is far smaller than in a squirrel cage rotor bar where similar cross-section constitutes of single solid wire. This fact is supported eg. by results published in [72] which is excerpted by Fig. 16 and Fig. 63 in chapter 4.1.1. [93], [94] concern influence of proximity effect among the rotor bars. Due to normally low operation slip frequency, and distance between the bars, this effect can be neglected.

Effect of higher harmonics transferred to the rotor from stator supply can occur especially when IM is supplied from a converter (which corresponds with findings presented in chapter 4.1.1), but stronger effect is an influence of rotor (slip) frequency or better to say the skin effect

caused by these frequencies. [7] presents an experimentally obtained waveform of dependence of leakage inductance $L_{\sigma r}$ on slip (rotor) frequency f_r of a 160 kW induction machine from a railway traction vehicle, presented in Fig. 23.

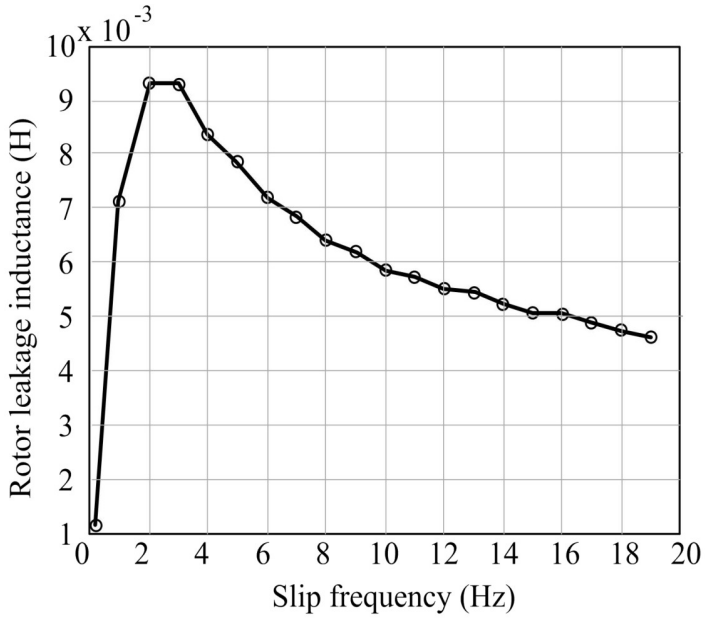

Fig. 23: Rotor leakage inductance $L_{\sigma r}$ as a function of rotor (slip) frequency f_r [7].

Here we can see that higher the slip frequency is, the lower the leakage inductance. This means as well that a value of $L_{\sigma r}$ obtained by conventional methods (laboratory standard tests) can be very different from those that are present during operation of the machine as $L_{\sigma r}$ is obtained from a locked rotor test (chapter 5.1.2) usually conducted by line frequency (50/60 Hz) while during operation the slip frequency is low (units of hertz).

4.1.5 Stator Leakage Inductance

Stator winding of an induction machine is usually conducted out of more strands (filaments) to prevent the skin effect [95]. Smaller machines have the winding wound from an insulated wire. Machines with larger rated powers have also the stator winding from solid rod-like conductors with larger cross-sections to hold the larger current. Even in this case, the winding is carried out at least from units of separated conductors. Particular strands then change their horizontal position throughout the slot [9], [95]. This is called Roebel's permutation [9]. If the cross section of strands does not allow to change the position within the length of the same slot, then the strands are at least switched at the ends of the stator in a way, that they have different position in a next slot [9]. Due to these arrangements, the influence of skin effect is mitigated. These measures mitigate also the proximity effect which can influence also the inductance, as showed in chapter 4.1.8. Effects of saturation can be considered, as described in chapter 4.1.3, but in most cases are not taken into account [2], [89].

4.1.6 Magnetizing Inductance

Magnetizing inductance represents the main part of the magnetic flux in the machine, better to say magnetic flux that flows through both windings. Therefore much of the flux path is inside the steel packets of stator and rotor and therefore can saturate. Magnetizing inductance thus change with magnetic flux. An approximate shape of magnetizing inductance dependency on magnetic flux Ψ_m is depicted in Fig. 24.

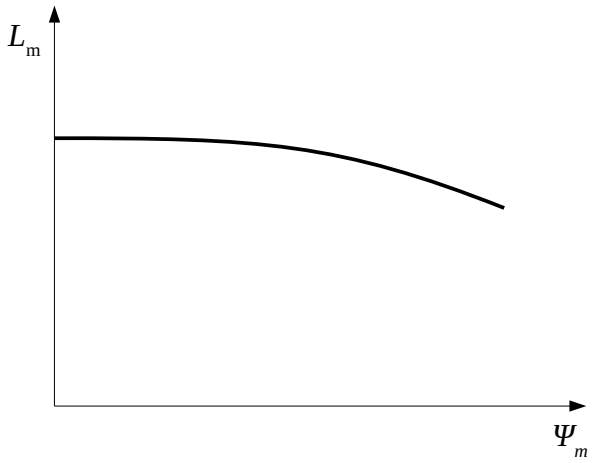

Fig. 24: Magnetizing inductance L_m as a function of flux.

Magnetizing inductance can be defined as

$$L_m = \frac{\Psi_m}{I_m} , \tag{51}$$

where I_m is a magnetizing current. To determine the flux, it is useful to get its value from I_m as $\Psi_m = f(I_m)$. The non-linear course is approximated by some mathematical function e.g. in [7] by polynomial function

$$\Psi_m = f(I_m) = a_0 + a_1 I_m + a_2 I_m^2 , \tag{52}$$

where a quadratic fitting method is selected and a_0, a_1 and a_2 determined from data of the no-load test (chapter 5.1.2) or some other method for obtaining some form of magnetizing curve.

The saturation effects can be seen also on dependence of L_m on I_m which curve is presented e.g. in [7] from data obtained from 160kW induction machine, presented in Fig. 25.

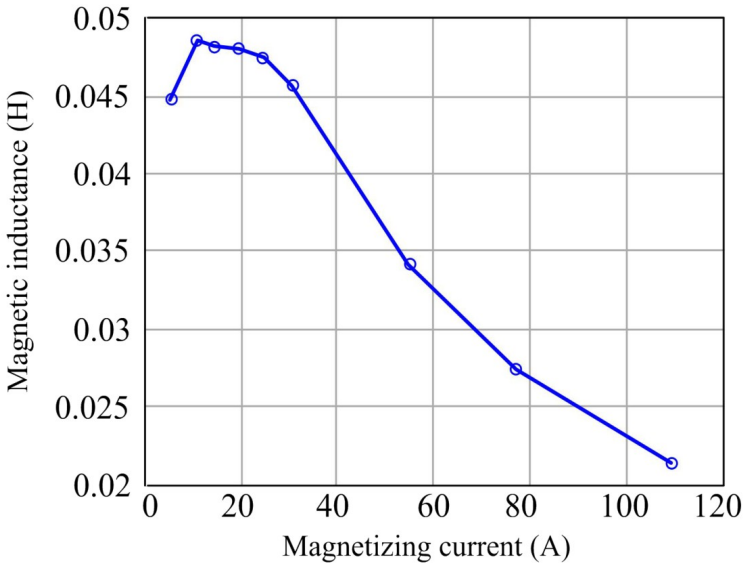

Fig. 25: L_m as a function of I_m [7].

In [2] authors presented that the non-linearity of L_m caused by saturation can be seen also on a course of L_m as a function of stator current magnetizing component I_{sd}. This is depicted in Fig. 26.

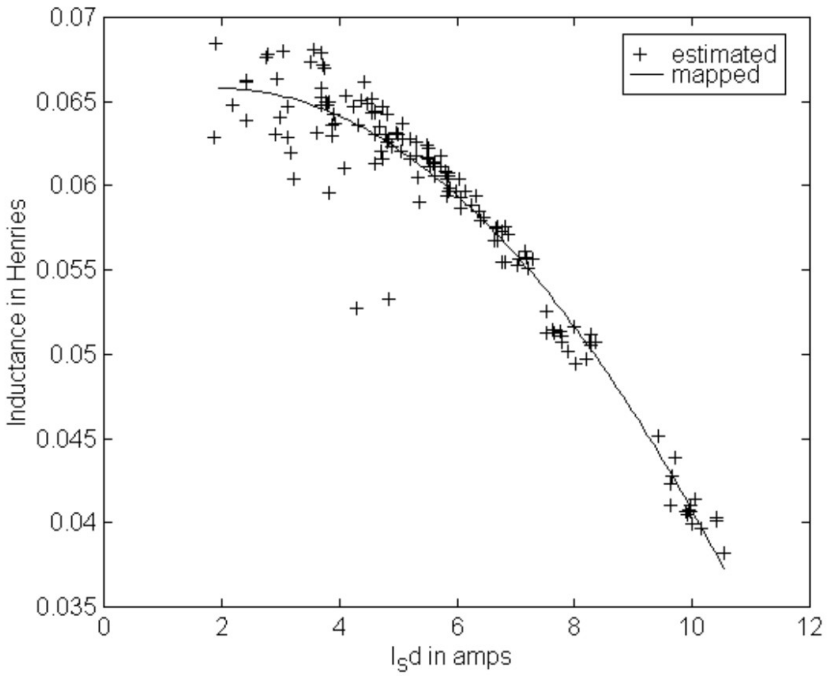

Fig. 26: L_m as a function of stator current component I_{sd} [2].

Both of the dependencies of L_m presented in above mentioned sources can be seen also in the experimental data shown in chapter 7 e.g. in Fig. 49, Fig. 55, Fig. 65 or Fig. 72.

4.1.7 Temperature Influence to Resistances

The most significant quantity that has a cardinal influence on the resistance is the temperature of the conductor. Relation between the temperature and the resistance can be described by a well know equation

$$R_{\vartheta 2} = R_{20}\left(1+\alpha_{20}\left(\vartheta_2-20\right)\right), \tag{53}$$

where $R_{\vartheta 2}$ is the resistance value for the given temperature ϑ_2, ϑ_2 is this given temperature and α_{20} is a the temperature coefficient of resistance measured at 20°C. For recalculating to 20°C, R_{20} has to be expressed by dividing the whole equation with the content of the brackets on the right side.

A more accurate and more general description of the temperature - resistance relation is given by [87], [96]:

$$R_{\vartheta 2} = R_{\vartheta 1}\left(1+\alpha_{\rho 1}\left(\vartheta_2-\vartheta_1\right)+\alpha_{\rho 2}\left(\vartheta_2-\vartheta_1\right)^2\right), \tag{54}$$

where $R_{\vartheta 1}$ is the resistance at an arbitrary base temperature ϑ_1, $\alpha_{\rho 1}$ is a linear temperature coefficient and $\alpha_{\rho 2}$ is a linear temperature coefficient. However, temperature - resistance relation of most metals used in industry under usual operating conditions (e.g. from -40°C to 300°C) is very close to linear behaviour so the omitting of the quadratic constituent of (54) can be done with insignificant influence to the result, so the (53) is commonly used in praxis [7].

Another formula for recalculating the resistance between two temperatures (and more general one) is [7], [97]:

$$R_{\vartheta 2} = R_{\vartheta 1}.\frac{\tau_t+\vartheta_2}{\tau_t+\vartheta_1}\ , \tag{55}$$

where τ_t is a temperature coefficient given by

$$\tau_t = \frac{1}{\alpha_{20}} - \vartheta_{20}\ . \tag{56}$$

Equation (55) is in fact derived from (53), but offers the calculation between two arbitrary temperatures. In case of copper, which is nowadays the most common material for both stator and rotor winding of induction machines, its temperature dependence of resistivity is linear from approximately 60 K (-213°C) to its melting point [96], [98], [99] Therefore the temperature coefficient α_{20Cu} can be used in this whole temperature range as a general temperature coefficient α_{Cu} and the relation (53) can be used used then for recalculation of resistance not only to the 20°C (or the temperature at which α is measured) but to any arbitrary temperature in the range mentioned above, as in (57):

$$R_{\vartheta 2} = R_{\vartheta 1}\left(1+\alpha_{20Cu}\left(\vartheta_1-\vartheta_2\right)\right)\ . \tag{57}$$

4.1.8 Stator Resistance

It is clear that there is a significant influence of temperature to stator resistance. Relations describing this phenomenon were presented in chapter 4.1.7. The influence of frequency and saturation on stator resistance is usually not considered [2]. Saturation should not have any influence to resistance as it is connected with magnetic effects and therefore with inductances. However the frequency based phenomena can have some effect based on construction – geometry of particular machine. As mentioned in chapter 4.1.5, the stator winding of an induction machine is usually made with mitigation of skin effect in mind.

In [8], authors conducted a study on frequency influence to stator resistance in case that the stator winding had been made out of solid bar conductors. Shape of the conductors was rectangular as well as the stator slots. Results of this study stated that significant effects occur for stator frequencies higher than 500 Hz and for conductor height from 5 mm.

In [95] authors deal not only with skin effect but with the proximity effect as well. Proximity effect is in brief a change of current distribution in a conductor due to influence of magnetic fields from other nearby placed conductors. This phenomenon is of course associated eith alternating current, related with induction. Magnetic field from adjacent conductors with the same direction of current induce eddy currents in the conductor itself. This pushes the current density in the conductor itself to the areas farthest from those other conductors. Deforming the current density makes the effective resistance of the conductor to rise. We can think of that the proximity effect is working against the skin effect as it is pushing towards centre of the conductor while the latter pushes the current to the surface. In case of stranded stator winding (made out of multiple turns of thinner conductor) the skin effect is minimized. In case that stator winding is made of smaller number of bars both effects can show depending on how the permutations of position described in chapter 4.1.5 can be carried out. Again the fact that these effects are strongly related with geometry and construction of the machine must be highlighted.

[95] confirms that the skin effect is negligible compared to proximity effect in stranded windings. The study taken a 1250 kW three phase six pole machine with squirrel cage rotor. Stator winding was two-layer, in 72 open slots 14 mm wide and 80 mm deep with 9 rectangular bars in layer of winding. Together there were 18 bars in a slot with the bar dimensions h_v = 3,3 mm being height and b_v = 10,6 mm being the conductor width. The authors tried a simulation when the bars were not permuted (same position of the bars in the slot and also the same position in each slot in the same pole) and got the results that at 50 Hz the resistance increased by 34% compared to its DC value, and at 2 kHz by a factor of 300. Fig. 27 shows the dependence of the stator current and inductance of the stator winding compared to their DC values on a ratio of bar height h_v to skin depth δ.

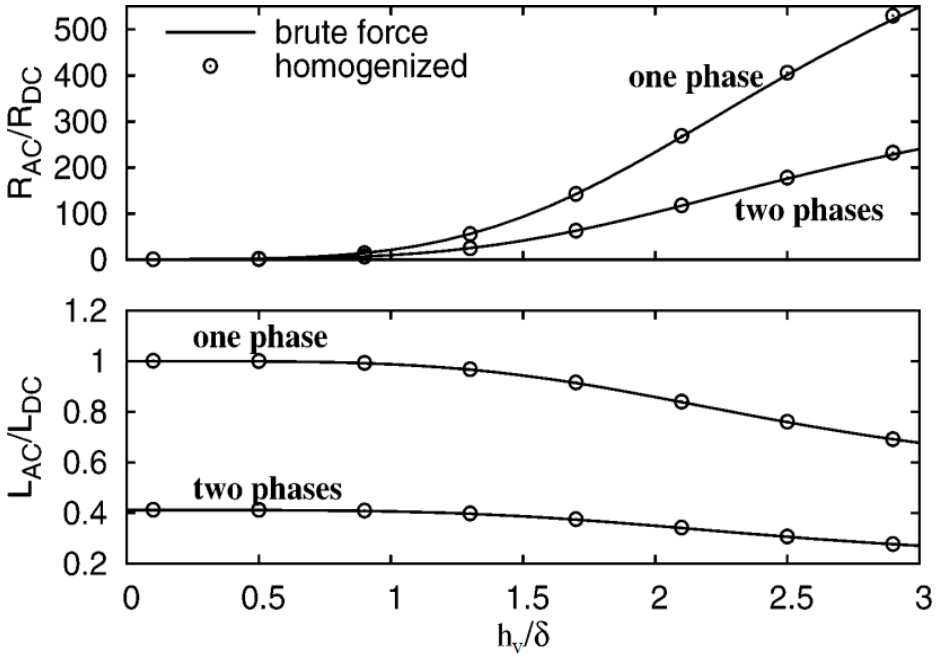

Fig. 27: Proximity effect influence on inductance and resistance in stator winding [95].

The data in Fig. 27 were obtained by means of FEM. Brute force are the direct FEM results while the homogenized points are analytically optimised. The waveform designated as one phase belongs to case when the two groups of conductors in a slot belong to the same phase. Two phase waveform means that each group belonged to a different phase, thus the current was 120° shifted between the phases. It is seen that even this measure has a significant contribution to lowering the proximity effect. Other significant result of [95] is that when the skin effect counter measures (described above or in chapter 4.1.5) are applied, the proximity effect can be neglected for lower frequencies. However with the rising switching frequencies in inverter fed drives, this phenomenon can become more significant.

4.1.9 Rotor Resistance

As described in chapter 4.1.7, temperature has a significant influence to resistance of metals so to the rotor resistance as well. Material of rotor winding can be copper or aluminium in case of squirrel cage rotors. Copper is however preferred also for squirrel cage rotors due to lower resistivity which can contribute to higher overall efficiency of the machine. Somehow exotic materials such as bronze or brass for specific applications are also cited [9].

Another significant phenomenon is the influence of skin effect which shows up in squirrel cage rotors. This is described in chapter 4.1.2. In wound rotors, skin effect is mitigated but the proximity effect could occur. However, similarly to stator winding, the counter measures against skin effect (chapter 4.1.8) work in similar principle as in case of stator winding also against proximity effect.

In [7] authors present an experimentally obtained waveform of rotor resistance increase due to rising slip (rotor) frequency f_r of a 160 kW induction machine from a railway traction vehicle, presented in Fig. 28.

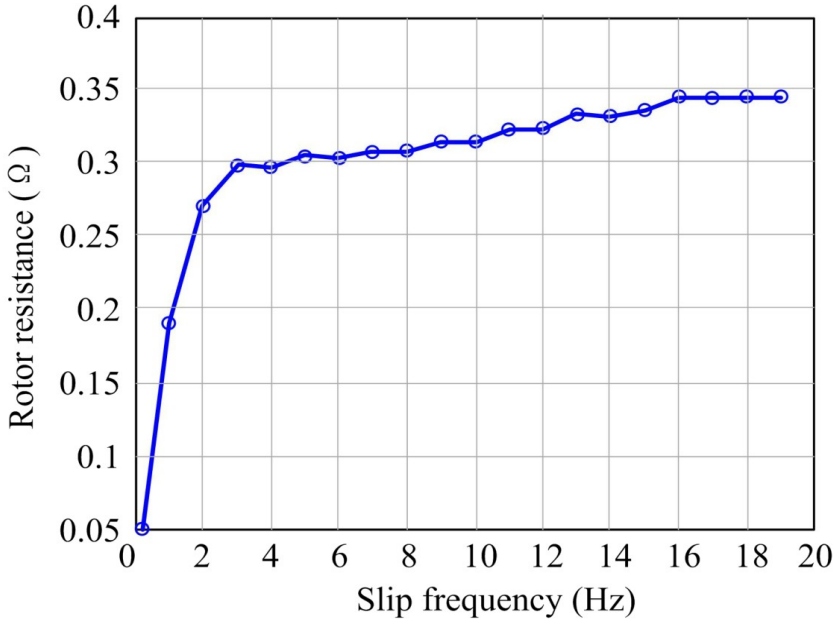

Fig. 28: Rotor resistance R_r as a function of rotor (slip) frequency f_r [7].

We can see a sharp increase in range under 2,5 Hz. Behaviour of rotor resistance in case of particular machine however depends on geometry of the bars (and slots). Rising of the rotor resistance with the rising rotor frequency can be seen also in experimental results presented in chapter 7, e.g. Fig. 50 or Fig. 64. This behaviour is also confirmed by other publications, e.g. [2], [9], [84], [100].

4.2 Behaviour of Machine Under Changed Parameters

Main quantity that is usually demanded from an electromechanical converter, the induction machine not being an exception, is the torque. Torque in the air gap of an induction machine M_δ can be described (with the designation from T equivalent circuit - Fig. 11) as:

$$M_\delta = k_M \left(\hat{\Psi}_m \otimes \hat{I}_r \right) = \frac{3 R_r}{\omega_r} \cdot \left[\frac{U_i^2}{\omega_s^2} \cdot \frac{1}{\left(\frac{R_r}{\omega_r} \right)^2 + L_{\sigma r}^2} \right] . \tag{58}$$

Here we can see that the rising value of R_r decreases the torque of the machine if other values are constant.

As an example, how the change of parameters that is not detected in the controller, can influence a control strategy, IFOC has been chosen as it is widely used for its simplicity and effectiveness [68], [101]. The main idea behind FOC is to control an induction machine similarly as a DC machine with separate control of flux and torque current (field and armature winding in case of DC machine). As mentioned in chapter 3.3 an inverse Γ equivalent circuit (Fig. 14) is often used for representation of its principle. Current $\hat{I}_{2\Gamma}$ which flows through the resistance $R_{r\Gamma}$ represents a torque producing component of the total stator current while $\hat{I}_{\mu\Gamma}$ a magnetizing one. It should

be noted that these currents correspond with stator current components Isd, Isq. The designation here is used to correspond with the marking used in inverse Γ equivalent circuit in Fig. 14. Fig. 29 shows, how the current is decomposed into respective components.

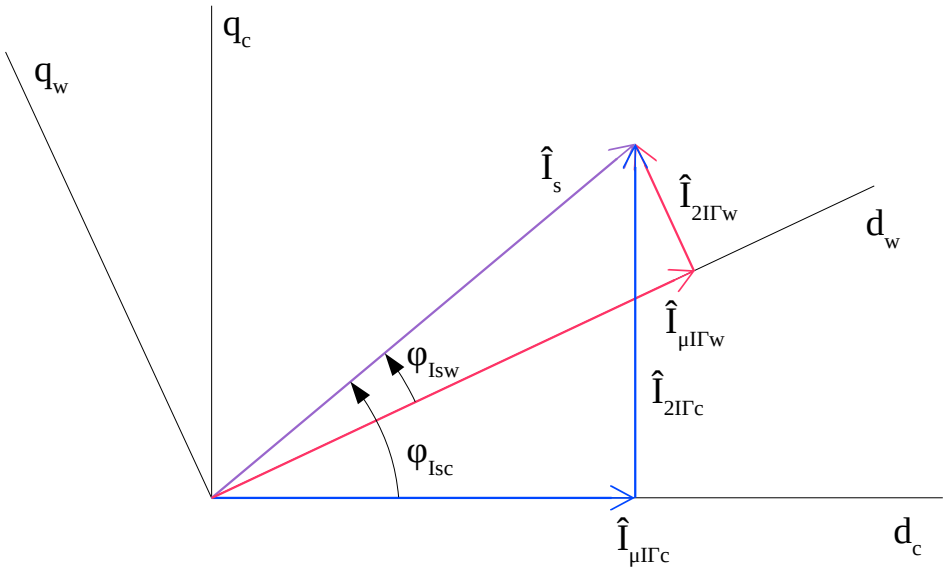

Fig. 29: Vector diagram of current decomposition for cold and warm rotor winding resistance.

It further illustrates the situation when the real rotor winding is warm and therefore its real resistance $R_{rI\Gamma} = R_{rI\Gamma w}$ (index "*w*" for warm), but the controller still operates with value $R_{rI\Gamma} = R_{rI\Gamma c}$ (index "c" for cold). Controller thus determines the position of the axis d_c (cold) and decomposes the stator current vector $\hat{I}_s$ into components – $\hat{I}_{\mu I\Gamma c}$ and $\hat{I}_{2I\Gamma c}$ (cold). However the real position of the axis d is d_w (warm). Therefore real components of the vector $\hat{I}_s$ are $\hat{I}_{\mu I\Gamma w}$ and $\hat{I}_{2I\Gamma w}$ (warm). Fig. 29 shows that not only angles but also magnitudes of decomposed vectors are different. Magnetic flux controller stabilizes the magnetic flux of the machine based on the component $\hat{I}_{\mu I\Gamma c}$ but the real magnetic flux is higher. Therefore a motor magnetic circuit can be saturated. Based on wrong position of of the decomposed currents magnetic flux position will be also wrong.

The angle φ_I can be calculated for general case from

$$tg(\varphi_I) = \frac{\hat{I}_{2I\Gamma}}{\hat{I}_{\mu I\Gamma}} = \frac{\frac{\hat{U}_{2I\Gamma}}{R_{rI\Gamma}/s}}{\frac{\hat{U}_{2I\Gamma}}{\omega_s L_{\mu I\Gamma}}} = \frac{\omega_s L_{\mu I\Gamma}}{R_{rI\Gamma}/s} = \frac{\frac{\omega_s L_{\mu I\Gamma}}{R_{rI\Gamma}}}{\frac{\omega_s - \omega_m}{\omega_s}} = \frac{(\omega_s - \omega_m) L_{\mu I\Gamma}}{R_{rI\Gamma}} = \frac{\omega_r L_{\mu I\Gamma}}{R_{rI\Gamma}} \cdot \quad (59)$$

This equation confirms what is evident from inverse Γ equivalent circuit in Fig. 14 - that the particular current components depend on values of magnetizing inductance and rotor resistance. Therefore it is seen that temperature change or frequency circumstances can influence the angle through resistance and saturation circumstances through inductance. This transfers also into T

equivalent scheme to L_m and R_r which are though considered as key parameters for IFOC [102], [103]. Ratio between L_m and R_r is called a rotor time constant τ_r:

$$\tau_r = \frac{L_m}{R_r} \cdot \tag{60}$$

4.2.1 Influence of the Rotor Winding Temperature on the Magnetic Flux Amplitude

For rotor magnetic flux amplitude following equation can be stated

$$\left|\hat{\Psi}_r\right| = \frac{R_r \cdot \left|\hat{I}_s\right|}{\sqrt{\frac{R_r}{L_\mu} + \omega_r^2}} \cdot \tag{61}$$

Based on this relation, influence of rotor resistance (and thus temperature), can be described.

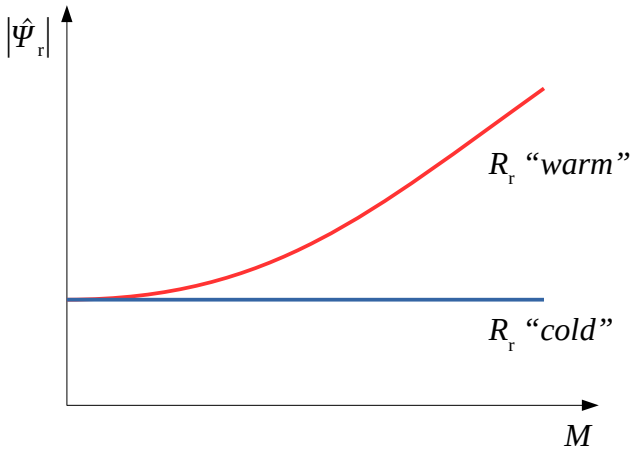

Fig. 30: Rotor magnetic flux as a function of torque.

Fig. 30 illustrates the influence of the rotor resistance value R_r on the value of rotor magnetic flux amplitude $\left|\hat{\Psi}_r\right|$. For the "cold" rotor resistance R_r (blue line) and for the corresponding values of the rotor angular speed ω_r as the function of the motor mechanical torque the $\left|\hat{\Psi}_r\right|$ is constant and has the rated value.

Red line in Fig. 30 represent higher "warm" rotor resistance R_r for the same values of rotor angular speed ω_r. The rotor flux increases in this case with the torque of the machine.

4.2.2 Verification by Simulation

To compare the behaviour of the motor and its model in cold and warm state, two identical models were created in the Matlab – Simulink environment, one for the "cold" motor, and one for the "warm" state. Focus has been taken on evaluating of the change of the rotor resistance, so all inputs of the rotor resistance were equipped with a gain block to adjust its value. For the test, the rotor resistance of the warm motor is set two times higher than in a cold state, which corresponds

to change of temperature e.g. from -25°C to 185°C. Such a temperature range can be seen as extreme at a first glance, but it can be real in conditions of railway traction drives in arctic regions: from cold start in winter to temperatures during heavy hauling operations. It should be noted that for example Class 180 / H allows the maximum temperature winding of 200°C [104]. Induction motor parameters were set as for 1AY112L6, the 3,5 kW rated power machine used also in experimental verification of the method (its parameters are stated in chapter 7.2).

Simulation started as free running – load torque to be set to M_{load} = 0 Nm. At simulation time t = 3 s, step change in load torque has been performed and the load torque was set to M_{load} = 15 Nm (half of the machine rated torque) which results into the first step change of quantities depicted in Fig. 31 and Fig. 32. After the second step change (simulation time t = 6 s), the load torque was set to M_{load} = 30 Nm (full machine rated torque) which results in the second step of the quantities.

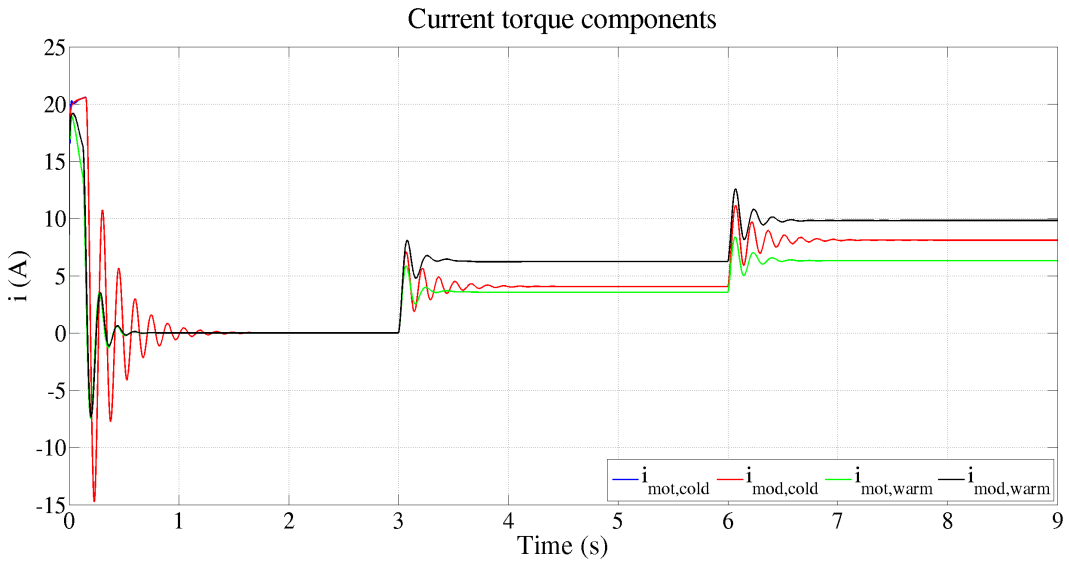

Fig. 31: Current torque components from the simulation of a warmed machine.

Fig. 31 shows the torque components of stator current, namely the stator current torque component of the machine (designation $i_{mot,cold}$) and its model ($i_{mod,cold}$) in a "cold" state and the stator current torque component of the machine (marked $i_{mot,warm}$) and its model ($i_{mod,warm}$) in a "warm" state. The waveform of $i_{mot,cold}$ (blue waveform) is not visible, because it is covered by the waveform of $i_{mod,cold}$ (red waveform), which it exactly copies. It is the result of the fact that motor and its model are in absolute conformity.

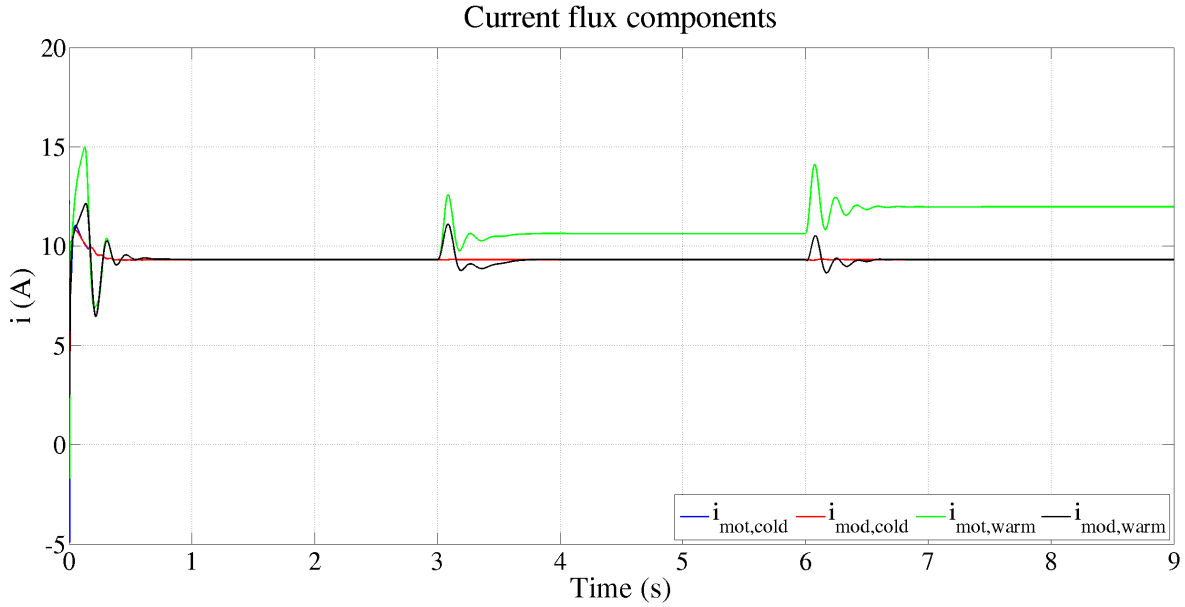

Fig. 32: Current flux components from the simulation of a warmed machine.

In Fig. 32 the flux components of stator current are shown, namely the stator current flux component of the machine (marked $i_{mot,cold}$) and its model ($i_{mod,cold}$) in a cold state and the stator current flux component of the motor (marked $i_{mot,warm}$) and its model ($i_{mod,warm}$) in a warm state. The waveform of $i_{mot,cold}$ (blue) is again completely covered with $i_{mot,cold}$ (red) as the motor and its model are in conformity.

Simulation confirms theoretical assumptions about the influence of the change of the rotor resistance on the control performance of the motor. In a “cold” state, model assumes the same value of the rotor resistance as it really is in the real machine. When the machine warms up, the real value of the rotor resistance increases, but the model computes still with the value of the “cold” state. “Warm” machine increases field excitation, which is evident in the increase of the stator current flux component, but the model does not assume this, because of incorrect value of the rotor resistance. In the real machine the torque component of the stator current decreases, but the model assumes its increase.

In a “cold” state, values of the stator current components of a real IM and its model are in conformity. But in the “warm” state, components computed by the model are different from those in a real motor. This difference is bigger with a higher load torque. This difference causes that the field oriented control cannot behave optimally.

To sum up, magnetizing inductance L_m and rotor resistance R_r are the two parameters to be considered as most important for monitoring to obtain correct parameters for proper operation of field oriented control of an induction machine [1], [13], [30], [31].

5 Overview of the Methods for Parameter Identification of Induction Machines

To operate modern control strategies of the induction machine, certain parameters of the machine need to be known before start of the operation of the drive. These can be obtained either in a non-experimental way from the producer or by searching in other information sources. In fact, manufacturers normally do not provide these parameters. It should be mentioned, that parameters of the same type of the machine can vary up to 10-15 % from the manufacturing process [105], [106], so even if the manufacturer provided these data, it would imply that every single unit would need to be tested. (It is not necessary to add that this would result in a cost increase which a lot of customers would not be willing to pay for). The same problem would arise even if parameters for the machine type were be found in other sources.

Because of those facts, only experimental methods are viable in most of cases. These can be divided into following groups [1], [5], [105], [107], [108]:

- ***conventional methods*** (no-load, locked rotor and conventional DC test), also called *standard tests* or *laboratory standard tests* – mostly laboratory based methods due to usage of sinusoidal voltage sources or special-purpose jigs. These methods are useful for the verification of new technologies. Modifications of these methods with drive converters could in some cases be used also for commissioning of the drives so these would be classified rather as on-site off-line method, as follows:
- ***on-site methods*** – suitable for obtaining machine parameters in the place of installation of the drive. These can be further divided into off-line and on-line:
  - ***off-line parameter identification methods*** – methods used for obtaining parameters during initialization of the drive or before start after shut down.. These can be further divided into subcategories based on the conditions of the drive commissioning:
    - ***self-commissioning methods*** – methods suitable for self-commissioning should be able to gather the required machine parameters at standstill as the load may be already coupled to a load. These methods can be used for observing parameters after shut down of the drive.
    - ***commissioning methods*** – the main difference from the previously mentioned methods is that the machine is allowed to rotate. In this category, modifications of conventional methods carried out with an inverter can be found as well.
  - ***on-line parameter identification methods*** – methods used for identification of parameters during the operation of the drive ensuring that the controller respects parameter changes.

Some authors use different classification e.g. [10], [41], [84], using the term *on-line* for all on-site methods and from this group putting aside a category called *Monitoring at standstill* which is similar to *methods suitable for self-commisioning* while having no overall term for methods used

during the machine operation. The authors in [2] use term *off site methods* for all testing that take place outside of the place of installation. As a most common procedure of this group it mentions *conventional methods* (no-load and locked rotor tests). Then it distinguishes a group called *on site and off line methods* for all the methods carried out on the place of installation and a third group called *on-line* methods. In general and based on the examples mentioned above it can be said, that all of the authors generally follow the basic idea of distinguishing between methods suitable for parameter identification before the drive is put into the operation, and during the operation. In this work, the above described classification will be maintained.

Methods classified as off-line serves, as mentioned above, for ensuring the basic knowledge of the machine parameters. For the best performance of a drive, changes of parameters should be respected and because of this, greater effort of the research is focused on on-line methods.

In following chapters, the presented categories of the parameter identification methods of induction machines will be described. As the research in this field is very broad, an overwhelming number of methods have been developed and published so far. Therefore, only a few representative methods will be presented in each category. For completeness not only on-line methods, which are core of this work, but conventional methods as well as off-line methods overview is presented. Both of these groups are connected to on-line methods as they are de facto their prerequisities.

5.1 Conventional Methods

Conventional methods, also known as Standard tests, [1]–[3], [42], [109] are carried out when laboratory equipment is available. Definition of its procedure and way of evaluation of its results are given in standards e.g IEEE Standard Test Procedure for Polyphase Induction Motors and Generators [3], NEMA MG-1: Motors and Generators [110], or the IEC/EN 60034-2-1 [4]. These tests are normally performed with a sinusoidal voltage source (e.g. grid or rotational generator). If the inverter is used for these tests, parameters obtained this way should conform to those from the test with sinusoidal supply if the calculation is made for the fundamental components of the inverter supply [111].

5.1.1 Conventional DC Test

Under the term *DC test* we understand measurement of the stator resistance. Since this value is usually very small (units of Ohms or less) the 4-wire measurement should be used. The tested motor is connected to an adjustable DC supply which enables to set the stator current to be approximately 10% of the machine's rated value I_{sn} (RMS value). Stator current and voltage at motor terminals are measured and evaluated by Ohm's law. All three phases should be measured and an average from these three values should be taken as the final value. An equivalent circuit is defined for phase values of quantities so if the motor terminals do not allow access to both ends of individual phases (which means that the phases are already internally star or delta connected), the resistance has to be recalculated to phase values. Measurements should be carried out for all three terminal combinations as in the previous case (i.e. if terminals were be marked *a, b* and *c* then it means combinations *a*-*b*, *a*-*c* and *b*-*c*) and an average value should be taken as the final one. If the

resulting average value of resistance between the terminals is $R_{SDCtmeas}$ then the stator resistance phase value R_s will be:

for star (wye) connection

$$R_s = \frac{R_{SDCtmeas}}{2} \tag{62}$$

and for delta connection

$$R_s = \frac{3\,R_{SDCtmeas}}{2} \tag{63}$$

Accuracy of this measurement can be increased by repeating it at least twice.

The evaluation of this measurement is not complete if temperature dependence of resistance is not taken into consideration. Unless the tested motor is equipped with a temperature sensor inside the stator winding, it is not possible to measure the temperature of the winding itself. For this reason, the DC test should be carried out as the first one or the motor should be left disconnected for several hours so it can be stated, that the temperature of the whole mass of the motor is the same as the ambient temperature which is measured easily. Usually, the resistance is recalculated for the temperature of 20°C according to the (53).

5.1.2 No-load Test

The *no-load test* (in some sources called also *running-light test*) is carried out with the motor running freely while being supplied from a three phase AC source with a variable voltage and a constant frequency. As there is no load connected to the motor, the rotor can rotate at almost synchronous speed. Without any substantial loss of accuracy the rotor current $\hat{I}_r$ can be then assumed to be equal to zero and thus the whole right branch of the equivalent scheme can be neglected (Fig. 33).

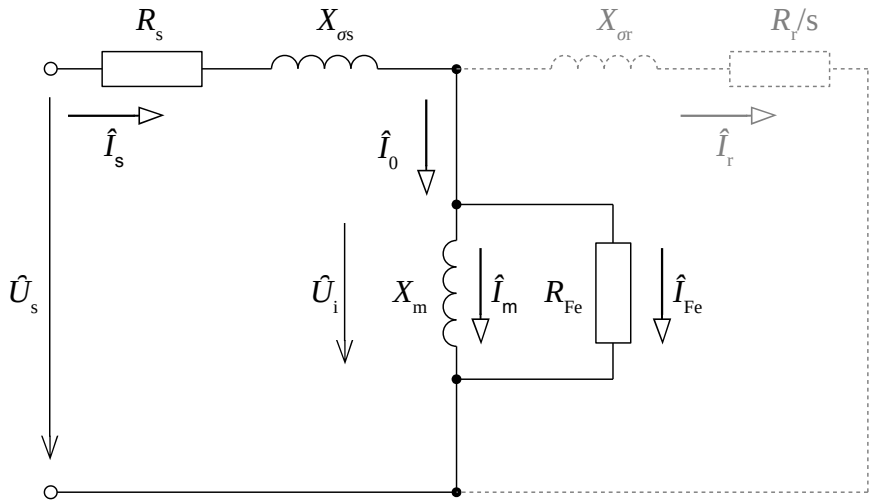

Fig. 33: Equivalent circuit of the machine by no-load test.

This test usually follows the DC test, so the initial temperature of the motor can be assumed to be the same. At the beginning the supply voltage is set to 120% of the machine's rated value U_{sn} which is the first point of the measurement. Measured quantities are stator voltage U_{s0}, phase value of stator current I_{s0}, and input power P_{I0}. Following this first point, the voltage is decreased in steps to 25% of U_{sn}. After each change of the voltage, the monitored quantities should be measured after they stabilize themselves.

If we subtract the copper losses P_{Cu} defined as

$$P_{\mathrm{Cu}} = 3\, R_{\mathrm{s}} I_{\mathrm{s}0}^2 \tag{64}$$

from input power P_{I0} we get a sum of mechanical losses P_{mech} and iron losses P_{Fe}. If we extrapolate the dependence of this sum on the voltage U_{s0} to the zero voltage ($U_{s0} = 0$), we can separate mechanical losses from this sum because in this theoretical point, no current would flow through the circuit and thus there would be no iron losses. The mechanical losses are given by sum of friction losses P_{fric} and ventilation losses P_{vent}. If the machine has a separate cooling, which is usually the case of high powered machines, P_{mech} consists of P_{fric} only.

Quantities P_{I0} and I_{s0} for calculations are taken from the point where $U_{s0} = U_{sn}$. Phase values have to be used at applicable places in the equations, since the equivalent scheme is defined as a one phase. Then, we can obtain following parameters and quantities of the scheme:

- sum of $X_{\sigma s}$ and X_{m}
- U_{i} $\left(U_{\mathrm{i}} = \left|\hat{U}_{\mathrm{i}}\right|\right)$
- R_{Fe}

according to following equations:

$$Z_{\mathrm{s}0} = \frac{U_{\mathrm{sn}}}{I_{\mathrm{s}0}} = \sqrt{R_{\mathrm{s}}^2 + \left(X_{\mathrm{s}\sigma} + X_{\mathrm{m}}\right)^2} \tag{65}$$

$$U_{\mathrm{i}} = U_{\mathrm{sn}} - R_{\mathrm{s}} I_{\mathrm{s}0} \tag{66}$$

$$R_{\mathrm{Fe}} = \frac{3\, U_{\mathrm{i}}^2}{P_{\mathrm{Fe}}} \tag{67}$$

Sum of $X_{\sigma s}$ and X_{m} can be separated only after values of the locked rotor test are obtained.

In case of high power machines, voltage drop over R_s is often neglected and instead of calculating the value of U_i, U_s is taken directly as the internal voltage U_i.

If this no-load test is repeated at various frequencies, dependency of R_{Fe} and Z_{s0} on frequency and dependency of P_{mech} on speed of the motor can be obtained as well.

Dependency of back EMF (inner voltage) U_i on magnetization current I_m can be used as a characteristics of magnetic circuit of the machine. Influence of saturation compared with linearised part of magnetic curve is shown on Fig. 34.

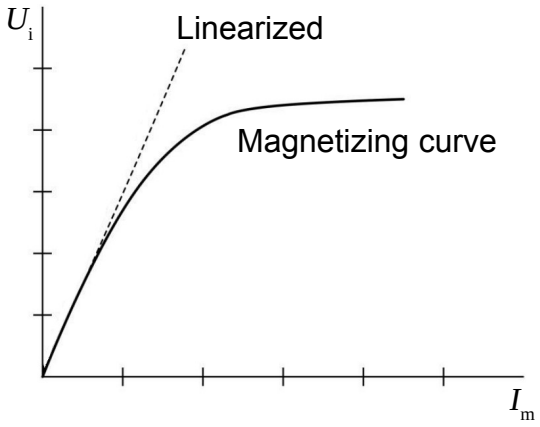

Fig. 34: Magnetizing curve.

This curve can be used also for estimating variation of L_m with I_m using (68):

$$L_m = \frac{U_m}{I_m} \cdot \tag{68}$$

5.1.3 Locked Rotor Test

During the *locked rotor test* (sometimes *blocked rotor test or short circuit test*) rotor of the tested machine is mechanically blocked so it cannot move. The machine is supplied from variable AC supply with a constant frequency during the test. If the rotor is wound, it is short-circuited. While the rotor cannot rotate slip $s = 1$. Impedance of stator – rotor loop is far smaller than the impedance across the middle branch of the equivalent scheme, so the current I_0 can be neglected compared to currents I_s and I_r and thus the whole middle branch can be neglected as well (Fig. 35).

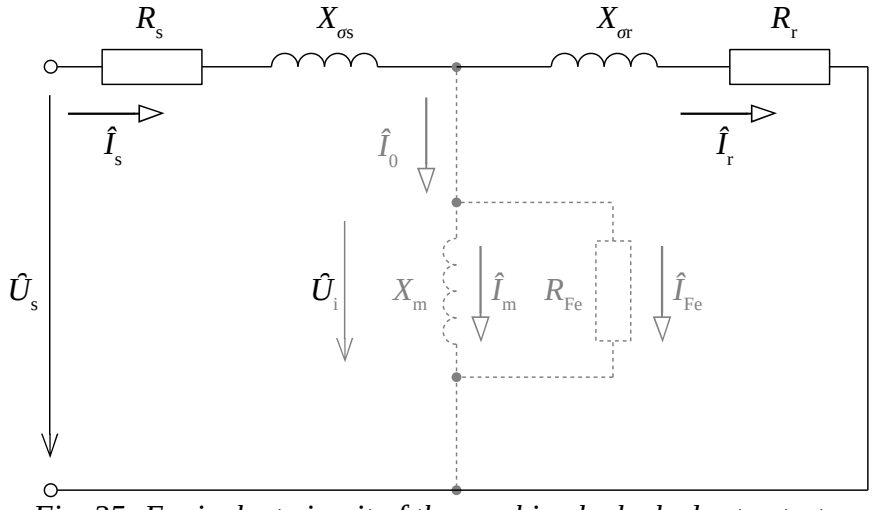

Fig. 35: Equivalent circuit of the machine by locked rotor test.

After commencing the test, voltage is increased until the current flowing through the machine reaches 120% of its rated value I_{sn}. Voltage is comparatively low as the impedance in this mode is small. Voltage is then lowered step-by-step until zero while stator voltage, stator current and input

power are measured. This procedure should ensure that the temperature is more or less constant during the whole test.

At the point where stator current is equal to the rated value ($|\hat{I}_s| = I_{sn}$), the input power P_{Ibr}, the phase value of the stator current I_{sbr} and the phase value of the stator voltage U_{sbr} are read. According to Fig. 35, impedance of this equivalent scheme can be calculated as

$$Z_{br} = \frac{U_{sbr}}{I_{sbr}} = \sqrt{(R_s + R'_r)^2 + (X_{s\sigma} + X'_{r\sigma})^2} \tag{69}$$

The real part of this impedance (R_{br}) can be calculated as

$$R_{br} = R_s + R'_r = Z_{br} \cos\varphi_{br} \tag{70}$$

where

$$\cos\varphi_{br} = \frac{P_{Ibr}}{3 U_{sbr} I_{sbr}} \tag{71}$$

From the R_{br} we can get R'_r , the rotor resistance referred to the stator, by subtracting the stator resistance value, which has already been obtained by the DC test.

Again, the temperature dependence of the resistance should be taken into account, so if the motor is not equipped with a temperature sensor, the actual value of the stator resistance should be measured right after the end of the test with the aim of temperature estimation. Temperature of the stator and the rotor is assumed to be same. Both resistances should be then recalculated to the same temperature.

A more complicated issue arises with the sum of stator and rotor leakage reactances $X_{\sigma s}$ and $X_{\sigma r}$. This sum is divided to its respective components according to the knowledge of the motor design obtained from the producer. If relevant documentation is not available the most common ratio which is used is 1:1. This is valid especially for high powered machines. Some (mostly American) producers provide information about the type of the motor according to NEMA-MG1-2009 standard [110] as a nameplate value (Design type A, B, C or D).

According to [3] the ratio between $X_{\sigma s}$ and $X_{\sigma r}$ is 1:1 for type A, D and for induction machines with a wound rotor. For class B, the ratio of $X_{s\sigma}$ to $X_{r\sigma}$ is stated as 0,67 and for type C it is given as 0,43. Schematic cuttings of rotor bars of the respective classes are shown on Fig. 36.

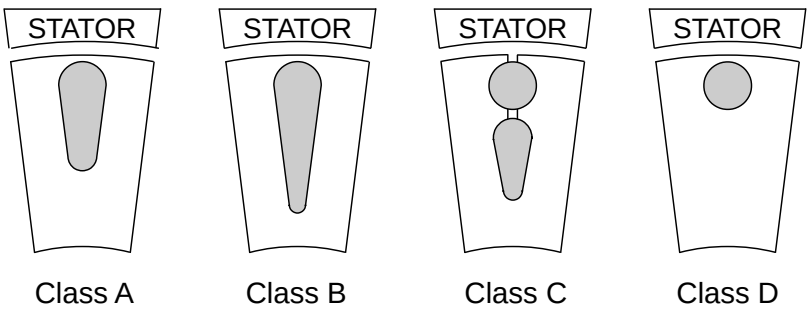

Fig. 36: Rotor bars according to NEMA-MG1-2009.

European norm IEC/EN 60034-2-1 [4] states in part 7.5.2, that the data about the motor design should be used to specify the ratio between $X_{\sigma s}$ and $X_{\sigma r}$. Otherwise, it recommends to use the ratio 1:1 for single cage motors and 0,67 for motors with double-cage or deep bar rotors which correspond with class B of the American standard.

Another problem of locked rotor test is high rotor frequency ($s = 1$) which does not meet the conditions of normal operation. In operation at rated speed, the slip of the machine is in units of percent ($s \rightarrow 0$). The same situation is with the machines working with a frequency converter. The converter changes the frequency of the magnetic field and the rotor revolves with the speed close to the speed of the field in the whole speed range of the drive which means that the slip and the rotor frequency are low in the whole operational range. When the rotor frequency is high, the skin effect increases the value of effective rotor resistance and so, the rotor resistance obtained by this test does not conform to the actual value at normal run.

This can be resolved by conducting this test at various frequencies which enables us to obtain a dependency of rotor resistance R'_r on frequency. By extrapolation of this dependency to zero frequency, DC value of rotor resistance R'_r can be obtained as it is depicted in Fig. 37.

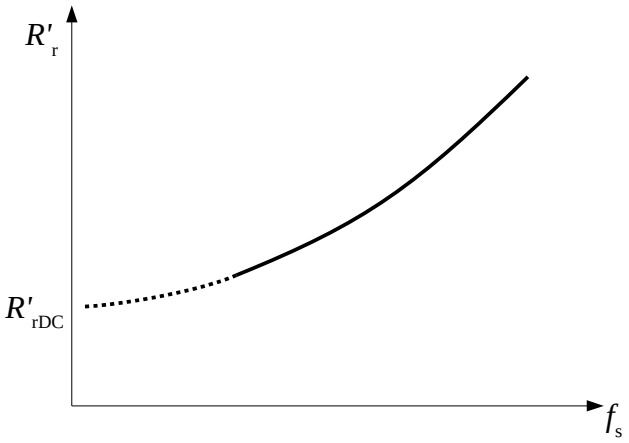

Fig. 37: Variation of effective rotor resistance with stator frequency.

5.2 Methods for On-site Identification of Parameters

Conventional methods described in the previous chapter are very effective for estimation of parameters of induction machines, but their laboratory nature makes them unsuitable for on-site usage in many cases. Firstly, some of the procedures of the conventional tests could be difficult to follow within on-site performance. For instance mechanical blocking of the rotor can be a considerable hurdle, as it would need a special test bench of a special jig which would be used only once. In other cases, decoupling of the machine from the load could be an inconvenient problem for carrying out the no-load test (e.g. traction vehicles with firmly joined gearbox). Secondly, there is economics and effectiveness. It is very common nowadays, that motor and inverter of the drive come from different manufacturers. For effective commissioning of such solution, the most effective manner is to install the machine and the inverter to their final positions as any extra

manipulation (e.g. blocking the rotor) would need more people and time, and thus would be also more expensive.

Because the parameters of the machine are unknown in most of cases and they can differ from the manufacturing process [106], identification of parameters of the machine needs to be performed for every machine being used in variable speed drives. To sum up, these are the main reasons why several methods suitable for convenient on-site identification of parameters were developed. These methods are described in the following chapters in brief.

5.3 Off-line Methods

As described at the beginning of chapter 5, under the term *off-line methods* we understand methods used for obtaining parameters required for vector control during initialization of the drive or before the drive is switched on after shut down. Based on whether the load is already coupled to the machine, these are further divided into commissioning and self-commissioning methods.

5.3.1 Methods Suitable for Self-commissioning

Methods suitable for self-commissioning should be able to gather the required machine parameters at standstill as the load may be already coupled to the machine. Therefore they can be used for observing parameters after shut down of the drive as well. In general, it can be said that the drive is switched on and waiting for command to start moving. The procedure is then expected to be fully automated. The applied voltage must be DC or single phase AC to ensure that the machine will stay in standstill.

5.3.2 Identification from Manufacturer’s or Geometry Data

These methods try to use the rated values or name-plate data or geometry of a machine, if it is known. Results obtained by such methods are usually not very precise, but can be used as initial values for other types methods or for non-demanding applications. Further, these methods can not reflect the actual machine state such as temperature, age, etc. Method presented in [112] uses rated output power, maximum or breakdown torque, starting torque, rated input power and reactive power at full load which can be obtained or calculated from catalogue data. With the least square algorithm, set of equations is solved that describe the machine’s equivalent circuit that works for NEMA class A and B [110] (Fig. 36). In [113] a frog-leaping genetic algorithm again is used for similar attitude with input values being rated torque, rated power factor, rated current, maximum torque, starting torque and starting current. Methods using geometry data of the machine are used more during the design of the machine and obtaining the geometry data from the manufacturer is usually not an easy task due to intellectual property protection. A comprehensive summary of these approaches are given in [114], [115].

5.3.3 DC Supply

DC supply is ideal for the determination of stator resistance which is usually the first parameter that is being identified. The resistance is calculated from DC voltage and corresponding DC current. In this test the three phase converter operates as a chopper with PWM modulation. The voltage on the motor terminals is usually reconstructed from the DC-link voltage and the switching pattern as described in chapter 2. Problems can arise with the influence of voltage drop on switching devices. This can be prevented e.g. with measuring with two different voltages and corresponding two current levels, such as described in [47], [116], [117]. Other non-linearities of the converter, such as the output voltage delay, switching devices dead times or influence of switching frequency can be mitigated either by known properties of the converter (e.g. measured and pre-programmed separately) or by by other measures taken during measurement. For example in [116], measurements with two different PWM frequencies are taken to obtain data for two inverter non-linearity curves for final compensation.

Phases of the induction machine can be connected by the supply converter in two principal ways as shown in Fig. 38 where U_{DCO} is a DC voltage lowered by the converter to limit the current within the limits of the machine. To gain a better precision, the measurement can be repeated with permutation of phase connection (e.g. a-bc, b-ac, c-ab). Moreover, the possible asymmetries that can be revealed by particular measurements could be used for diagnostics of the machine.

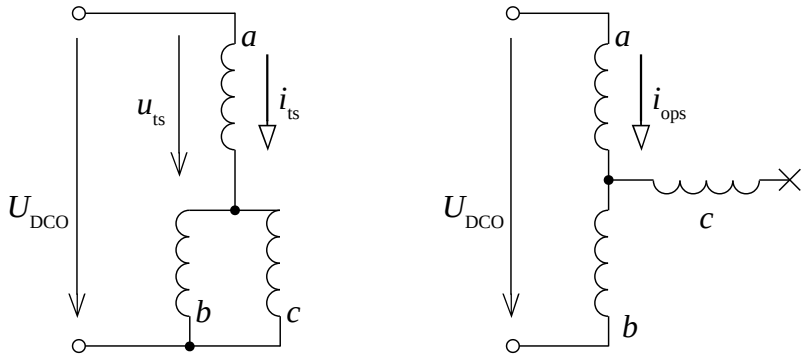

Fig. 38: Possible principal connections of the stator phase windings during the DC test.

To determine of the remaining parameters, a transient current response to the switch on or switch off of the DC supply is used. Responses of current are recorded and evaluated using various mathematical apparatus such as Laplace transformation or least squares algorithm [84]. An example of such waveforms is shown in Fig. 38 taken from [117]. Here for example, the leakage inductance $L_{\sigma\Gamma}$ of an inverse Γ equivalent circuit is obtained from integration of voltage section L_{suInt} divided by current difference L_{siDif} (with respect to sampling frequency and sample scales).

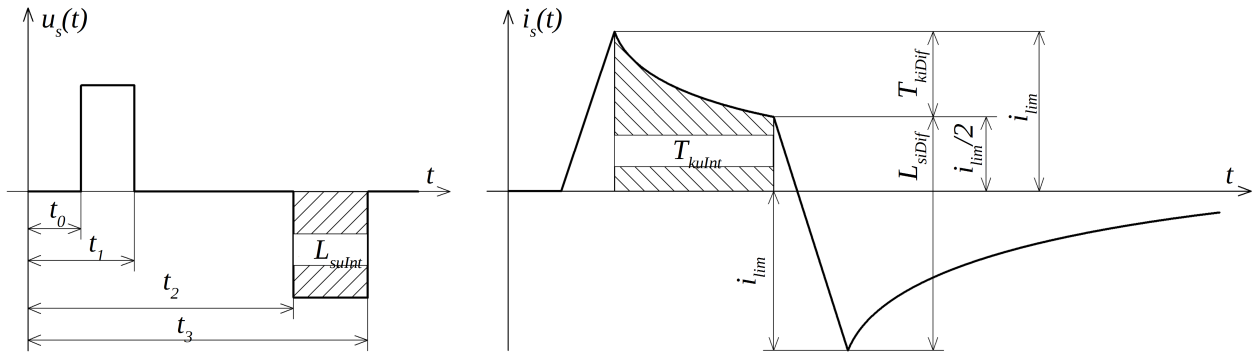

Fig. 39: Example of stator voltage and current waveforms used in Off-line identification using DC voltage [117].

Similar procedure, called DC-decay test is used in [40] to compute main flux of the machine.

5.3.4 AC Supply

No rotating magnetic field is produced in the air gap and therefore no torque is produced if the AC supply is applied as a single-phase. The connection of phases can be again done as shown in Fig. 38. Various methods use different frequencies, however usage of high-frequency (HF) signals is limited by properties of the converter, especially the switching devices used (high power devices has comparatively low switching frequency). Following this, some authors consider frequencies higher than the rated machine frequency as HF, such as [118] does for 250 Hz. Results of usage of HF signals will be influenced by by skin-effect which has to be compensated or neglected, but on the other can be used for predicting the machine behaviour in certain situations or for observing a geometry of the machine such as deep bars in the rotor cage.

Many of the methods that are using AC supply are based on standstill frequency response [119]. These methods are in general looking for a transfer function that would describe the dependency of a single-phase current on the AC output voltage of the inverter [118], [120], [121]. A voltage vector reconstruction based on AC supply response is presented in [122] where recursive least square algorithm is used for final estimation of parameter. A predictive algorithm is used in [123] for evaluating the responses of the machine to pseudo-random AC excitation. Usage of the pseudo-random signals is advantageous in noisy environment where other methods could be hindered by noise or noise removal procedures. Authors of [124] benefits from phase delay between sinusoidal voltage and current (from units to tenths of hertz) which they use for rotor resistance and rotor time constant determination. Moreover, they use measurements with different frequencies to evaluate the effect of skin effect to rotor resistance and can thus establish a look-up table for the dependence of rotor resistance on stator frequency. On the contrary, two different frequencies close to each other to prevent influence by skin effect are used by [125]. Some of the methods using the AC single-phase supply enable the identification of the machine magnetizing curve [116], [126].

5.3.5 Methods Suitable for Commissioning

Among the methods that are not considered as suitable for self-commissioning but for commissioning are also those which requires comparatively difficult mathematical apparatus. This could be based for example on a fact, that some of these methods would need more powerful control hardware than actually needed for the control of the drive itself. However, the main difference from the previously mentioned methods suitable for self-commissioning is that the machine is allowed to rotate.

It is obvious, that under these conditions, the no-load test similar to that one from Conventional methods (chapter 5.1.2) can be carried out, only with respect to the properties of the inverter (voltage drop and the dependence of the estimated output voltage on the output current). Parameters obtained this way should conform to those from Conventional test with sinusoidal supply if the calculation is made for the fundamental components of the inverter supply [111].

Pseudo-locked rotor tests are conducted in a very similar way to a common locked rotor test. Stand-still of the machine is again ensured by connection of two phases together in parallel in the same manner as shown in Fig. 38 left. No torque will be generated under this condition. The evaluation is conducted according to the same pattern as in (69)-(71) with respect to the fact that the measured impedance is 3/2 of that of the single phase.

Other possibility is to use a transient during start of the machine which is done in [127] with the help of genetic algorithms. To achieve precise results, surprisingly complicated algorithm are used by some authors: least square error minimization in [128], or artificial neural network in [129], pseudo-random binary-sequence voltage excitation and an adaptive observer in [130] or a maximum likelihood estimation method for obtaining transfer function parameters [131]. On the contrary a simple trial and error method for rotor time constant tuning is described in [132] which uses information from a speed sensor. The drive is operated in the torque mode, with rated rotor flux reference. At certain speed of rotation, an alternating square-wave torque reference is applied. If the rotor time constant value used in the controller is correct, the actual torque is also an alternating square-wave, so the speed response follows a triangular function. Deviation of the speed profile from the expected one is used for tuning the time constant which resembles a MRAS scheme, however this solution does not require the model reference.

It can be said in general that commissioning methods are a minority compared with stand-still self-commissioning methods because the latter offer advantages of a coupled load. The rotating machine can be beneficial when mechanical parameters are to be obtained. An example is presented in [133] where transient during start and shut-down are used. Principles that can be used in commissioning methods can be used also in on-line methods in most cases, especially if the load is allowed to be connected and rotated, which further shrinks this category of methods.

5.3.5.1 Magnetising Curve Identification for a Rotating Machine

Most of the methods inherit somehow the basic idea of the no-load test measurement, so identification of the machine’s magnetizing curve becomes a simple task if the machine is allowed to rotate under no-load conditions during the on-site commissioning.

If we define an analytical approximation of the magnetizing curve in a suitable functional form and perform a series of steady state harmonic voltage measurements in the field weakening region, it becomes possible to observe the magnetizing curve approximation just by visual inspection of the measurement results [44]. An illustration of this method is given in Fig. 40, where measured line-to-line fundamental voltage component is shown, together with the reconstructed magnetizing curve.

Analytical approximation used was in form

$$i_{\mathrm{m}} = a\psi_{\mu} + (1-a)\,\psi_{\mu}^{b} \tag{72}$$

where i_{m} and ψ_{μ} are in per-unit system. Fundamental stator voltage is measured for different values of parameters *a* and *b*, as these are unknown and must be obtained by repeating the measurement till it gives sufficient results. For the case described, it was determined that $b = 7$. The correct value is $a = 0.9$ since it gives the flattest voltage behaviour in the field-weakening region, which starts at starts at 1150 r/min for the measured machine [44]. The reconstructed inverse magnetizing curve analytical approximation is depicted on the right side of Fig. 40. This method, as described in [44] has to be evaluated by human operator which makes it unsuitable for self-commissioning.

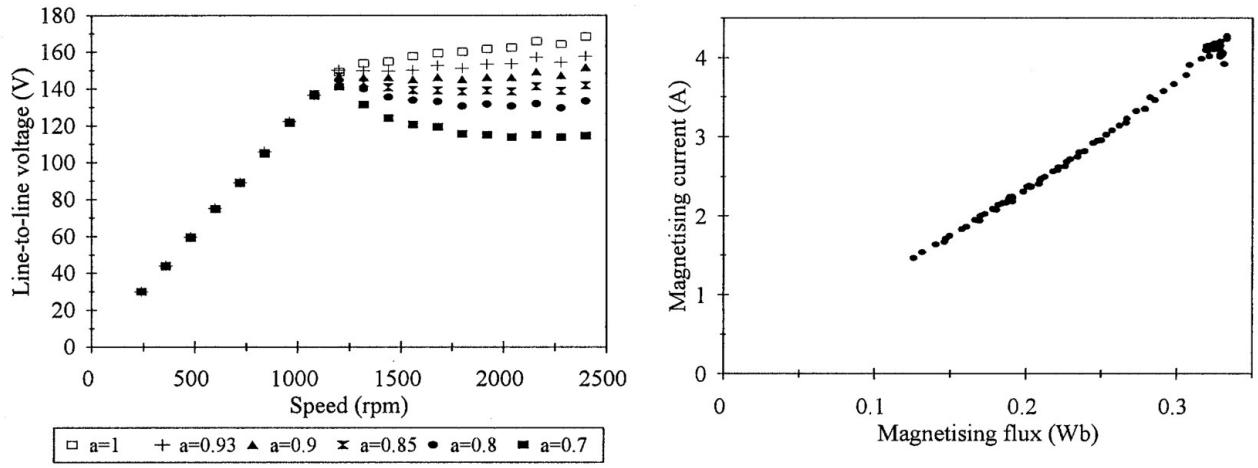

Fig. 40: Fundamental stator voltage for different settings of parameter. a of the inverse magnetizing curve [44].

5.4 On-line Methods

As mentioned before, off-line methods serve for ensuring the basic knowledge of the machine parameters before the start. For the best performance of a drive, changes of parameters should be respected and because of this, greater efforts of the research are focused to on-line methods which monitor the parameters during the operation.

Some techniques known from off-line methods were adapted. The rotor time constant estimation methods are in the centre of interest, because the rotor resistance value has the crucial influence to the working point of the machine while being influenced by temperature. Methods differ not only in the manner how the required motor reaction is erected, but also in measured signals and mainly in approaches used for measured signals evaluation. A major issue of majority of on-line methods is their relatively low accuracy in field of low load [5].

5.4.1 Methods Based on Injected Test Signal

A family of these methods [28], [29], [134]–[138] creates a special test signal that is superimposed (injected) to the stator supply quantities and a response to this this signal is being analysed from samples of stator quantities (e.g. [134]). Methods that are based on observing stator current are preferred as stator voltage is complicated to be measured and in most of cases (chapter 2), drive installations are not equipped with a sensor to measure voltage at motor terminals. Spectral analysis, mostly fast Fourrier transform that is suitable for a microcontroller realization is used to evaluate measured samples.

For further calculation the fundamentals determined from the measured data are used for an equivalent circuit of a motor that is described as a dq axes model (see (28)). Selection of the excitation signal properties is crucial as it should ideally excite all unknown parameters in the model of the machine. The signal should lead to high and different parameter sensitivities and should contain necessary components with sufficiently high amplitudes. Precautions should be taken to carry out some torque-producing action, so the systems where torque-producing current component is left undisturbed are preferred.

Problems can arise in case of light or no-load operation of the drive when slip is very low and thus the induced currents are very small, because their influence is hard to be detected. This could be overcame by injecting of negative sequence components. Method described in [135] uses a sinusoidal perturbation that is injected into the flux-producing current component. Two flux search coils are installed which enables the rotor resistance to be estimated under any load, but this additional hardware is considered as highly impractical. Method described in [136] uses FFT to analyse the currents and voltages with a help of average speed of the machine. Superimposed signal can take a form of a pseudo-random binary sequence applied by injecting it into the d-axis and correlating with q-axis stator current response. The sign of correlation gives the direction for rotor time constant updating. This method however does not work satisfactorily under light loads [5]. Frequencies of the injected signals can be limited by the properties of the converter, similarly as in case of AC excitation self-commissioning methods (chapter 5.3.4). DC signal injection is thus more favourable from this point of view, however it can cause unwanted torque pulsations [1]. Second order harmonics introduced to the test signal can prevent such pulsations as proposed in [28]. The unnecessary power losses caused by the additional signal can be prevented by using it only in dedicated moments [29]. Most of the signal injection based methods are used mainly for thermal monitoring of the machine for protection and diagnostics [29], [137], [138] through identifying the stator resistance (and evaluating its change during time). In this case, the disadvantages of the signal injection methods are mostly compensated by the fact they they can be recalled only once a longer period as temperature changes have longer time constants.

5.4.2 Methods Based on Observers

The principle of an observer based methods lies in creating a parallel virtual (modelled) system that should behave as the original system. This system is called an observer. An input signal of the real system is measured (here the stator quantities) and applied also to the modelled system. In an ideal

case, measured response of the real system (motor) and the model should be the same so the state quantities in the model should correspond to those in the real system. However the real system is disturbed so an error between responses of a real and simulated system arise. These effects are compensated by adding a value of weighted difference between the measured output of a real system and an observer output to the values of state quantities.

In general, an observer is described by following matrix equations:

$$\begin{aligned} \hat{x}(k+1) &= [A - HC]\hat{x}(k) + Hy(k) + [B - HD]u(k) \\ \hat{y}(k) &= C\hat{x}(k) + Du(k) \end{aligned} \tag{73}$$

Where $\hat{x}(k)$ is an estimation of state quantities, $\hat{y}(k)$ is an estimation of output of the system, $y(k)$ is a measured output of the system and $u(k)$ is a known input to the system while *A*, *B*, *C*, *D* are parameters of the model of the system (observer) and *H* is a matrix of the observer.

Mathematical tools used for purposes of observer based techniques are mostly Extended Kalman Filter (EKF) [14], [22], [23], [139] or Extended Luenberger Observer (ELO) [18], [20], [21]. In case of Luenberger observer a quicker convergence can be reached while Kalman filter gets better results from noisy signals. Other observer techniques are used as well, for example a stator resistance estimation with sliding mode observer in [19] or adaptive observer for stator and rotor resistance in [17]. Using of observers, especially the Kálmán, is characterized by comparatively high computational demands [1]. To lower the computational burden, reduced-order EKF was proposed [140]. Systems with observers are most often used for stator and rotor resistance [18], [19], [21], [22] identification often in in sensor-less control methods.

5.4.3 Model Reference Adaptive System Based Methods (MRAS)

Model Reference Adaptive System based methods (MRAS), sometimes called “methods based on modelling” are based on an idea that one quantity is calculated in two different ways and results are compared. Relatively simple implementation makes this approach attractive, the difficulties can be seen only under facts, that two models are calculated and possibly also with the suitable adaptive system law. General structure of a MRAS system is shown in Fig. 41.

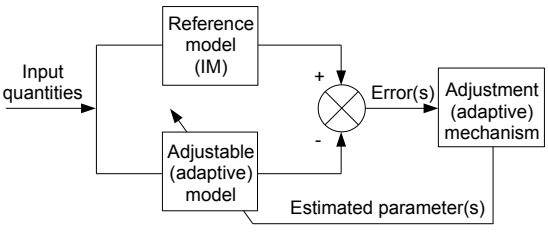

Fig. 41: General block scheme of MRAS.

In case of IM parameter identification, the reference model is the actual machine itself, so it is literally no model at all. Selected input quantities are used for the adaptive model where searched parameters are carried out in a manner that their values can be easily changed (tuned). Selected output quantities from the adaptive model are compared by quantities available from the IM and the result (error) is First value of the selected quantity is calculated with reference values of parameters stored in the controller while the second one is calculated from the measured quantities. The

difference of both signals is processed by adaptive mechanism (adaptive law) which can be for example and ordinary PI or I controller. It is assumed that the error is fully caused by the change of the searched parameter. Adaptive mechanism then adjust the value of searched parameter in the adjustable (adaptive) model [1], [5]. When the outputs of both models are equal (the error is minimal), the searched parameter(s) is considered to be equal to the real value. The error signal signal (output quantity from the model) can be chosen from variety of quantities: electromagnetic torque [141]–[143], rotor flux [144], stator voltage [142], [145], active power [141], [143], reactive power [30], [32], [32], [146] or back EMF [144], [147].

The accuracy of any of these methods depends on the accuracy of the applied model. A steady-state model of the induction machine can be used. Sensitivity of the model-based methods to variations of other parameters can be high as the models usually use constant parameters. This is in accordance with the fact that the accuracy of these methods are given mostly by the accuracy of the model. Improvements can be carried out e.g. by introducing variation of the magnetizing inductance with saturation or respecting the iron losses variation. MRAS methods are usually capable of estimating only one or two parameters limited by the speed of convergence and stability of the adaptive process [1]. Designing a suitable adaptive law for more parameters would be difficult as the ordinary PI or I controllers would not satisfy stability criteria. MRAS based methods are typically used for rotor resistance or rotor time constant estimation [32], [141]–[143], [145], in less cases for stator resistance [147], [148].

5.4.4 Recursive Least Square Methods

The basic idea behind Recursive Least Square (RLS) methods [84], [127], [149]–[151] is to minimize the second order (a square) of the difference between the estimated and actual values of parameters. Better to say, it is a minimization of a square of the error between estimated and real actual values. Based on this error minimization, the estimated parameters should converge to the right actual values. An iterative approach to this minimization can hinder usage of large matrix equations, but still, the algorithm can take long or can be otherwise demanding.

Machine is described by equations derived from voltage model such as in [149]:

$$\begin{pmatrix} \dfrac{\mathrm{d}i_{\mathrm{sd}}}{\mathrm{d}t} i_{\mathrm{sd}} - \omega_{\mathrm{r}} u_{\mathrm{sq}} - \left(\dfrac{\mathrm{d}u_{\mathrm{sd}}}{\mathrm{d}t} + \omega_{\mathrm{r}} i_{\mathrm{sq}} \right) - u_{\mathrm{sd}} \\ \dfrac{\mathrm{d}i_{\mathrm{sq}}}{\mathrm{d}t} i_{\mathrm{sq}} - \omega_{\mathrm{r}} i_{\mathrm{sd}} - \left(\dfrac{\mathrm{d}u_{\mathrm{sq}}}{\mathrm{d}t} + \omega_{\mathrm{r}} u_{\mathrm{sd}} \right) - u_{\mathrm{sq}} \end{pmatrix} \begin{pmatrix} K_1 \\ K_2 \\ K_3 \\ K_4 \\ K_5 \end{pmatrix} = \begin{pmatrix} \dfrac{-\mathrm{d}^2 i_{\mathrm{sd}}}{\mathrm{d}t^2} - \omega_{\mathrm{r}} \dfrac{\mathrm{d}i_{\mathrm{sq}}}{\mathrm{d}t} \\ \dfrac{-\mathrm{d}^2 i_{\mathrm{sq}}}{\mathrm{d}t^2} - \omega_{\mathrm{r}} \dfrac{\mathrm{d}i_{\mathrm{sd}}}{\mathrm{d}t} \end{pmatrix} . \tag{74}$$

Parameters of the machine are hidden under K_{i} marking. Each author uses slightly different notation of the K_{i} coefficients [149], [150], [152], but if properly arranged, they should result in the same meaning.

For example, in [149], the constants are defined as follows:

$$K_1=\frac{R_s\tau_r+L_s}{\sigma L_s\tau_r}\quad K_2=\frac{R_s}{\sigma L_s\tau_r}\quad K_3=\frac{1}{\sigma\tau_r}\quad K_4=\frac{1}{\sigma L_s\tau_r}\quad K_5=\frac{1}{\sigma L_s\tau_r}\ , \tag{75}$$

where σ is the leakage factor defined as

$$\sigma=1-\frac{L_m^2}{L_s L_r}\ . \tag{76}$$

In general, the matrix equation in (74) can be rewritten into notation **Ax** = **b**. Here, **A** is called data matrix, **b** observation vector and **x** a vector of unknowns (parameters $\underline{K}_i$). The RLS algorithm is then used to solve this equation. Data for the other variables in the equations can be obtained from both transient or steady-state operation of the drive, but in steady-state, not all of the parameters can be determined as they are not excited and the derivatives are equal to zero [150]. Namely, these data are stator currents and voltages and their derivatives , e.g. in dq reference frame as shown in (74).

5.4.5 Artificial Intelligence and Genetic Algorithms Based Methods

Recent development opened up usage of artificial intelligence realized by neural networks, better to say Artificial Neural Networks (ANN) [153]–[156], Genetic Algorithms (GA) [74], [127], [157] and Optimization Algorithms (OA) [158]–[160]. These methods are however characterized by high computational demands and thus their deployment could be limited outside cost optimized applications. A real-time control accelerator may be needed adjacent to a microcontroller to implement ANN as presented in [15]. They are further complicated by the needs of extra time and resources are needed for ANNs as they need to have training samples or training algorithm. Large number of calculations is needed by OAs such as Particle Swarm Optimization. On the contrary, GAs have demanding requirements on storage of historical data [16]. and thus generally on the memory of the control hardware. Nevertheless, methods based on artificial intelligence are in a focus of researchers and the long-term continually dropping cost of microcontrollers is opening possibilities also for these methods.

5.4.6 Other On-line Methods

Among other techniques of on-line parameter determination are those utilizing special switching techniques of the current regulated PWM inverter, which allows measurement of the induced voltage across a disconnected stator phase. This method needs the additional voltage sensor so it is less preferable in industry.

Recent emphasis on sensorless vector control has led to a development of a number of schemes for simultaneous rotor speed and rotor time constant on-line estimation, that are applicable in conjunction with the appropriate speed estimation model-based algorithms. These methods of rotor time constant estimation belong in vast majority of cases to one of the groups already reviewed in this section.

Some authors however try to describe temperature behaviour of the machine to determine temperature precisely and then to use this estimated temperature to calculate the change of temperature dependent parameters of the machine, such as [161].

Despite the growing popularity of sensorless schemes of induction machine drives, some authors propose installing of additional temperature sensors. Temperature sensor mounted to the stator winding of the machine was used in [7]. Authors then calculated the values of both stator and rotor resistances assuming the same temperature through the whole machine volume, based on the temperature change measured by the aforementioned sensor. In [35], the authors mounted a wireless temperature sensor on the rotor of a machine beside a wired one attached to the stator winding.

Among methods that do not suit to any of the previously mentioned groups are also methods based on voltage model calculation. A combination of information from a mechanical speed sensor and a steady-state voltage model was used in [13] to calculate rotor resistance which change was used to obtain the temperature change of the rotor of the induction machine in a battery electric vehicle drive. In [31], the same combination of speed sensor and steady-state voltage model was used for estimation of rotor magnetic flux and its angle. These two methods served also as an inspiration for the solution presented in this work as it represent a computationally modest approach of parameter identification suitable for variety of drives.

6 Proposed On-line Method for Resource-constrained Microcontrollers

A number of different on-line methods was developed for monitoring machine parameters during operation as being showed in chapter 5.4. However, a lot of them are computationally or memory demanding or are very complex to implement and thus are not suitable for microcontrollers with limited resources.

This thesis proposes the new method of simultaneous on-line identification of rotor resistance and magnetizing inductance based on voltage model calculation, suitable for IFOC, FIFOC and similar control strategies. It is focused on drives with induction machines that are equipped with a mechanical speed sensor, a microcontroller with limited resources and a part of their working cycle is in a steady-state mode. These could be existing drives with an older microcontroller system whose hardware cannot cope with computational or memory intensive algorithms or new drives that need a speed sensor due to technical standards, or for high precision speed or position measurement, but otherwise are equipped with low-cost microcontrollers.

A drive in consideration has a structure and sensors as depicted in Fig. 3, so it is expected that values of I_{sd}, I_{sq}, U_{sd}, U_{sq}, ω_s and ω_r are supposed to be known in the microcontroller as described in chapter 2 and that the method would not need any other inputs of any extra hardware than previously stated.

6.1 Mathematical Derivation

Vector equations (32), (33) and (34) for the voltage model of the induction machine, represented by an equivalent circuit in Fig. 11, can be rewritten for clarity into four equations (77), (78), (79) and (80).

$$\hat{U}_s = R_s \hat{I}_s + \mathrm{j}\omega_s L_{s\sigma} \hat{I}_s + \hat{U}_i \tag{77}$$

$$\hat{U}_i = \mathrm{j}\omega_s L_m \hat{I}_m \tag{78}$$

$$\hat{U}_i = \frac{R_r}{s} \hat{I}_r + \mathrm{j}\omega_s L_{r\sigma} \hat{I}_r \tag{79}$$

$$\hat{I}_m = \hat{I}_s - \hat{I}_r \tag{80}$$

These vector equations ((77), (78), (79), (80)) can be expressed also in a form of their components in dq reference frame, which is a common form of representation of vectors in microcontrollers as shown in (81), (82), (83) and (84).

$$\begin{aligned} U_{sd} &= R_s \cdot I_{sd} - \omega_s \cdot L_{\sigma s} \cdot I_{sq} + U_{id} \\ U_{sq} &= R_s \cdot I_{sq} - \omega_s \cdot L_{\sigma s} \cdot I_{sd} + U_{iq} \end{aligned} \tag{81}$$

$$\begin{aligned} U_{\mathrm{id}} &= -\omega_{\mathrm{s}} \cdot L_{\mathrm{m}} \cdot I_{\mathrm{mq}} \\ U_{\mathrm{iq}} &= -\omega_{\mathrm{s}} \cdot L_{\mathrm{m}} \cdot I_{\mathrm{md}} \end{aligned} \tag{82}$$

$$\begin{aligned} U_{\mathrm{id}} &= \frac{R_{\mathrm{r}}}{s} \cdot I_{\mathrm{rd}} - \omega_{\mathrm{s}} \cdot L_{\sigma\mathrm{r}} \cdot I_{\mathrm{rq}} \\ U_{\mathrm{iq}} &= \frac{R_{\mathrm{r}}}{s} \cdot I_{\mathrm{rq}} - \omega_{\mathrm{s}} \cdot L_{\sigma\mathrm{r}} \cdot I_{\mathrm{rd}} \end{aligned} \tag{83}$$

$$\begin{aligned} I_{\mathrm{md}} &= I_{\mathrm{sd}} - I_{\mathrm{rd}} \\ I_{\mathrm{mq}} &= I_{\mathrm{sq}} - I_{\mathrm{rq}} \end{aligned} \tag{84}$$

Values of I_{sd}, I_{sq}, U_{sd}, U_{sq}, ω_{s} and ω_{r} are supposed to be known in the microcontroller as described in chapter 2. Further, the values of parameters $L_{\sigma\mathrm{s}}$, $L_{\sigma\mathrm{r}}$ and R_{s} are also assumed to be known either provided by manufacturer or by standard (laboratory) tests (conventional methods) [3] or some off-line method. Assuming the steady-state of the machine, all those quantities are assumed to be constant during the calculation.

Back EMF components U_{id} and U_{iq} can be calculated from (81) as all other quantities are known:

$$\begin{aligned} U_{\mathrm{id}} &= U_{\mathrm{sd}} + \omega_{\mathrm{s}} \cdot L_{\sigma\mathrm{s}} \cdot I_{\mathrm{sq}} - R_{\mathrm{s}} \cdot I_{\mathrm{sd}} \\ U_{\mathrm{iq}} &= U_{\mathrm{sq}} - \omega_{\mathrm{s}} \cdot L_{\sigma\mathrm{s}} \cdot I_{\mathrm{sd}} - R_{\mathrm{s}} \cdot I_{\mathrm{sq}} \end{aligned} . \tag{85}$$

One of the vectors, e.g. the stator voltage, can be aligned with an axis of the dq reference frame resulting in the particular component of such vector being equal to zero. This zero component could be possibly omitted from the notation of the equations but for generality it is assumed in this paper that the vectors can have any position.

For clarity and simplification of the notation of the calculation, equivalent rotor resistance R_{req} is defined as

$$R_{\mathrm{req}} = \frac{R_{\mathrm{r}}}{s} = R_{\mathrm{r}} \cdot \frac{\omega_{\mathrm{s}}}{\omega_{\mathrm{s}} - \omega_{\mathrm{m}}} \cdot \tag{86}$$

Rotor current components I_{rd}, I_{rq} can be calculated by merging and rearranging (83) as:

$$\begin{aligned} I_{\mathrm{rd}} &= \frac{R_{\mathrm{req}} \cdot U_{\mathrm{id}} + \omega_{\mathrm{s}} \cdot L_{\sigma\mathrm{r}} \cdot U_{\mathrm{iq}}}{R_{\mathrm{req}}^2 + \omega_{\mathrm{s}}^2 \cdot L_{\sigma\mathrm{r}}^2} \\ I_{\mathrm{rq}} &= \frac{R_{\mathrm{req}} \cdot U_{\mathrm{iq}} - \omega_{\mathrm{s}} \cdot L_{\sigma\mathrm{r}} \cdot U_{\mathrm{id}}}{R_{\mathrm{req}}^2 + \omega_{\mathrm{s}}^2 \cdot L_{\sigma\mathrm{r}}^2} \end{aligned} . \tag{87}$$

From the equivalent circuit (Fig. 11) it is obvious that magnetizing current components I_{md}, I_{mq} can be expressed not only as stated in (84), but also as

$$\begin{aligned} I_{\mathrm{md}} &= \frac{U_{\mathrm{iq}}}{\omega_{\mathrm{s}} \cdot L_{\mathrm{m}}} \\ I_{\mathrm{mq}} &= -\frac{U_{\mathrm{id}}}{\omega_{\mathrm{s}} \cdot L_{\mathrm{m}}} \end{aligned} . \tag{88}$$

Substituting I_{md}, I_{mq} from (88) to (84) and I_{rd}, I_{rq} from (87) to (88), (88) can be rewritten as

$$\begin{aligned} \frac{U_{iq}}{\omega_s \cdot L_m} &= I_{sd} - \frac{R_{req} \cdot U_{id} + \omega_s \cdot L_{\sigma r} \cdot U_{iq}}{R_{req}^2 + \omega_s^2 \cdot L_{\sigma r}^2} \\ -\frac{U_{id}}{\omega_s \cdot L_m} &= I_{sq} - \frac{R_{req} \cdot U_{iq} + \omega_s \cdot L_{\sigma r} \cdot U_{id}}{R_{req}^2 + \omega_s^2 \cdot L_{\sigma r}^2} \end{aligned} . \tag{89}$$

Converting I_{sd}, I_{sq} to a common denominator with the rest of the right side of (89) forms

$$\begin{aligned} \frac{U_{iq}}{\omega_s \cdot L_m} &= \frac{R_{req}^2 \cdot I_{sd} + \omega_s^2 \cdot L_{\sigma r}^2 \cdot I_{sd} - R_{req} \cdot U_{id} - \omega_s \cdot L_{\sigma r} \cdot U_{iq}}{R_{req}^2 + \omega_s^2 \cdot L_{\sigma r}^2} \\ -\frac{U_{id}}{\omega_s \cdot L_m} &= \frac{R_{req}^2 \cdot I_{sq} + \omega_s^2 \cdot L_{\sigma r}^2 \cdot I_{sq} - R_{req} \cdot U_{iq} - \omega_s \cdot L_{\sigma r} \cdot U_{id}}{R_{req}^2 + \omega_s^2 \cdot L_{\sigma r}^2} \end{aligned} . \tag{90}$$

Now first equation in (90) is multiplied with U_{id} and second equation in (90) with U_{iq} and then added together to eliminate the left sides and to get a single equation (91):

$$\begin{aligned} 0 = &\frac{R_{req}^2 \cdot I_{sd} \cdot U_{id} + \omega_s^2 \cdot L_{\sigma r}^2 \cdot I_{sd} \cdot U_{id} - R_{req} \cdot U_{id}^2 - \omega_s \cdot L_{\sigma r} \cdot U_{iq} \cdot U_{id}}{R_{req}^2 + \omega_s^2 \cdot L_{\sigma r}^2} + \\ + &\frac{R_{req}^2 \cdot I_{sq} \cdot U_{iq} + \omega_s^2 \cdot L_{\sigma r}^2 \cdot I_{sq} \cdot U_{iq} - R_{req} \cdot U_{iq}^2 - \omega_s \cdot L_{\sigma r} \cdot U_{id} \cdot U_{iq}}{R_{req}^2 + \omega_s^2 \cdot L_{\sigma r}^2} \end{aligned} . \tag{91}$$

Rearranging matching constituents of (91) forms

$$0 = \frac{R_{req}^2 \cdot (I_{sd} \cdot U_{id} + I_{sq} \cdot U_{iq}) + \omega_s^2 \cdot L_{\sigma r}^2 \cdot (I_{sd} \cdot U_{id} + I_{sq} \cdot U_{iq}) - R_{req} \cdot (U_{id}^2 \cdot U_{iq}^2)}{R_{req}^2 + \omega_s^2 \cdot L_{\sigma r}^2} . \tag{92}$$

As the left side of (92) is equal to zero, denominator can be removed. The expression in nominator of (92) can be rearranged as

$$R_{req}^2 - R_{req} \cdot \frac{U_{id}^2 \cdot U_{iq}^2}{I_{sd} \cdot U_{id} + I_{sq} \cdot U_{iq}} + \omega_s^2 \cdot L_{\sigma r}^2 = 0 , \tag{93}$$

which is a reduced quadratic equation of the type $x^2 + px + q = 0$ that can be solved by common formula for finding its roots. For clarity, the denominator of p is defined as an inner power of the machine P_i and nominator of p as a squared magnitude of back EMF vector $|U_i^2|$:

$$\begin{aligned} P_i &= I_{sd} \cdot U_{id} + I_{sq} \cdot U_{iq} \\ |U_i| &= U_{id}^2 \cdot U_{iq}^2 \end{aligned} . \tag{94}$$

For motoric mode of the machine, the inner power P_i is positive and therefore positive sign of the square root in quadratic formula is used:

$$R_{req} = \frac{1}{2} \left(\frac{|U_i|^2}{P_i} + \sqrt{\left(\frac{|U_i|^2}{P_i} \right)^2 + 4 \cdot \omega_s^2 \cdot L_{\sigma r}^2} \right) . \tag{95}$$

If the machine acts as a generator (regenerative braking) than the inner power is negative and therefore the negative sign is used, which is shown in (96). The resulting value of R_{req} will then be

negative. Despite of that, the resulting value of R_r will be positive, as the value of slip s is also negative in regenerative brake mode of the machine.

$$R_{req} = \frac{1}{2}\left(\frac{|U_i|^2}{P_i} - \sqrt{\left(\frac{|U_i|^2}{P_i} \right)^2 + 4 \cdot \omega_s^2 \cdot L_{\sigma r}^2} \right) \tag{96}$$

Final value of R_r is than easily calculated from R_{req} by multiplying it with slip s. With a known value of R_{req} (or R_r), magnetizing inductance L_m can be calculated from second or preferably first equation of (88) as it does not contain a negative sign. The calculation is performed only with half of components of the vectors $\hat{U}_i$ and $\hat{I}_m$. which can have different signs based on actual vector positions. To prevent the negative resulting value of L_m, absolute value of the right side is added, forming the final equation for calculating L_m as:

$$L_m = \left| \frac{U_{iq}}{\omega_s \cdot I_{md}} \right| \cdot \tag{97}$$

As the deriving of the calculation is based on a vector description which can be both in scale of maximum values (amplitudes) of RMS values, the calculation gives the same results both for maximum or RMS input values.

6.2 Microcontroller Algorithm

Based on previous deduction a list of equations that need to be performed by microcontroller is presented in this chapter. First, back EMF components are calculated from stator current and voltage (98), (99). Then inner power (100) and squared magnitude of the back EMF vector (101) values are needed for the coefficient p (102) of the reduced quadratic equation. The q coefficient is calculated in (103) and the discriminant in (104). Calculation of R_{req} depends on whether the machine is in motoric or regenerative brake mode. In (105), motoric mode is shown, meaning that the + sign is used (see 6.1, (95),(96)). In this equation probably a biggest hurdle for the tiniest resource-constraint microcontrollers is present which is the square root calculation. Following the equivalent rotor resistance R_{req} calculation, its value is used to calculate the rotor current component (106), which is needed for calculation of L_m. As showed in chapter 6.1, only one component is sufficient. The choice of the component is arbitrary and could be based on other criteria specific to target implementation. In our case, d-axis component was chosen as it enables to use the first equation of (88) for final L_m calculation - which does not contain a negative sign. In the denominator of this equation (106), the value of the q component is used once again as this part has the same value (see (87)) - this could save a few computations if memory for its temporary storage is available. The rotor current component is needed for the magnetizing current component calculation (107). Again, only one component is suitable for calculation of L_m. Its choice has to correspond with the choice of rotor current component – both of them have to be from the same axis. With the value of magnetizing current component, L_m can be finally calculated (108). Absolute value is here to prevent a negative resultant value of L_m in case that the components of the back EMF and magnetizing current would have different signs due to orientation their respective vectors. If the control algorithm aligns the vectors in a way that they lie in the same quadrants of the dq

plane, than the absolute value could be omitted. Rotor resistance R_r could be calculated already after (105), but is left till the end of the calculation in order to have the resulting values of parameters in the last two equations. So in (109) R_{req} is multiplied by the value of the actual slip s (see (86)) to get the R_r.

$$U_{id} = U_{sd} + \omega_s \cdot L_{\sigma s} \cdot I_{sq} - R_s \cdot I_{sd} \tag{98}$$

$$U_{iq} = U_{sq} - \omega_s \cdot L_{\sigma s} \cdot I_{sd} - R_s \cdot I_{sq} \tag{99}$$

$$P_i = I_{sd} \cdot U_{id} + I_{sq} \cdot U_{iq} \tag{100}$$

$$|U_i|^2 = U_{id}^2 \cdot U_{iq}^2 \tag{101}$$

$$p = \frac{|U_i|^2}{P_i} \tag{102}$$

$$q = \omega_s^2 \cdot L_{\sigma r}^2 \tag{103}$$

$$D = p^2 - 4 \cdot q \tag{104}$$

$$R_{req} = \frac{p + \sqrt{D}}{2} \tag{105}$$

$$I_{rd} = \frac{R_{req} \cdot U_{id} + \omega_s \cdot L_{\sigma r} \cdot U_{iq}}{R_{req}^2 + q} \tag{106}$$

$$I_{md} = I_{sd} - I_{rd} \tag{107}$$

$$L_m = \left| \frac{U_{iq}}{\omega_s \cdot I_{md}} \right| \tag{108}$$

$$R_r = R_{req} \cdot \frac{\omega_s - \omega_m}{\omega_s} \tag{109}$$

6.2.1 Other Assumptions for the Method Principle

An estimation of the proper value of R_r by the proposed method depends on accuracy of the speed measurement. If the drive is not equipped with a sensor with a suitable number of pulses per revolution, approaches like longer measurement or measurement of period of the pulse can be deployed. Prolonging the speed measurement should not be a problem as the drive should operate in steady-state mode during measurement. Parameters $L_{\sigma s}$, $L_{\sigma r}$ and R_s are assumed to be constant. This simplification can be done without a significant loss of accuracy in the case of $L_{\sigma s}$, $L_{\sigma r}$ as described in chapters 4.1.3, 4.1.4 and 4.1.5. Thus it is not influenced by a change of temperature and the effect of saturation can be also considered negligible. R_s is however influenced by the temperature, but its influence on the calculation is not so significant in most of the operation range. The voltage drop on the $L_{\sigma s}$ is higher than that on the R_s and this difference rises with the rising stator frequency and torque producing stator current component I_{sq}. Moreover, the temperature of the rotor is normally higher than that of the stator [13] which means that change of R_s is smaller than the change of R_r.

The actual error in estimation caused by improper value of R_s depends though on actual conditions in the machine – the relation of voltage drops on R_s compared to that one on I_{sq}, and are thus also machine-specific. As an example, we can take the 3,5 kW IM, that was tested in experiments (chapter 7.2). In case that the temperature of the stator winding changes by 100°C, the R_s will rise by 39 %. The error between when the controller executes the estimation with the „cold“ value and the result that would be obtained by „warm“ value of R_s is 13,5 % (the correct „warm“ value is 13,5 % higher than „cold“ one) for load torque of 9,5 Nm (I_{sq} = 3,2 A), but only 3,3 % for 23 Nm (I_{sq} = 6,3 A).

Frequency should not have any significant effect of the R_s as the stator winding is normally manufactured as parallel filaments to prevent the skin effect (chapter 4.1.8).

Both R_r and L_m can be regarded as slowly varying during steady-state operation. In this mode, R_r is mostly influenced by temperature change which rises slowly, as can be seen e.g. from Fig. 45 or Fig. 54. The flux which can influence the value of L_m by saturating the magnetic circuit also does not change quickly during normal operation of control strategies like IFOC of FIFOC. Therefore the method is enough to be executed within minutes during steady-state operation. In the case of change of a working point of the drive it should be executed after this change as magnetizing current or slip change can result in a sharp change of R_r or L_m. Averaging of multiple measurements of input quantities is advised to prevent variation of results.

7 Experimental Testing of the Developed On-line Method

Developed on-line method was tested on 4 different induction machines with rated power 3,5 kW, 15 kW, 180 kW and 1640 kW. Amount of tests on particular machines differ based on time available time and workforce in the particular test room and hurdles faced during implementation. The 3,5 kW and 15 kW machines are general purpose induction machines while the 180 kW is being used in traction drives of electric multiple units and 1640 kW in traction drives of locomotives. The aim to test at least a warming test and run with different loads was however completed in all four cases. Tests details are covered by following subchapters. As stated in chapter 6.1, maximum (amplitudes) or RMS input values can be chosen for input. The following experiments use maximum values in all cases. Voltage vector is aligned with the q axis, so the d component (U_{sd}) is zero in all presented cases.

7.1 Methods of Justifying the Obtained Results

It is generally difficult to compare the estimated parameter values with some reference. Laboratory standard tests [3] for example use the line frequency (50 Hz in our case) for locked rotor test meaning that slip frequency is equal to 50 Hz. On the other hand, during operation of the drive with scalar control or IFOC, slip frequency is low (in order of hertz). Magnetizing inductance has a similar problem with comparison of its estimated value to the value obtained by standard tests: the proposed identification method determines its value for particular working point while the standard test value is obtained from no-load measurement. Furthermore, there is an influence of higher harmonics during operation with converter while the standard tests are often carried out supplied from grid and grid connected induction regulators with different harmonic composition than converter operation.

To justify the method principle and obtained results, following methods and phenomena were used:

- Reverse calculation of stator current components with model with estimated parameter values
- Estimation of the rotor resistance with different method and comparison of the results
- Comparison of rotor resistance change observed by the proposed method with temperature resistance change formula
- Observation of effects of saturation to the magnetizing inductance
- Influence of rotor frequency to rotor resistance value

7.1.1 Reverse Calculation of Selected Quantities with Model with Estimated Parameter Values

To demonstrate that the derivation of the equations of the proposed method is correct, reverse calculation of selected quantities with the help of estimated parameters is carried out. Block scheme of the principle of this approach is depicted in Fig. 42. The idea behind this verification is to calculate some measurable quantity from the mathematical model of the machine with the help of estimated parameters and then compare measured and calculated values. In the presented case, stator current components were selected. With the proposed on-line identification method, R_r and L_m are estimated and then their values are used in a mathematical model of the machine. In this model, represented again by a T-equivalent circuit (Fig. 11), the knowledge of all the equivalent circuit parameters and some of the measurable quantities, namely stator voltage components U_{sd}, U_{sq}, stator angular frequency ω_s and rotor angular frequency ω_m is used. From these, the stator current components I_{sdc}, I_{sqc} are calculated with the letter "c" in their subscript standing for "calculated".

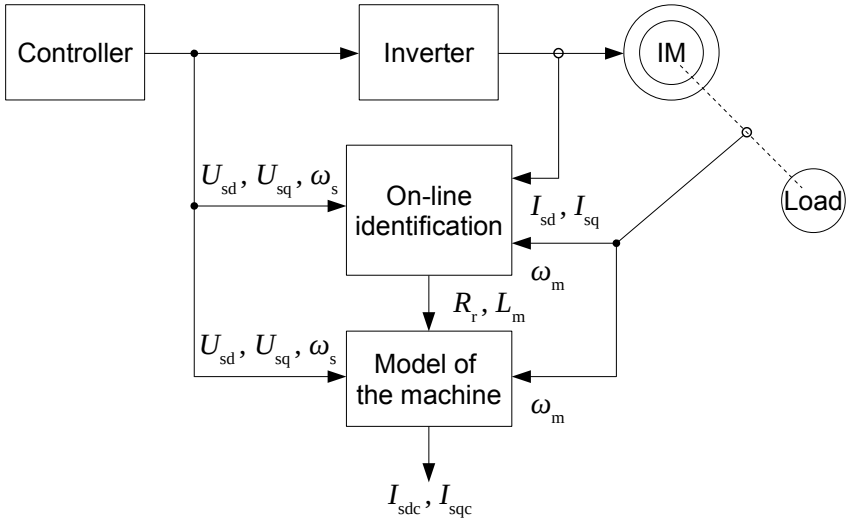

Fig. 42: Block scheme of the reverse calculation verification.

The calculated values of I_{sdc}, I_{sqc} are exactly the same as those that can be measured (I_{sd}, I_{sq}), because this T-equivalent circuit is not capable of introducing some other parasitic effects. Despite that, it demonstrates that the values of R_r and L_m have values appropriate for the T-equivalent circuit representation of the machine.

Values of I_{sdc} and I_{sqc} can be seen in tables in chapters 7.2.2, , 7.4.2 and 7.5.2 for particular machines, where they are stated within *Values calculated for verification* part of these tables.

7.1.2 Estimation of the Rotor Resistance with Different Method and Comparison of the Results

A method published in [13] (let's call it Tran and Nègre's method for clear distinguishing) can estimate the rotor resistance with the values that are already available for the purposes of the

proposed on-line identification method plus the magnetizing inductance value. This thus offers also a kind of cross control as it is possible to calculate the rotor resistance with another approach with a parameter given by the method proposed by this thesis.

Estimation of the rotor resistance by Tran and Nègre's method is based on following equation:

$$R_{\mathrm{rv}} = \frac{-(\omega_{\mathrm{s}} - \omega_{\mathrm{m}}) \cdot [\Psi_{\mathrm{sd}} \cdot L_{\mathrm{r}} + I_{\mathrm{sd}} \cdot (L_{\mathrm{m}}^2 - L_{\mathrm{s}} \cdot L_{\mathrm{r}})]}{\Psi_{\mathrm{sq}} - L_{\mathrm{s}} \cdot I_{\mathrm{sq}}}, \tag{110}$$

where stator magnetic flux components Ψ_{sd}, Ψ_{sq} are defined as

$$\Psi_{\mathrm{sd}} = \frac{U_{\mathrm{sq}} - R_{\mathrm{s}} \cdot I_{\mathrm{sq}}}{\omega_{\mathrm{s}}}, \Psi_{\mathrm{sq}} = \frac{U_{\mathrm{sd}} + R_{\mathrm{s}} \cdot I_{\mathrm{sd}}}{\omega_{\mathrm{s}}}, \tag{111}$$

and L_{s} and L_{r} being stator and rotor inductances respectively, defined as

$$L_{\mathrm{s}} = L_{\sigma\mathrm{s}} + L_{\mathrm{m}}, L_{\mathrm{r}} = L_{\sigma\mathrm{r}} + L_{\mathrm{m}}. \tag{112}$$

Other symbols used in these equations have the same meaning as elsewhere in this theses with their meaning explained in List of Symbols - Nomenclature section. Value of L_{m} used for this verification is that one obtained by method proposed in this theses. Rotor resistances estimated by this Tran and Nègre's approach have the same values as those estimated by the method in this theses which confirms its correctness. This can be seen in tables in chapters 7.2.2, , 7.4.2 and 7.5.2 for particular machines, where the resistance calculated by this method is stated within *Values calculated for verification* part of these tables, marked a R_{rv}.

7.1.3 Comparison of Rotor Resistance Change Observed by the Proposed Method with Temperature Resistance Change Formula

This justification is based on comparison of rotor resistance R_{r} change during the warming test with a value calculated by the well-known equation for temperature dependence of metals (57) for the same warming. It is assuming the linear behaviour of this dependence, as stated in chapter 4.1.7. This change of resistance estimated by the proposed method is in good accordance with values calculated by (57). This is shown by all four warming tests of the four tested induction machines, namely in (113) and Fig. 45 for 3,5 kW machine, (114) and Fig. 54 for 15 kW machine, (115) and Fig. 61 for 180 kW and (116) and Fig. 69 for 1640 kW machine.

7.1.4 Observation of Effects of Saturation to the Magnetizing Inductance

The influence of saturation to magnetizing is described in more detail in chapter 4.1.6. Due to saturation of the magnetic circuit of the machine, the value of L_{m} decreases. This dependence can be observed also as a dependence of magnetizing inductance on magnitude of magnetizing current $L_{\mathrm{m}} = f(|I_{\mathrm{m}}|)$ or on magnetizing component of stator current $L_{\mathrm{m}} = f(I_{\mathrm{sd}})$. These dependences are supported also by observations presented elsewhere (see chapter 4.1.6) and can be seen in results of experiments. In the results of experiments presented in this thesis, it can be seen in Fig. 49, Fig. 55, Fig. 57 and Fig. 65.

7.1.5 Influence of Rotor Frequency to Rotor Resistance Value

Rotor resistance is rising with the rising slip (rotor) frequency due to skin effect, as described in chapter 4.1.9. Due to lowering the effective conductor's cross section, the effective resistance is getting higher. This is valid for squirrel cage rotors made out of solid bar conductors, which were used in experiments in this work. The dependence of $R_r = f(f_r)$ can be seen also in results of experiments presented here, such as in Fig. 50, Fig. 56, Fig. 64 and Fig. 71.

7.2 Tests on the 3,5 kW Induction Machine

Laboratory workplace with induction machine 1AY112L-6 (producer EM Brno) has been the pivotal place for the development and measurements. Equipped with a test bench of this 3,5 kW induction machine coupled to a loading DC machine (see Fig. 44), converter, measurement apparatus control system it offered all the needed material for successful tuning of the method. Fig. 43 shows a block scheme of this workplace.

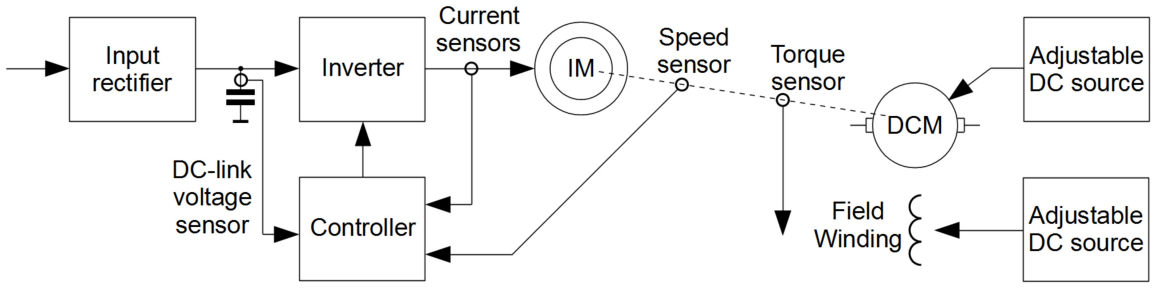

Fig. 43: Block scheme of the 3,5 kW machine test bench workplace.

The DC-link voltage sensor (LEM voltage transducer LV25-P) and current sensors (LEM LF205-S) were placed in a separate measurement module. Speed sensor (LARM IRC 300/1024) was connected at the rear end of the induction machine (between the end bell and cooling fan). It is an optical incremental encoder with 1024 impulses per revolution. Torque-measurements were provided by torque-measuring shaft (KTR DATAFLEX 22/100) connected between couplings of the common shaft between the two machines. The heart of the control system was a TI TM4C123G-H6PM microcontroller with 12-bit successive approximation AD converters.
As mentioned in chapter 7.1, it is not representative to compare values obtained by the proposed identification method with values obtained by conventional methods (laboratory standard tests, chapter 5.1). However these values should be stated here for completeness and also as a matter of interest. R_{rstd} = 1,04 Ω and L_{mstd} = 106 mH (*std* in the indices as *standard tests*).

Tab. 2: Rated values of 3,5 kW induction machine (1AY112L-6).

Rated values		**Construction details**	
Rated power P_n	3,5 kW	Number of poles $2p$ (-)	6
Rated supply voltage (line to line) U_{sn}	380 V	Connection	Y
Rated supply frequency f_{sn}	50 Hz	Type of rotor	Squirrel cage
Rated line current I_{sn}	11 A	Rotor conductor material	Copper
Rated cos φ	0,6	Class of insulation	F (180)
Rated efficiency η	80,6 %	Type of cooling	IC416
Rated speed n_n	965 min^{-1}	$L_{\sigma s}$: $L_{\sigma r}$ ratio	1:1
Rated torque M_n	30 N·m		

Tab. 3: Values of parameters of tested 3,5 kW machine used for identification method.

Parameter	**Value**
Stator resistance R_s	1,11 Ω
Stator leakage inductance $L_{\sigma s}$	8,25 mH
Rotor leakage inductance $L_{\sigma r}$	8,25 mH

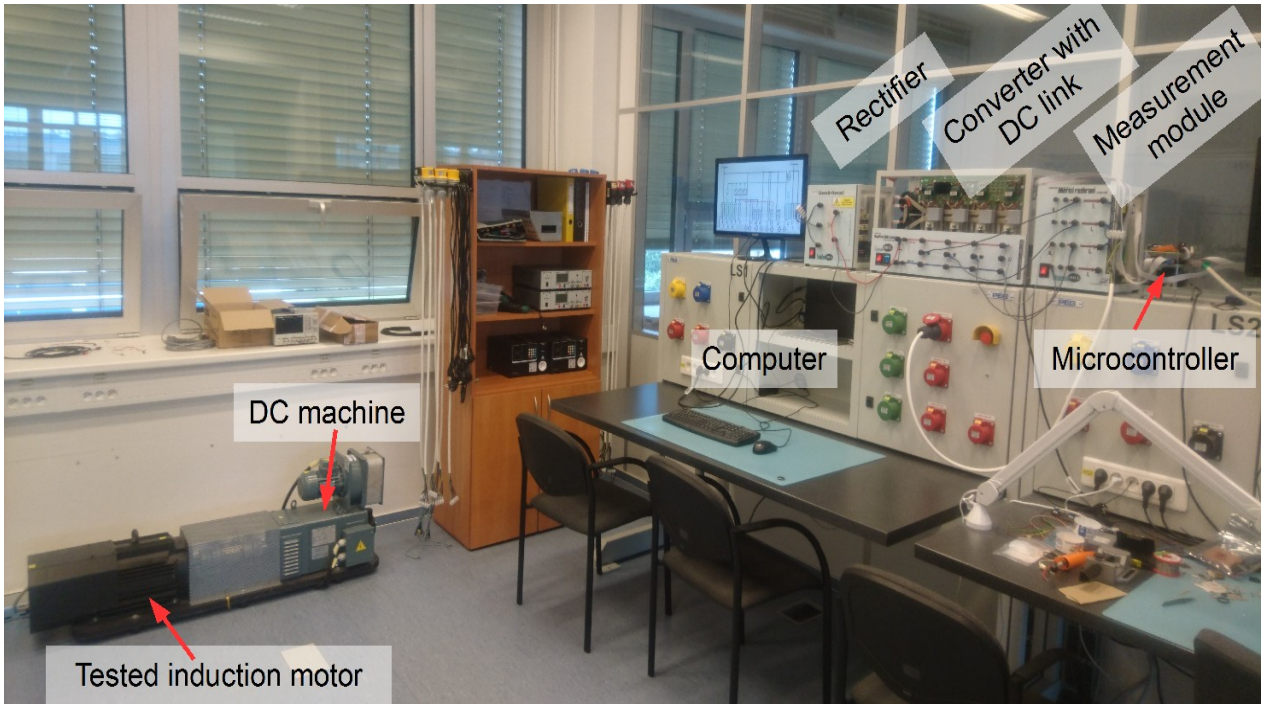

Fig. 44: Workplace of the 1AY112L-6 3,5 kW tested induction machine.

7.2.1 Warming Test

Warming test was performed by loading the tested induction machine with a constant load of 6 N·m for 60 minutes. Change of rotor resistance R_r and frame warming is depicted in Fig. 45. Data for each point were averaged from 12 sets of samples of input quantities, the time span between these samples was 10 seconds. Temperature of the machine frame was measured with a PT100 sensor. The initial temperature was 28 °C, the final temperature 75 °C, resulting in a warming of 47 °C. R_r rose from 0.99 Ω to 1.15 Ω which is an increase by 16%.

Considering the well-known equation for temperature dependence of metals (57), and assuming the linear behaviour of this dependence (as stated in chapter 4.1.7), this change of resistance estimated by the proposed method is in good accordance with it.

$$R_{\vartheta 2} = R_{\vartheta 1} \cdot (1 + 0{,}0038 \cdot 47) = 1{,}18 \cdot R_{\vartheta 1}, \tag{113}$$

where $\Delta\vartheta = 47$ °C is the warming during the test and $\alpha_{20Cu} = 0.0038\ \mathrm{K}^{-1}$ is the temperature coefficient for copper (material of the cage of the tested machine). The result of (113) means a rise by 18% from the initial value $R_{\vartheta 1}$ compared to 16% obtained by the proposed method. This comparison is however only rough as for example the absolute temperature of the rotor is unknown to us.

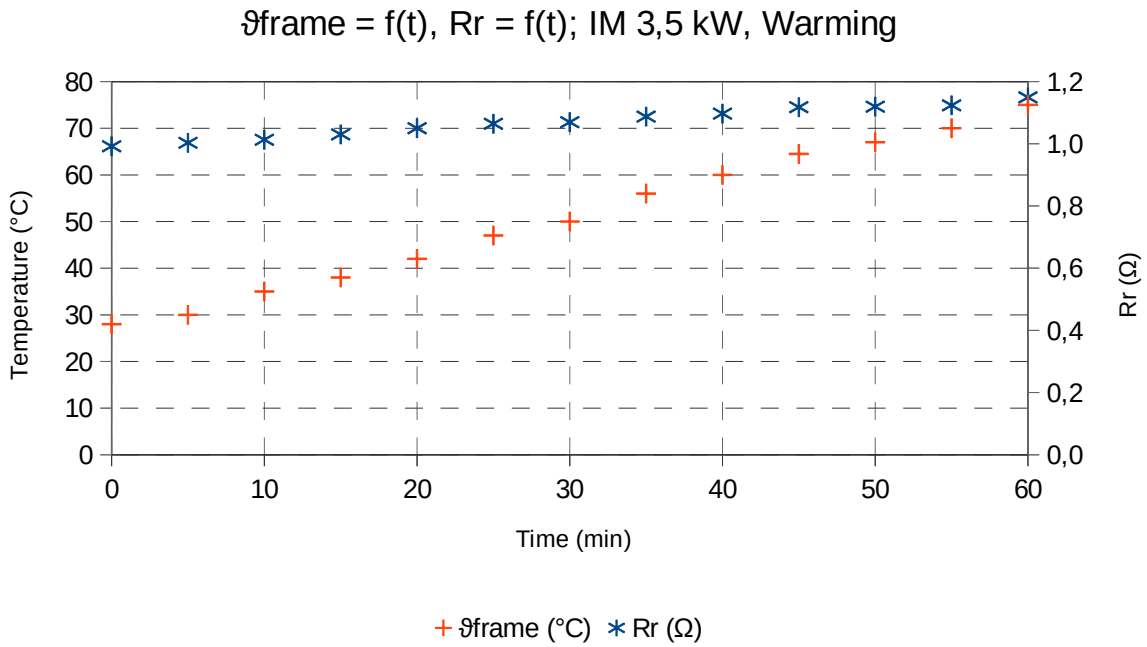

Fig. 45: R_r and machine frame temperature ϑ_{frame} change during warming test, IM 3,5 kW.

Fig. 46 shows values of L_m estimated by the proposed method in a course of time during the warming test. There is no visible influence of temperature upon magnetizing inductance which corresponds with theoretical assumptions (see chapter 4.1.6).

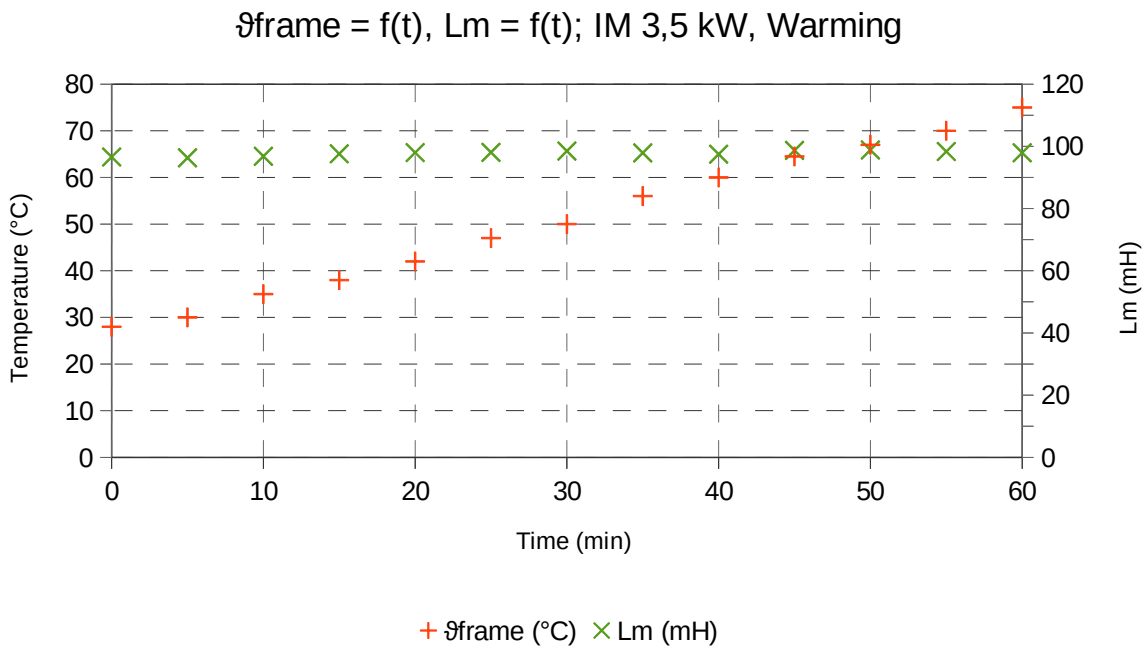

Fig. 46: L_m and frame temperature ϑ_{frame} in a course of time during warming test, IM 3,5 kW.

Both stator voltage and current were kept almost constant during this warming test (see Fig. 47) - stator current was supplied from a converter with a current loop. Because of that, there is a small variance of stator current. We used this variance to show the dependence of L_m on the magnetizing component of stator current (I_{sd}) in Fig. 48 where it is depicted in better scale. This dependence

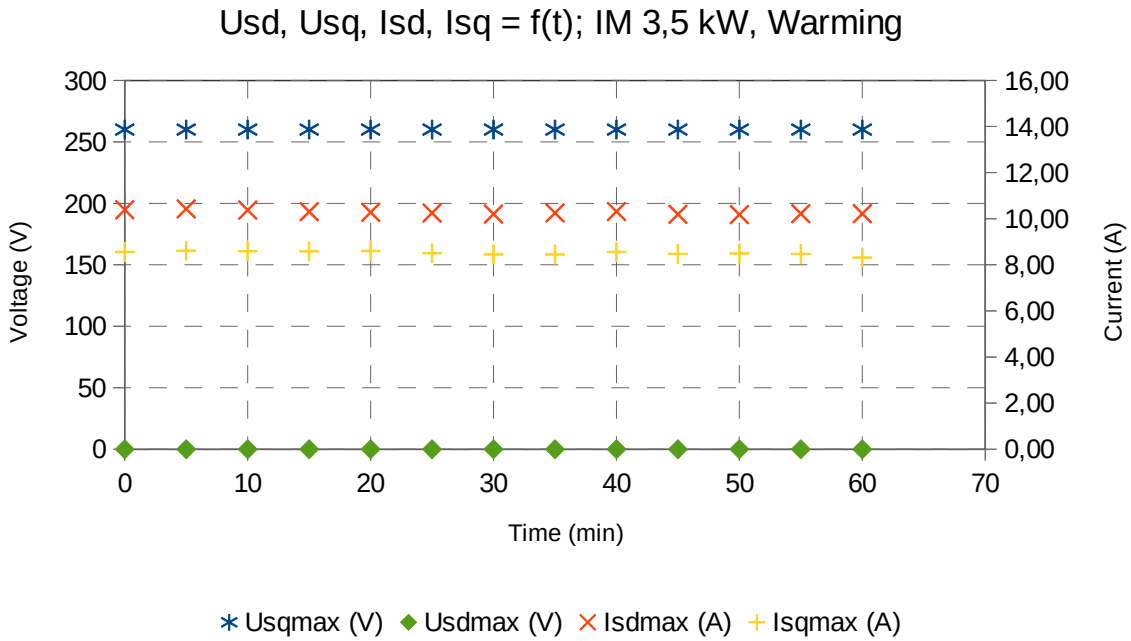

Fig. 47: Stator voltage components and stator current components during warming test, IM 3,5 kW.

under different loads and frequencies is shown also in Fig. 51. Saturation of the L_m is also visible as a function of magnetizing current magnitude $|I_m|$ shown in Fig. 49.Such dependences are presented

in [2], [7], [162] and discussed in chapter 4.1.6, so it can be regarded as another proof of the results obtained by the proposed method.

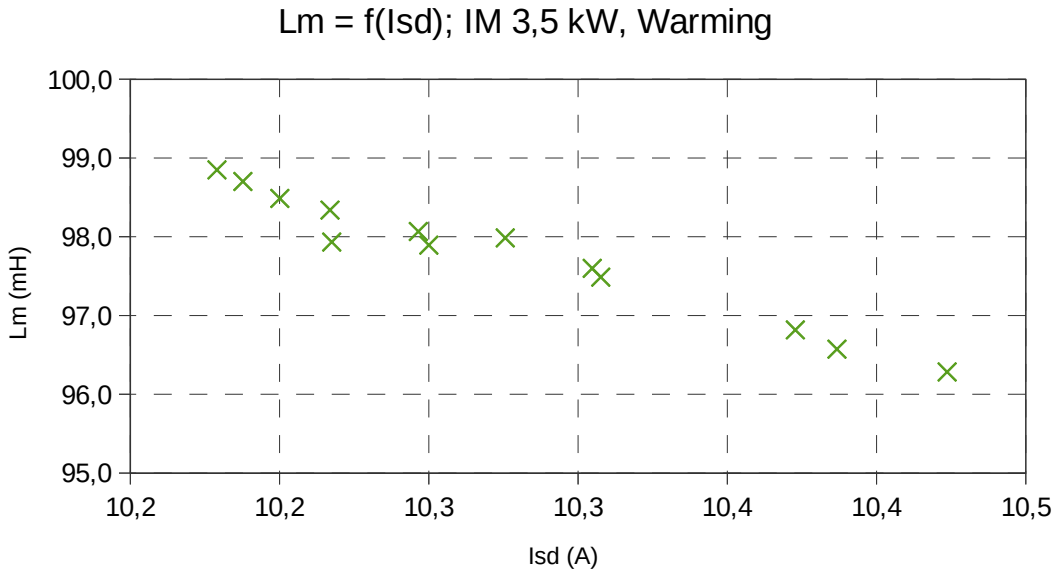

Fig. 48: L_m as a function of stator current component I_{sd} during warming test, IM 3,5 kW.

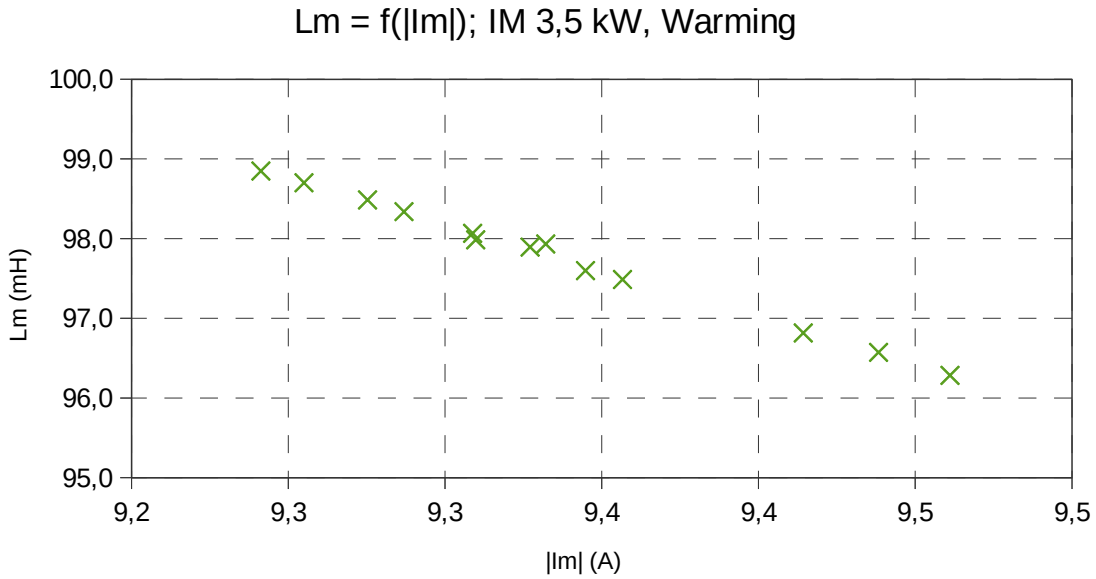

Fig. 49: L_m as a function of magnetizing current magnitude $|L_m|$ during warming test, IM 3,5 kW.

7.2.2 Tests with Different Loads and Frequencies

Another set of measurements was conducted with different load torques and four different stator frequencies, namely 20, 30, 40 and 50 Hz. Measurement at each frequency is represented by five working points with different loads. Temperature difference among measurement points did not exceed 5 °C so its influence should not be significant in this case. Each measurement point was averaged from five samples with a time span of 10 seconds.

Stator voltage is set according to U/f (voltage to frequency) ratio. For measurements at stator frequencies 20, 30 and 40 Hz, this ratio was 6,5. At 50 Hz, field weakening area was reached, therefore the U/f ratio was only 5,6. The voltage vector is again aligned with the q axis, so the d component (U_{sd}) is zero in all presented cases.

Tab. 4: Measurement at f_s = 20 Hz (ω_s = 125,66 rad·s^{-1}), U_{sd} = 0 V and U_{sq} = 130 V, IM 3,5 kW.

Measured input quantities					
M_{load} (N·m)	9,5	16,0	23,2	30,5	38,5
I_{sd} (A)	9,28	9,01	8,90	9,02	9,37
I_{sq} (A)	3,19	4,66	6,34	8,25	10,41
ω_m (rad·s^{-1})	123,58	121,84	119,68	117,14	113,82
f_r (Hz)	0,331	0,609	0,952	1,360	1,890
Estimated parameters					
R_r (Ω)	0,736	0,826	0,888	0,924	0,972
L_m (mH)	99,2	101,8	103,6	104,3	104,6
Values calculated for verification					
R_{rv} (Ω)	0,736	0,826	0,888	0,924	0,971
I_{sdc} (A)	9,28	9,01	8,90	9,20	9,37
I_{sqc} (A)	3,19	4,66	6,34	8,25	10,41

Tab. 5: Measurement at f_s = 30 Hz (ω_s = 188,50 rad·s^{-1}), U_{sd} = 0 V and U_{sq} = 195 V, IM 3,5 kW.

Measured input quantities					
M_{load} (N·m)	9,6	16,0	23,2	30,3	37,8
I_{sd} (A)	9,59	9,46	9,52	9,37	10,10
I_{sq} (A)	2,84	4,22	5,80	7,51	9,31
ω_m (rad·s^{-1})	186,41	184,84	182,87	180,75	178,17
f_r (Hz)	0,332	0,581	0,895	1,260	1,640

Measured input quantities					
Estimated parameters					
R_r (Ω)	0,783	0,847	0,905	0,928	0,967
L_m (mH)	97,5	99,1	99,4	99,3	98,8
Values calculated for verification					
R_{rv} (Ω)	0,783	0,847	0,905	0,928	0,967
I_{sdc} (A)	9,59	9,46	9,52	9,73	10,10
I_{sqc} (A)	2,84	4,22	5,80	7,51	9,31

Tab. 6: Measurement at f_s = 40 Hz (ω_s = 251,33 rad·s^{-1}), U_{sd} = 0 V and U_{sq} = 260 V, IM 3,5 kW.

Measured input quantities					
M_{load} (N·m)	9,7	16,0	23,0	30,2	37,9
I_{sd} (A)	9,71	9,67	9,78	10,07	10,48
I_{sq} (A)	2,60	3,92	5,47	7,08	8,76
ω_m (rad·s^{-1})	249,24	247,75	245,84	243,91	241,54
f_r (Hz)	0,332	0,570	0,873	1,180	1,550
Estimated parameters					
R_r (Ω)	0,826	0,878	0,926	0,940	0,976
L_m (mH)	97,0	99,8	97,8	97,0	96,0
Values calculated for verification					
R_{rv} (Ω)	0,825	0,878	0,926	0,940	0,976
I_{sdc} (A)	9,71	9,67	9,78	10,07	10,48
I_{sqc} (A)	2,60	3,92	5,47	7,08	8,76

Tab. 7: Measurement at f_s = 50 Hz (ω_s = 314,16 rad·s^{-1}), U_{sd} = 0 V and U_{sq} = 280 V, IM 3,5 kW.

Measured input quantities					
M_{load} (N·m)	9,7	15,6	23,3	30,4	37,4
I_{sd} (A)	7,73	7,88	8,09	8,85	9,44
I_{sq} (A)	2,61	4,13	5,83	7,82	9,52
ω_m (rad·s^{-1})	311,36	309,34	306,64	303,85	300,16
f_r (Hz)	0,445	0,776	1,200	1,640	2,230
Estimated parameters					

Measured input quantities					
R_r (Ω)	0,893	0,931	1,00	0,989	1,07
L_m (mH)	106,5	105,8	106,2	101,3	100,2
Values calculated for verification					
R_{rv} (Ω)	0,893	0,930	1,00	0,989	1,073
I_{sdc} (A)	7,73	7,88	8,09	8,85	9,44
I_{sqc} (A)	2,61	4,13	5,83	7,82	9,52

Fig. 50 shows the dependence of R_r to slip frequency f_r, which corresponds with the description in chapter 4.1.9 and 7.1.5. With the rising load torque M_{load} the mechanical speed decreased, which resulted in an increase of slip and therefore the slip frequency f_r. There is also a visible influence of stator frequency f_s. R_r is higher mainly due to skin effect in rotor bars which is more significant the higher the frequencies are.

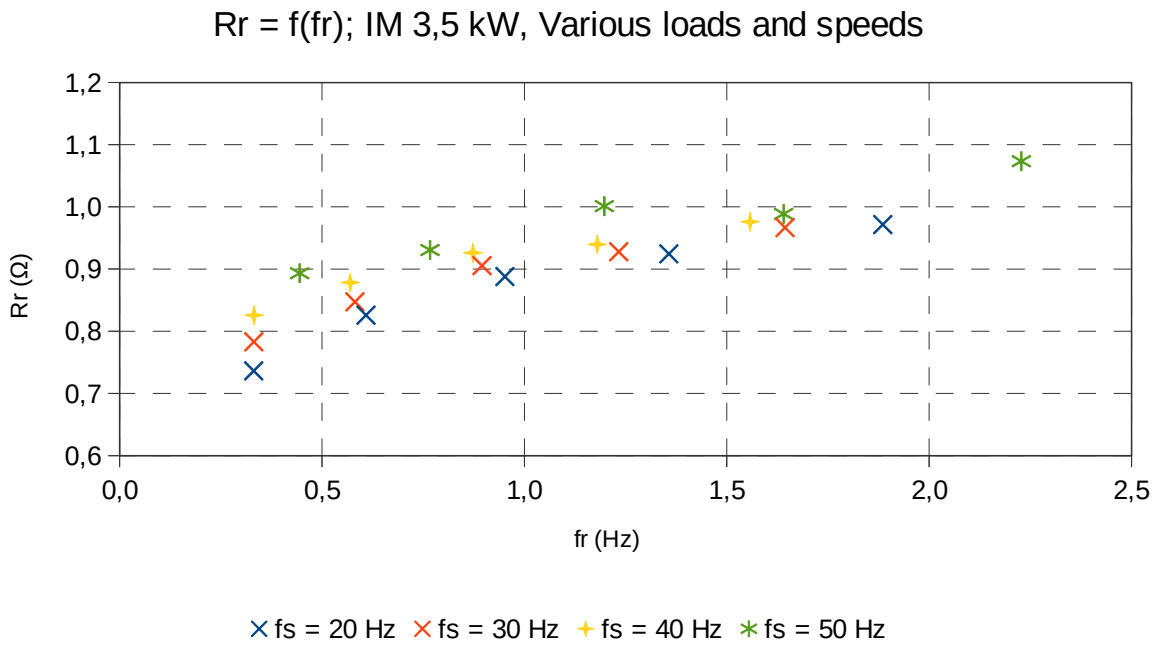

Fig. 50: R_r as a function of slip frequency f_r for different stator frequencies f_s, IM 3,5 kW.

There is again a visible dependence of L_m on the magnetizing component of stator current component I_{sd} (described in chapters 7.1.4 and mainly 4.1.6) shown in Fig. 51. In this figure, data from all the measurements with different loads and different frequencies are grouped and the trend corresponds with the expected results and findings published elsewhere. It can be further seen, that in three cases out of four, L_m decrease with the rising stator frequency f_s. However the highest switching frequency, on the contrary, has values of L_m higher than the rest of three. The cause of this should be the modulation that was used for particular stator frequency which can cause additional saturation.

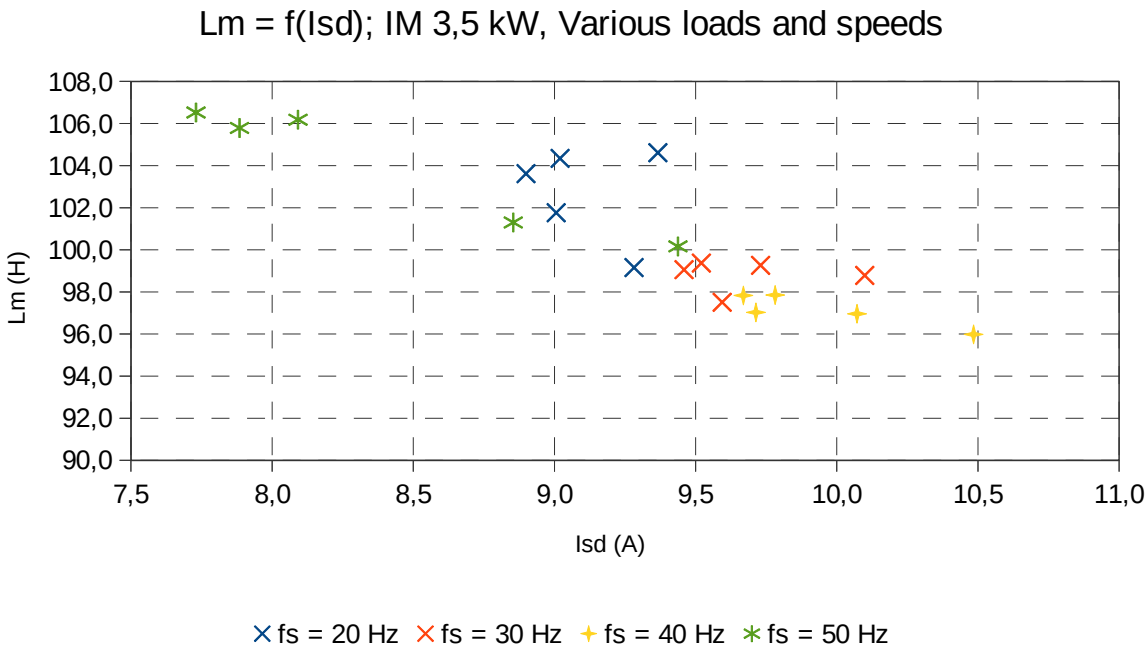

Fig. 51: L_m as a function of stator current component I_{sd} from measurements with different loads and different stator frequencies f_s, IM 3,5 kW.

7.3 Tests on the 15 kW Induction Machine

Another machine where the proposed method was tested was a 15 kW 1AOE132MK from EM Brno. As a load a DC dynamometer MS2812-4 was used (Fig. 53) so the overall configuration of the test bench workplace (Fig. 52) is similar to 3,5 kW machine (Fig. 43). The only difference is that there is inly a speed sensor (RC 300/1024 with 1024 impulses per revolution) on the common shaft. Torque measurement is carried out by the dynamometer. The controller as well as the converter and LEM sensors for voltage and currents were used the same as for the 3,5 kW machine, for their parameters see chapter 7.2. Rated values and construction details are in Tab. 8.

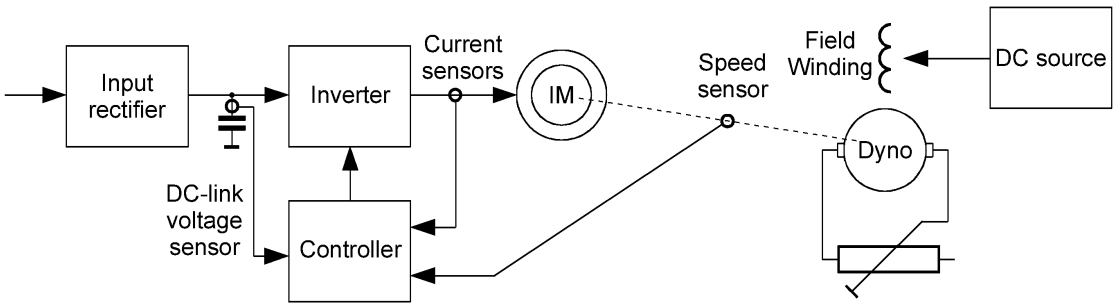

Fig. 52: Block scheme of the 15 kW machine test bench workplace.

Rotor resistance and magnetizing inductance obtained by conventional methods (laboratory standard tests) are R_{rstd} = 231 mΩ and L_{mstd} = 58,5 mH with the rest of parameters stated in Tab. 9.

Tab. 8: Rated values of 15 kW induction machine (1AOE132MK).

Rated values		Construction details	
Rated power P_n	15 kW	Number of poles *2p* (-)	4
Rated supply voltage (line to line) U_{sn}	380 V	Connection	Y
Rated supply frequency f_{sn}	50 Hz	Type of rotor	Squirrel cage
Rated line current I_{sn}	31,2 A	Rotor conductor material	Copper
Rated cos φ	0,805	Class of insulation	H (200)
Rated efficiency η	90,8 %	Type of cooling	IC411
Rated speed n_n	1455 min^{-1}	$L_{\sigma s}$: $L_{\sigma r}$ ratio	4:6
Rated torque M_n	98,1 Nm		

Tab. 9: Values of parameters of tested 15 kW machine used for identification method.

Parameter	Value
Stator resistance R_s	163,6 mΩ
Stator leakage inductance $L_{\sigma s}$	1,78 mH
Rotor leakage inductance $L_{\sigma r}$	2,68 mH

Fig. 53: 1AOE132MK-4 15 kW tested induction machine on a test bench stand.

7.3.1 Warming Test

Warming test was performed by loading the tested induction machine with a constant load of 88 Nm for 60 minutes with stator frequency f_s = 50 Hz and speed around rated machine speed. Change of rotor resistance R_r and frame warming (temperature of the frame) is depicted in Fig. 54. Data for each point were averaged from 12 sets of samples of input quantities, the time span between these samples was 10 seconds. Temperature of the machine frame was measured with a PT1000 sensor. The initial temperature was 44,8 °C, the final temperature 99,5 °C, resulting in a warming of 54,7 °C. R_r rose from 169 mΩ to 204 mΩ which is an increase by 21%.

Comparing it with the value from equation for temperature dependence of metals (57), (see chapter 4.1.7), in a form of (114), this change of resistance estimated by the proposed method is in good accordance with it:

$$R_{\vartheta 2} = R_{\vartheta 1} \cdot (1 + 0{,}0038 \cdot 54{,}7) = 1{,}21 \cdot R_{\vartheta 1}, \tag{114}$$

where $\Delta\vartheta$ = 54,7 °C is the warming during the test and α_{20Cu} = 0.0038 K^{-1} is the temperature coefficient of copper – the material of the rotor cage.

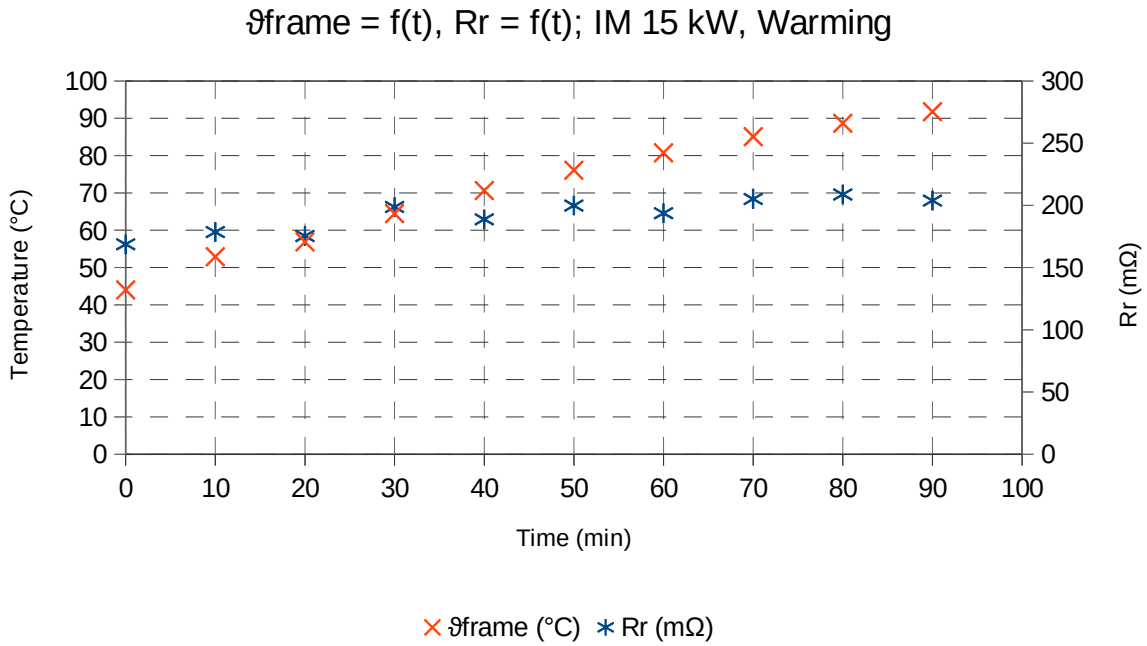

Fig. 54: R_r and machine frame temperature ϑ_{frame} change during warming test, IM 15 kW.

Magnetizing inductance is again almost constant. Nevertheless a small variance of stator current enables to show an influence of saturation to magnetizing inductance L_m. Dependence of L_m on magnetizing current magnitude $|I_m|$ is shown in in zoomed detail in Fig. 55 - a decline of L_m with the rising $|I_m|$ is clearly visible.

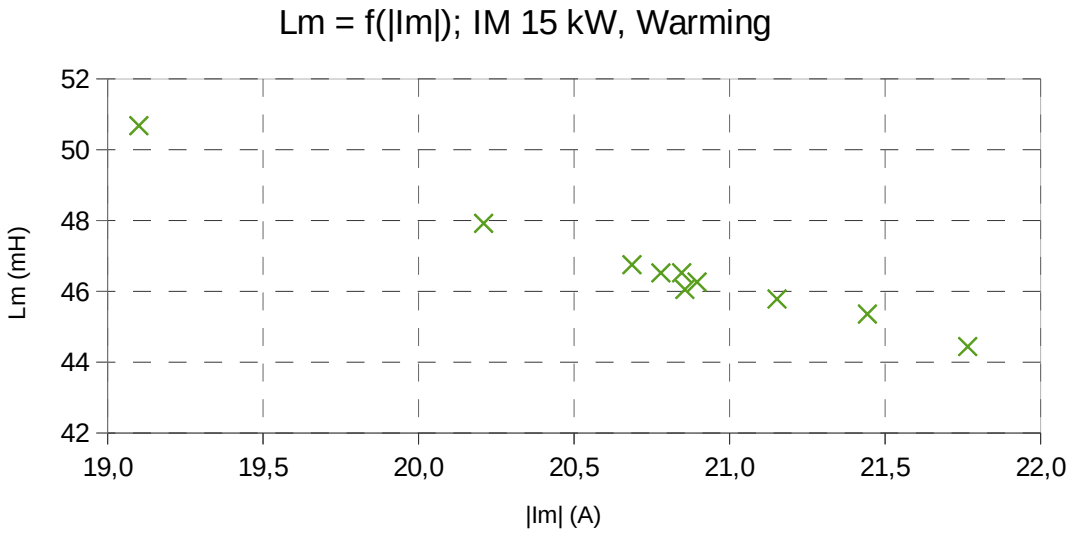

Fig. 55: L_m as a function of magnetizing current magnitude $|I_m|$ during warming test, IM 15 kW.

7.3.2 Test with Different Loads

Measurement was conducted with different load torques for stator frequency $f_s = 50$ Hz. Tab. 10 shows the data. Each measurement point was averaged from ten samples with a time span of 10 seconds.

Tab. 10: Measurement at $f_s = 50$ Hz ($\omega_s = 314{,}16$ rad·s^{-1}) and $U_{sd} = 0$ V, IM 15 kW.

Measured input quantities					
M_{load} (N·m)	15,9	36,1	56,3	73,8	86,2
U_{sq} (V)	328,27	326,62	324,79	323,79	322,60
I_{sd} (A)	24,80	24,20	24,06	24,34	25,38
I_{sq} (A)	5,40	11,93	18,62	24,48	28,72
ω_m (rad·s^{-1})	313,71	312,37	311,06	309,95	308,96
f_r (Hz)	0,071	0,285	0,494	0,669	0,827
Estimated parameters					
R_r (mΩ)	83,7	145,9	158,8	161,5	168,1
L_m (mH)	40,3	41,8	43,3	44,7	44,4
Values calculated for verification					
R_{rv} (Ω)	83,7	145,9	158,8	161,5	168,1
I_{sdc} (A)	24,80	24,20	24,06	24,34	25,38
I_{sqc} (A)	5,40	11,93	18,62	24,48	28,72

Temperature difference among measurement points did not exceed 5 °C so its influence should not be significant in this case. The voltage vector is again aligned with the q axis, so the d component (U_{sd}) is zero. Fig. 56 shows the dependence of R_r to slip frequency f_r, which corresponds with observations described in chapter 4.1.9 and also published elsewhere - R_r rises with the rising f_r mainly due to skin effect.

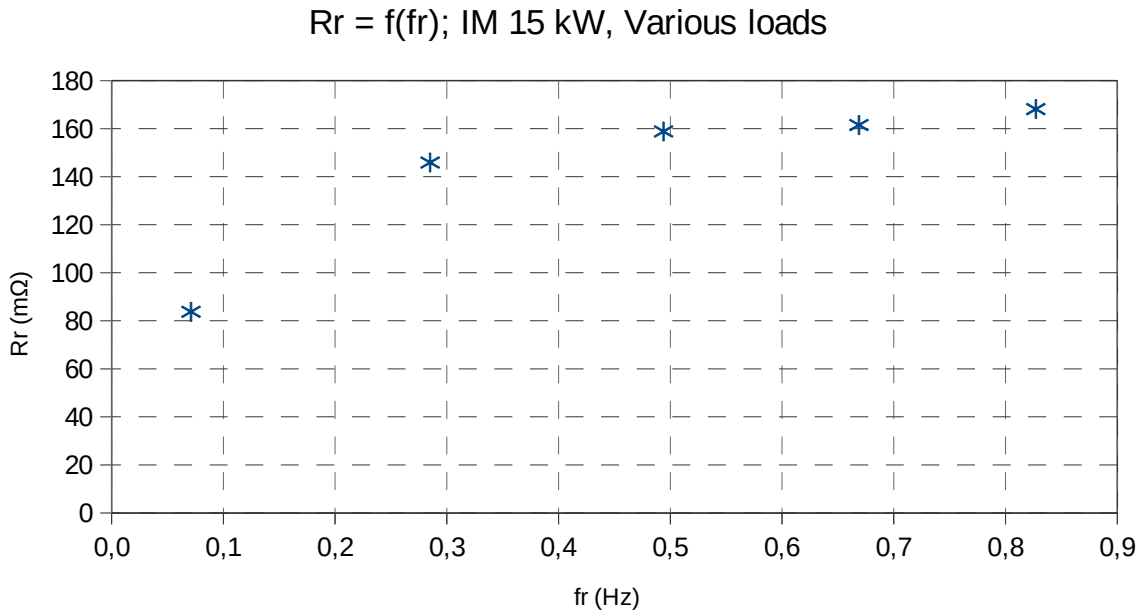

Fig. 56: R_r as a function of slip frequency f_r, IM 15 kW.

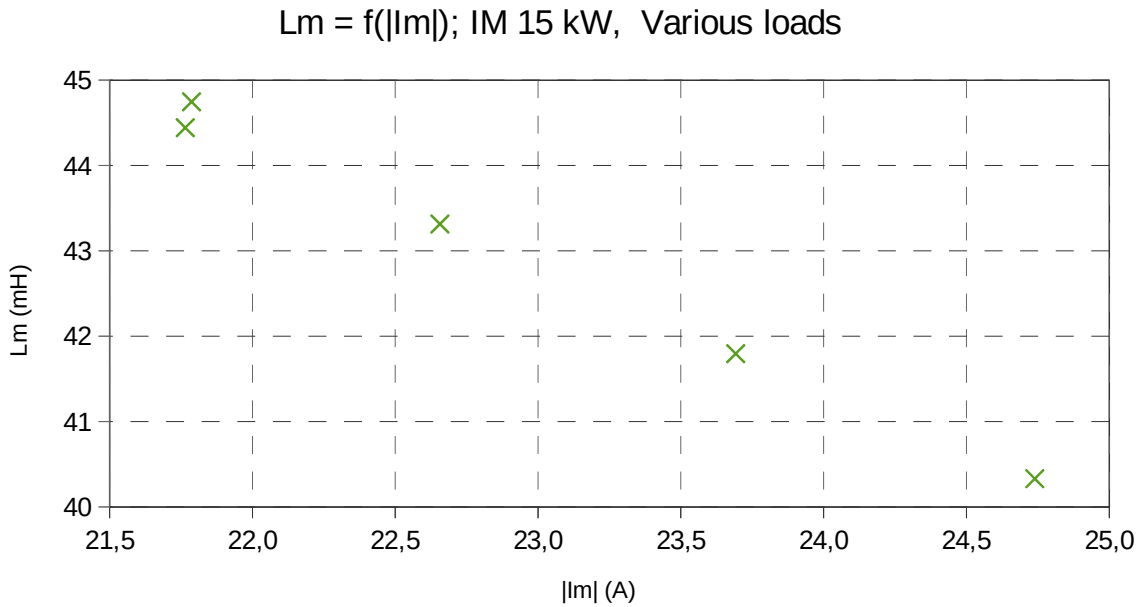

Fig. 57: L_m as a function of magnetizing current magnitude $|I_m|$ from measurements with different loads, IM 15 kW.

There is again a visible dependence of L_m on the magnetizing component of stator current component I_{sd} (described in chapter 4.1.6) shown in Fig. 57. In this figure, data from all the measurements with different loads and different frequencies are grouped and the trend corresponds with the findings stated in chapter 4.1.6 and published elsewhere.

7.4 Tests on the 180 kW induction machine

Tested machine YJ150B with rated power of 180 kW is a squirrel cage induction motor manufactured by CRRC Yongji (now part of CRRC). This machine is based on technology transfer form Hitachi company and is currently used mainly in electric multiple units for commuter transportation (S-bahn equivalents and metro trains such as type B metro cars in various Chinese cities). Technical details and rated values of this machine are shown in Tab. 11. As a load, induction machines YJ209A were used (Fig. 67 - machines with separate cooling on the left side).

Test bench workplace was equipped with four of these machines and further with three loading machines with the possibility to tune operation of multiple machines from a single converter. According to standard test the machines were very similar with the differences in parameters under 2%. Rotor resistance and magnetizing inductance obtained by conventional methods (laboratory standard tests) are R_{rstd} = 135 mΩ and L_{mstd} = 74,1 mH. Rest of parameters is stated in Tab. 12, rated values in Tab. 11. As the converter was not equipped with measurement of current for particular machines, only one machine was connected and the tests of the proposed on-line method were conducted only on this single machine. Block scheme of the test bench is presented in Fig. 58.

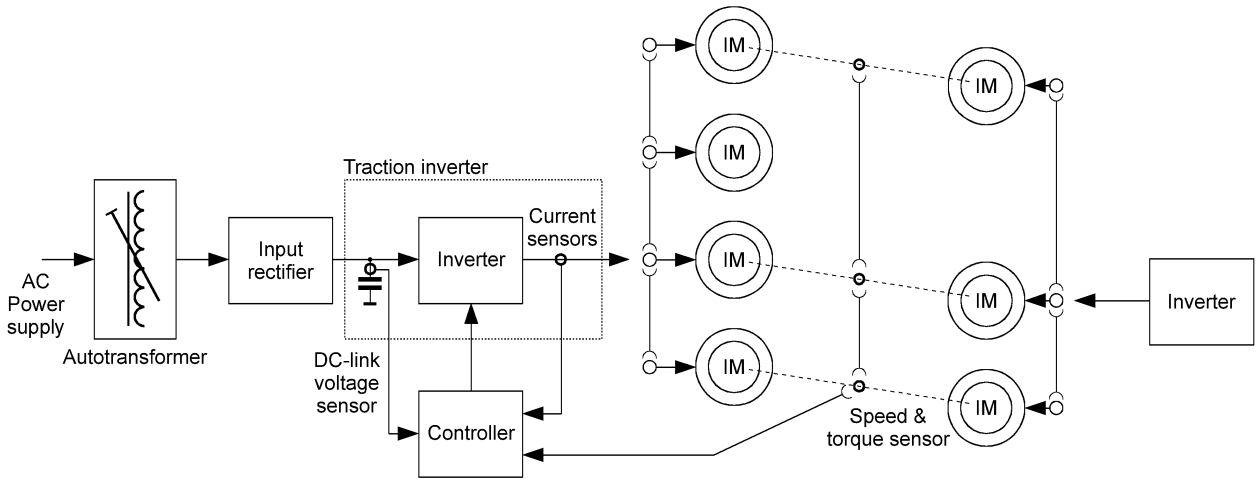

Fig. 58: Block scheme of the 180 kW machine test bench workplace.

The converter is also a traction equipment from a correspondent EMU as the tested induction machine. It is equipped FZ1200R33KF2C IGBT modules and installed in an underfloor container (Fig. 60). As it is meant to be connected directly to the catenary wires or third rail, it is supplied from an autotransformer and a diode rectifier in the laboratory. As a speed and torque combined sensor, JN-338-AN is used, phase currents were measured with LEM LF2006 current sensors, DC link voltage with DV 6400 transducer. Controller of the system was equipped with TMS320F28335

microcontroller with 12-bit AD converters. This microcontroller is a common platform of CRRC traction vehicles.

Fig. 59: Right: YJ150B 180kW induction machines on a test bench stand; Left: load machines YJ209A.

Fig. 60: Converter of the 180 kW machines test bench.

Tab. 11: Rated values of 180 kW induction machine (YJ150B).

Rated values		Construction details	
Rated power P_n	180 kW	Number of poles *2p* (-)	4
Rated supply voltage (line to line) U_{sn}	1100 V	Connection	Y
Rated supply frequency f_{sn}	68 Hz	Type of rotor	Squirrel cage
Rated line current I_{sn}	116 A	Rotor conductor material	Copper
Rated cos φ	0,87	Class of insulation	H (200)
Rated efficiency η	94 %	Type of cooling	IC411
Rated speed n_n	2015 min^{-1}	$L_{\sigma s}$: $L_{\sigma r}$ ratio	4:6
Rated torque M_n	853 N·m		

Tab. 12: Values of parameters of tested 180 kW machine used for identification method.

Parameter	Value
Stator resistance R_s	95,3 mΩ
Stator leakage inductance $L_{\sigma s}$	1,13 mH
Rotor leakage inductance $L_{\sigma r}$	1,69 mH

7.4.1 Warming Test

Warming test was performed by loading the tested induction machine with a constant load of 510 N·m, 16 kW at mechanical speed 305 min^{-1} for 55 minutes. Change of rotor resistance R_r is depicted in Fig. 61. Data for each point were averaged from 10 sets of samples of input quantities, the time span between these samples was 10 seconds.

Temperature of the machine frame was measured with a PT100 sensor. The initial temperature was 27,2 °C, the final temperature 49,1 °C, resulting in a warming of 22 °C. R_r rose from 40,3 mΩ to 43,7 mΩ which is an increase by 8 %.

Considering the well-known equation for temperature dependence of metals (57), and assuming the linear behaviour of this dependence (as stated in chapter 4.1.7), this change of resistance estimated by the proposed method is in accordance with it as shown in (115).

$$R_{\vartheta 2} = R_{\vartheta 1} \cdot (1 + 0{,}0038 \cdot 22) = 1{,}08 \cdot R_{\vartheta 1}, \tag{115}$$

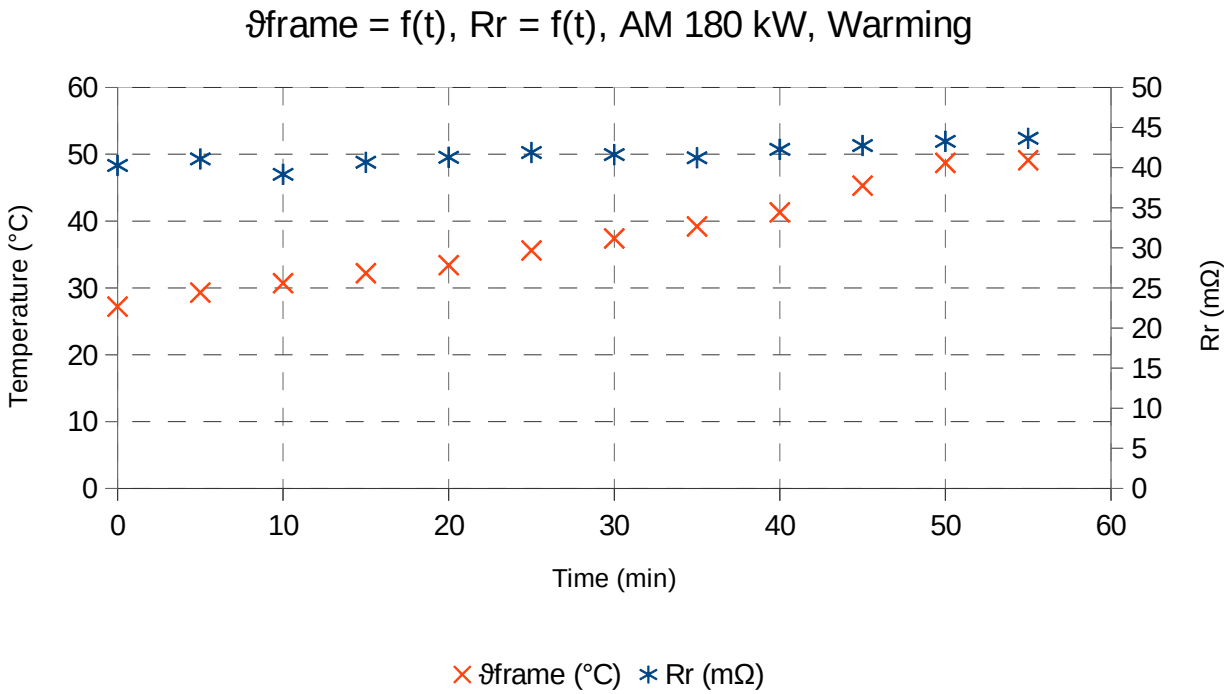

Fig. 61: R_r and machine frame temperature ϑ_{frame} change during warming test, IM 180 kW.

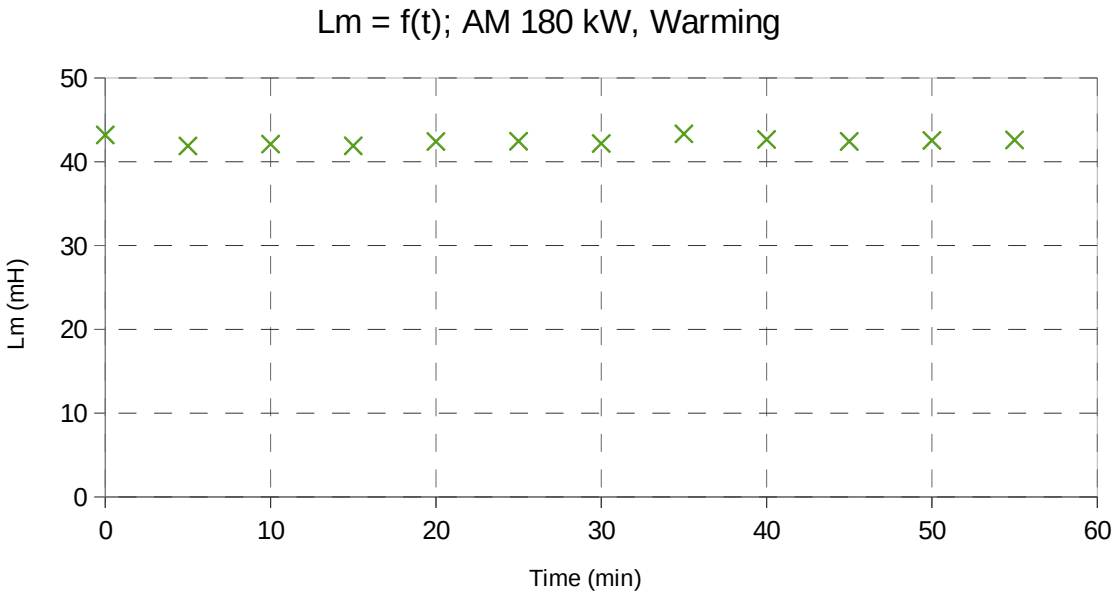

Fig. 62: L_m during warming test, IM 180 kW.

Fig. 62 shows values of L_m estimated by the proposed method in a course of time during the warming test. There is no visible influence of temperature upon magnetizing inductance which corresponds with theoretical assumptions (see chapter 4.1.6). However the small variance variance is present. If the existing variance of magnetizing current is used together with value of L_m as

$L_m = f(|I_m|)$, the clear decreasing dependence can be observed in Fig. 63. These expected results of saturation were presented and discussed in chapter 4.1.6.

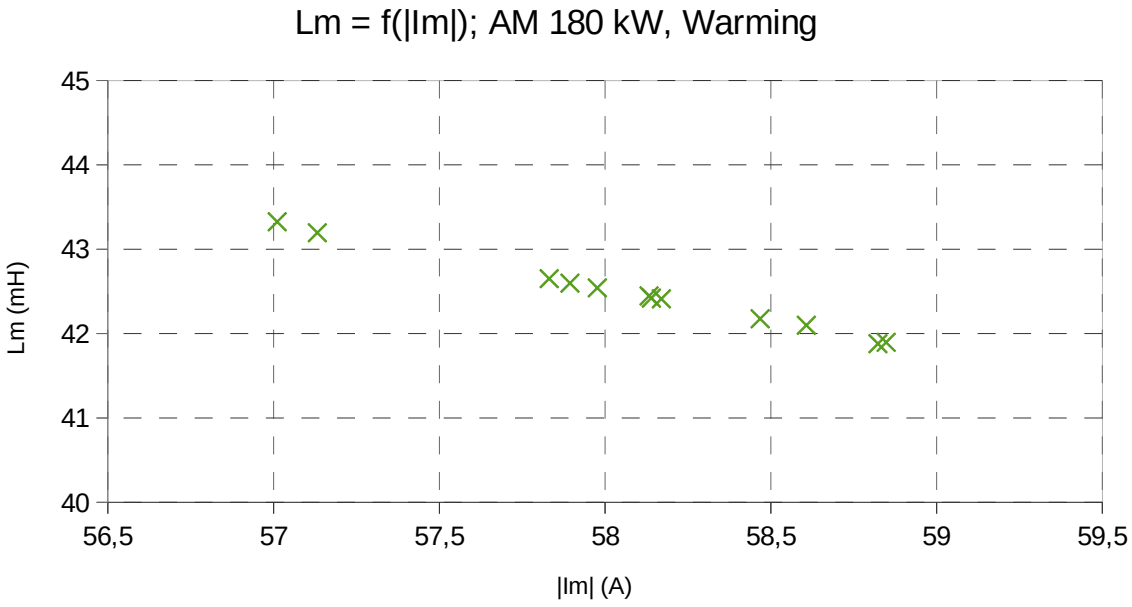

Fig. 63: L_m as a function of magnetizing current magnitude $|L_m|$ during warming test, IM 180 kW.

7.4.2 Tests with Different Loads and Frequencies

Another set of measurements was conducted with different load torques and different stator frequencies, namely 10, 20, 48, 53 and 63 Hz. Measurement at each frequency is represented by four working points with different loads. Temperature difference among measurement points did not exceed 5 °C so its influence should not be significant in this case. Each measurement point was averaged from ten samples with a time span of 10 seconds.

Stator voltage is set according to U/f (voltage to frequency) ratio. Controller of the converter however is not capable of maintaining this ratio at a fixed value, so it varied from 15 to 16,5 and therefore, value of ω_s is also presented for each point. The voltage vector is again aligned with the q axis, so the d component (U_{sd}) is zero in all presented cases. Important measured and calculated data are presented in Tab. 13, Tab. 14, Tab. 15, Tab. 16 and Tab. 17.

Tab. 13: Measurement at f_s = 10 Hz (U_{sd} = 0 V), IM 180 kW.

Measured input quantities				
M_{load} (N·m)	239	537	815	1090
U_{sq} (V)	152,63	156,15	162,08	174,63
ω_s (rad·s^{-1})	63,90	65,24	66,52	67,81
I_{sd} (A)	67,59	70,39	79,24	95,85
I_{sq} (A)	40,12	83,46	125,89	166,37

Measured input quantities				
ω_m (rad s^{-1})	63,40	63,92	64,42	64,88
f_r (Hz)	0,08	0,21	0,33	0,47
Estimated parameters				
R_r (mΩ)	28,73	33,99	34,83	37,40
L_m (mH)	33,11	33,37	33,48	32,24
Values calculated for verification				
R_{rv} (mΩ)	28,73	33,99	34,83	37,40
I_{sdc} (A)	67,59	70,39	79,24	95,85
I_{sqc} (A)	40,12	83,46	125,89	166,37

Tab. 14: Measurement at f_s = 20 Hz (U_{sd} = 0 V), IM 180 kW.

Measured input quantities				
M_{load} (N·m)	290	581	877	1181
U_{sq} (V)	315,79	321,3	330,13	341,69
ω_s (rad·s^{-1})	126,78	128,14	129,49	130,86
I_{sd} (A)	80,05	85,02	95,73	110,74
I_{sq} (A)	42,84	83,08	123,41	163,47
ω_m (rad s^{-1})	126,33	126,94	127,52	128,10
f_r (Hz)	0,07	0,19	0,31	0,44
Estimated parameters				
R_r (mΩ)	24,32	32,67	35,49	37,37
L_m (mH)	29,69	29,62	29,16	28,72
Values calculated for verification				
R_{rv} (mΩ)	24,32	32,67	35,49	37,37
I_{sdc} (A)	80,05	85,02	95,73	110,74
I_{sqc} (A)	42,84	83,08	123,41	163,47

Tab. 15: Measurement at f_s = 48 Hz (U_{sd} = 0 V), IM 180 kW.

Measured input quantities				
M_{load} (N·m)	351	656	968	1289
U_{sq} (V)	766,82	779,04	796,96	818,36

Measured input quantities				
ω_s (rad·s^{-1})	302,96	304,36	305,92	307,62
I_{sd} (A)	90,00	98,02	111,2	130,4
I_{sq} (A)	49,29	91,23	130,49	170,58
ω_m (rad·s^{-1})	302,31	302,97	303,68	304,54
f_r (Hz)	0,10	0,22	0,36	0,49
Estimated parameters				
R_r (mΩ)	30,22	34,93	39,09	40,81
L_m (mH)	27,25	27,00	26,45	25,39
Values calculated for verification				
R_{rv} (mΩ)	30,22	34,93	39,10	40,81
I_{sdc} (A)	90,00	98,02	111,06	130,4
I_{sqc} (A)	49,29	91,23	130,49	170,58

Tab. 16: Measurement at f_s = 53 Hz (U_{sd} = 0 V), IM 180 kW.

Measured input quantities				
M_{load} (N·m)	351	656	968	1289
U_{sq} (V)	848,91	859,35	876,62	904,09
ω_s (rad·s^{-1})	336,62	337,97	339,48	341,28
I_{sd} (A)	88,18	95,88	111,14	130,74
I_{sq} (A)	50,77	90,56	131,17	170,35
ω_m (rad s^{-1})	335,66	336,31	337,00	337,89
f_r (Hz)	0,15	0,27	0,39	0,54
Estimated parameters				
R_r (mΩ)	43,30	41,81	42,57	44,71
L_m (mH)	27,86	27,56	26,40	25,33
Values calculated for verification				
R_{rv} (mΩ)	43,30	41,81	42,57	44,71
I_{sdc} (A)	88,18	95,88	111,14	130,74
I_{sqc} (A)	50,77	90,56	131,17	170,35

Tab. 17: Measurement at f_s = 63 Hz (U_{sd} = 0 V), IM 180 kW.

Measured input quantities				
M_{load} (N·m)	450	780	1111	1369
U_{sq} (V)	1003,95	1011,18	1036,74	1021,6
ω_s (rad·s^{-1})	400,06	401,65	403,36	405,92
I_{sd} (A)	90,07	99,9	117,82	129,61
I_{sq} (A)	62,45	110,63	150,85	190,06
ω_m (rad s^{-1})	399,03	399,74	400,50	401,90
f_r (Hz)	0,16	0,30	0,45	0,64
Estimated parameters				
R_r (mΩ)	37,34	38,41	41,97	44,71
L_m (mH)	27,62	27,67	26,48	27,94
Values calculated for verification				
R_{rv} (mΩ)	37,34	38,41	41,97	44,71
I_{sdc} (A)	90,08	99,90	117,82	129,61
I_{sqc} (A)	62,45	110,63	150,85	190,06

Fig. 64 shows the dependence of R_r to slip frequency f_r, which corresponds with the description in chapter 4.1.9 and 7.1.5. With the rising load torque M_{load} the mechanical speed decreased, which resulted in an increase of slip and therefore the slip frequency f_r. There is also a visible influence of stator frequency f_s. Not all the points behave as expected which is caused by the modulation used, which is unfortunately unknown. The number of switching pulses per period can influence the the skin effect. In general, R_r is higher mainly due to skin effect in rotor bars which is more significant the higher the frequencies are.

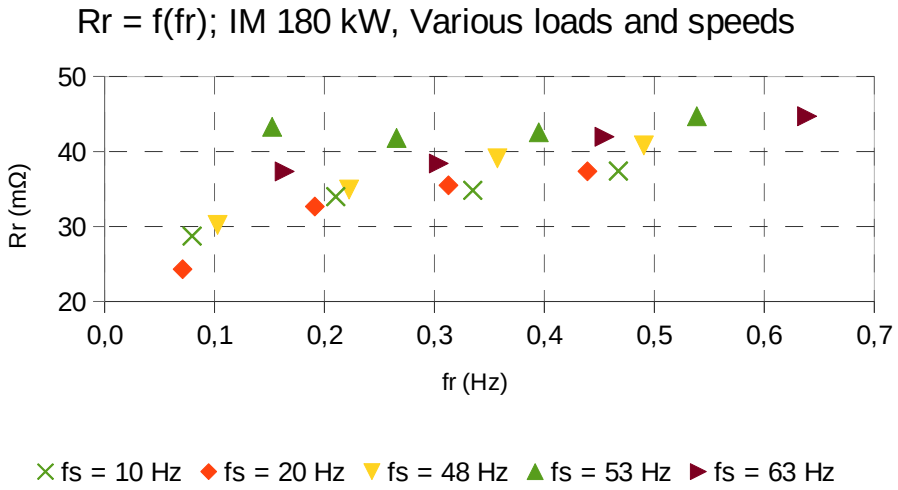

Fig. 64: R_r as a function of slip frequency f_r for different stator frequencies f_s, IM 180 kW.

There is again a visible dependence of L_m on the magnetizing component of stator current component I_{sd} (described in chapters 7.1.4 and mainly 4.1.6) shown in Fig. 65. In this figure, data from all the measurements with different loads and different frequencies are grouped and the trend corresponds with the expected results and findings published elsewhere.

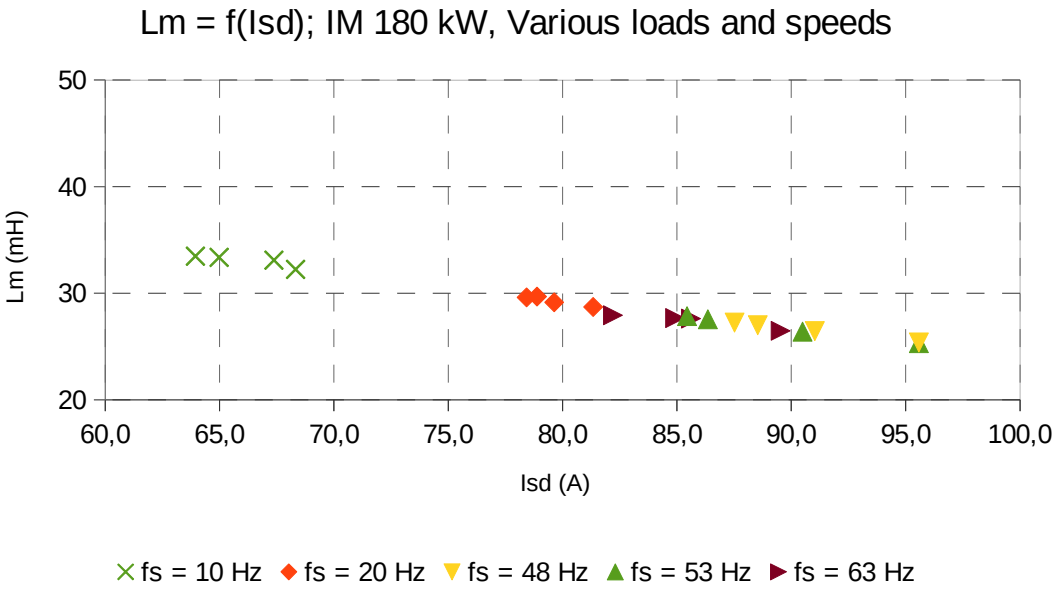

Fig. 65: L_m as a function of stator current component I_{sd} from measurements with different loads and different stator frequencies f_s, IM 180 kW.

7.5 Tests on the 1640 kW Induction Machine

Finally the method was tested on a YJ130A induction machine (Fig. 67) with rated power of 1640 kW. Manufacturer is the CNR Yongji (now part of CRRC). This machine is used in traction drives of high power locomotives (e.g. HXD3B Co'Co' locomotive). It is again a squirrel cage rotor machine with a separate air cooling (the air duct adaptor can be seen on the top-front of the machine, not yet connected to the ventilation distribution system in the figures). As a load, another induction machine (type JD127) was used connected to the same shaft (Fig. 67 - right). Rated values and construction details of the tested machine are shown in Tab. 18. Parameter values used for identification method are listed in Tab. 19, while R_{rstd} = 59,3 mΩ and L_{mstd} = 27,2 mH. all these were obtained by standard tests. are Block scheme of the test bench is depicted in Fig. 66.

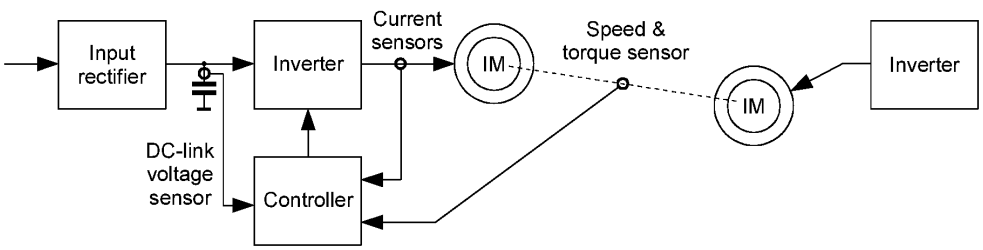

Fig. 66: Block scheme of the 1640 kW machine test bench workplace.

Tab. 18: Rated values of 1640 kW induction machine (YJ130A).

Rated values		Construction details	
Rated power P_n	1640 kW	Number of poles $2p$ (-)	6
Rated supply voltage (line to line) U_{sn}	2942 V	Connection	Y
Rated supply frequency f_{sn}	96,7 Hz	Type of rotor	Squirrel cage
Rated line current I_{sn}	382 A	Rotor conductor material	Copper
Rated cos φ	0,912	Class of insulation	H (200)
Rated efficiency η	95,8 %	Type of cooling	IC17
Rated speed n_n	1911 min^{-1}	$L_{\sigma s}$: $L_{\sigma r}$ ratio	4:6
Rated torque M_n	8170,1 N·m		

Tab. 19: Values of parameters of tested 1640 kW machine used for identification method.

Parameter	Value
Stator resistance R_s	35,8 mΩ
Stator leakage inductance $L_{\sigma s}$	0,58 mH
Rotor leakage inductance $L_{\sigma r}$	0,87 mH

Machine was powered from a locomotive converter (Fig. 68) with IGBT modules 5SNA 0600G650100. The converter is installed in locomotive machine room compatible cabinet (rack).

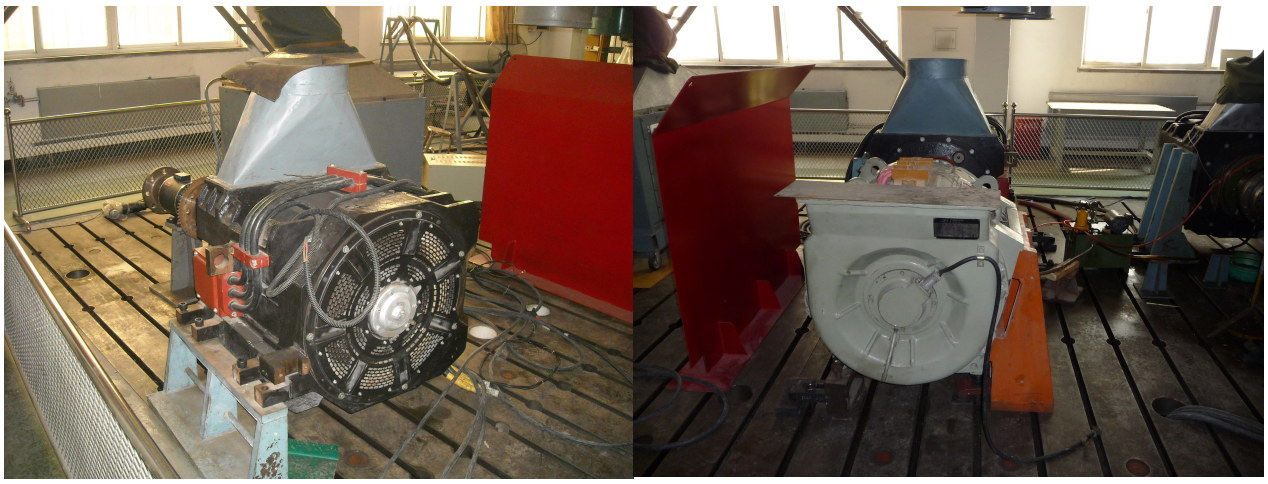

Fig. 67: Left: YJ130A 1640 kW tested induction machine; Right: coupled to a load machine (JD127).

Sensors used for measurements were as follows: current transducer LTC 1000-SFC/SP2, voltage transducer DV 6400, and combined speed and torque sensor JN-338-AN (this sensor is visible in Fig. 67 left where it is on a support and connected to the shaft of the machine – speed sensor visible

on the right figure of Fig. 67 on the end bell of the loading machine was not used).Controller of the system was equipped with TMS320F28335 microcontroller with 12-bit AD converters. This microcontroller is a common platform of CRRC traction vehicles, as mentioned in chapter 7.4.

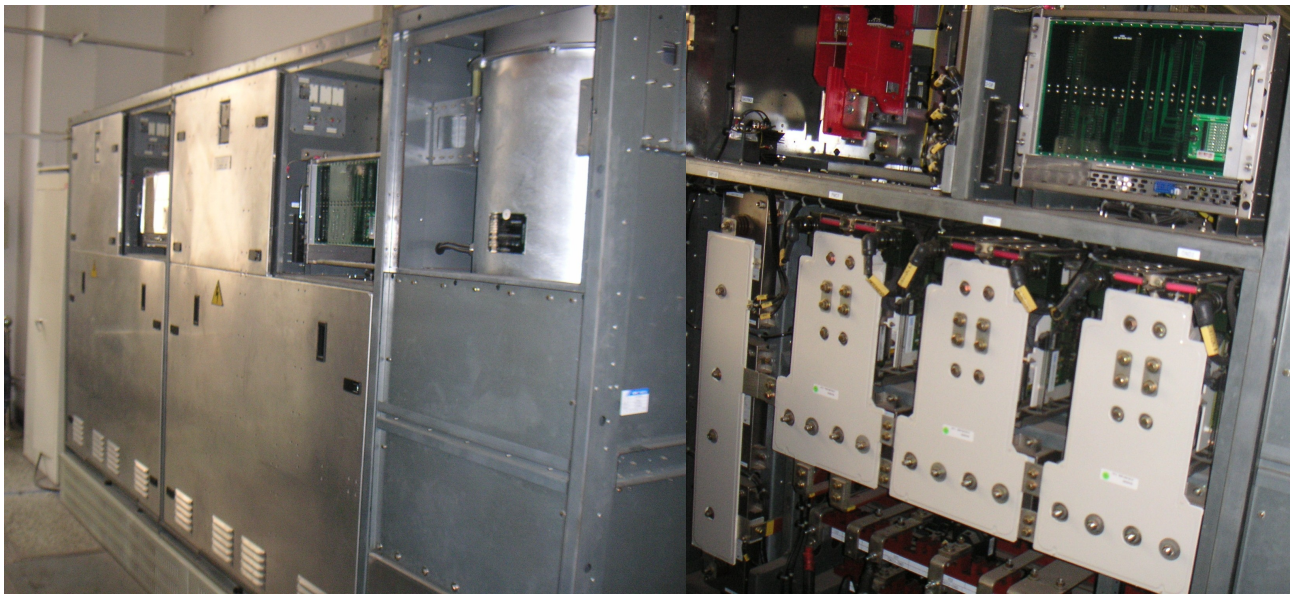

Fig. 68: Left: Converter of the 1640 kW machine test bench; Right: detail of its power modules.

7.5.1 Warming Test

Warming test was performed by loading the tested induction machine with a constant load around 8950 Nm, 562 kW at mechanical speed 600 min^{-1} for 55 minutes. Change of rotor resistance R_r and temperature of the frame ϑ_{frame} is depicted in Fig. 69. Data for each point were averaged from 10 sets of samples of input quantities, the time span between these samples was 10 seconds.

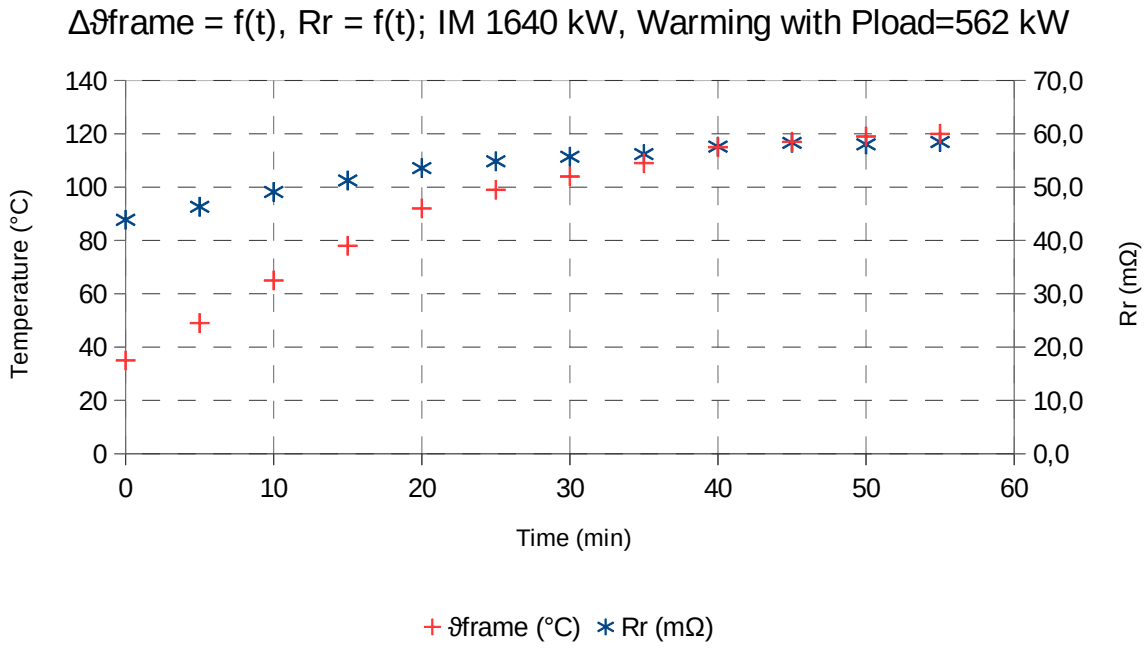

Fig. 69: R_r and machine frame temperature ϑ_{frame} change during warming test, IM 1640 kW.

Temperature of the machine frame was measured with a PT100 sensor. The initial temperature was 35 °C, the final temperature 120 °C, resulting in a warming of 85 °C. R_r rose from 44 mΩ to 58 mΩ which is an increase by 31,8 %. This is in a very good conformity with a value from (116) which is a comparison according to chapter 7.1.3.

$$R_{\vartheta 2} = R_{\vartheta 1} \cdot (1 + 0{,}0038 \cdot 85) = 1{,}323 \cdot R_{\vartheta 1}, \tag{116}$$

A dependence of L_m on the magnetizing component of stator current component I_{sd} (described in chapters 7.1.4 and mainly 4.1.6) shown in Fig. 70.

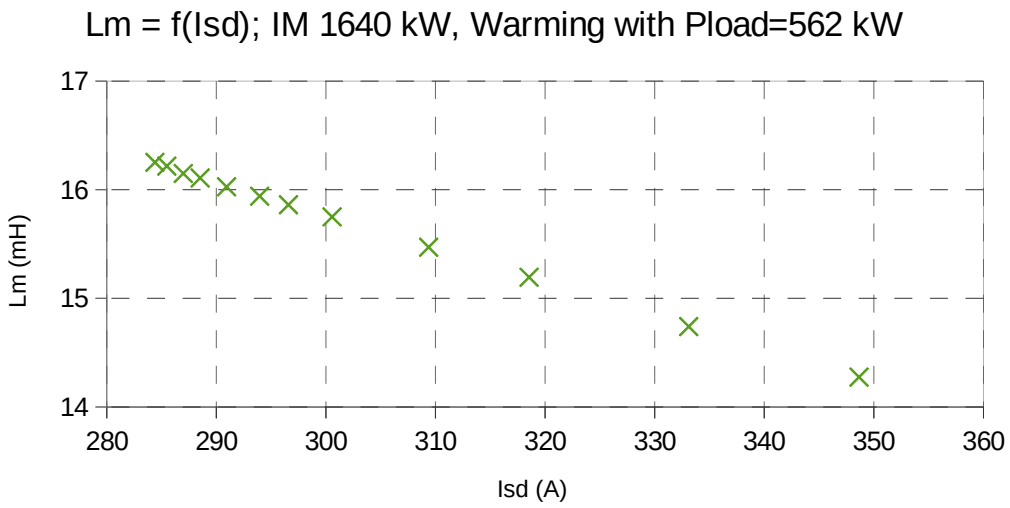

Fig. 70: L_m as a function of stator current component I_{sd} during warming test, IM 1640 kW.

7.5.2 Tests with Different Loads and Frequencies

Set of measurements with different load torques and different stator frequencies was conducted also in case of this machine. The stator frequencies were: 20, 30, 35, 55, 75 and 100 Hz. Measurement at each frequency is represented by couple of working points with different loads. Temperature difference among measurement points did not exceed 5 °C so its influence should not be significant in this case. Each measurement point was averaged from ten samples with a time span of 10 seconds.

Stator voltage is set according to U/f (voltage to frequency) ratio in range from 24 to 27. The voltage vector is again aligned with the q axis, so the d component (U_{sd}) is zero in all presented cases. Important measured and calculated data are presented in Tab. 20, Tab. 21, Tab. 22, Tab. 23, Tab. 24 and Tab. 25.

Tab. 20: Measurement at f_s = 20 Hz (U_{sd} = 0 V), IM 1640 kW.

Measured input quantities				
M_{load} (N·m)	2000	4000	6000	8000
U_{sq} (V)	564,33	572,14	581,57	593,46
ω_s (rad·s^{-1})	131,12	133,18	135,68	138,82
I_{sd} (A)	179,30	173,99	195,27	232,62
I_{sq} (A)	139,00	243,56	372,43	495,87
ω_m (rad s^{-1})	130,12	131,11	132,18	133,67
f_r (Hz)	0,16	0,33	0,56	0,82
Estimated parameters				
R_r (mΩ)	29,57	34,52	37,34	40,22
L_m (mH)	23,9	26,6	27,4	27,3
Values calculated for verification				
R_{rv} (mΩ)	29,57	34,52	37,34	40,22
I_{sdc} (A)	179,30	173,99	195,27	232,62
I_{sqc} (A)	139,00	243,56	372,43	495,87

Tab. 21: Measurement at f_s = 30 Hz (U_{sd} = 0 V), IM 1640 kW.

Measured input quantities				
M_{load} (N·m)	2000	4000	6000	8000
U_{sq} (V)	800,22	808,26	817,80	830,34
ω_s (rad·s^{-1})	193,56	195,68	198,21	201,53
I_{sd} (A)	177,93	179,95	202,70	249,64
I_{sq} (A)	127,16	234,49	358,03	501,31
ω_m (rad·s^{-1})	192,45	193,45	194,52	195,82
f_r (Hz)	0,18	0,35	0,59	0,91
Estimated parameters				
R_r (mΩ)	34,54	37,07	39,55	42,55
L_m (mH)	23,17	24,71	25,13	24,82
Values calculated for verification				
R_{rv} (mΩ)	34,54	37,07	39,55	42,55
I_{sdc} (A)	177,93	179,95	202,70	249,64
I_{sqc} (A)	127,16	234,49	358,03	501,31

Tab. 22: Measurement at f_s = 35 Hz (U_{sd} = 0 V), IM 1640 kW.

Measured input quantities				
M_{load} (N·m)	2000	4000	6000	8000
U_{sq} (V)	911,49	920,98	931,15	942,84
ω_s (rad·s^{-1})	223,01	225,53	228,22	231,31
I_{sd} (A)	178,01	184,63	209,01	249,28
I_{sq} (A)	129,95	248,70	364,90	484,75
ω_m (rad·s^{-1})	221,77	222,97	224,22	225,53
f_r (Hz)	0,20	0,41	0,64	0,92
Estimated parameters				
R_r (mΩ)	37,21	39,47	41,42	44,18
L_m (mH)	22,96	24,17	24,32	23,96
Values calculated for verification				
R_{rv} (mΩ)	37,21	39,47	41,42	44,18
I_{sdc} (A)	178,01	184,63	209,01	249,28
I_{sqc} (A)	129,95	248,70	364,90	484,75

Tab. 23: Measurement at f_s = 55 Hz (U_{sd} = 0 V), IM 1640 kW.

Measured input quantities					
M_{load} (N·m)	1000	2000	4000	6000	7000
U_{sq} (V)	1383,8	1388,7	1398,4	1410,2	1417,1
ω_s (rad·s^{-1})	348,06	349,34	351,92	355,04	356,88
I_{sd} (A)	166,78	169,53	184,65	214,91	237,15
I_{sq} (A)	56,02	117,87	230,65	354,39	417,08
ω_m (rad·s^{-1})	347,40	348,03	349,24	350,60	351,39
f_r (Hz)	0,11	0,21	0,43	0,71	0,87
Estimated parameters					
R_r (mΩ)	45,12	41,94	43,47	46,16	47,96
L_m (mH)	23,36	23,47	23,31	22,85	22,36
Values calculated for verification					
R_{rv} (mΩ)	45,12	41,94	43,47	46,16	47,96
I_{sdc} (A)	166,78	169,53	184,65	214,91	237,15
I_{sqc} (A)	56,02	117,87	230,65	354,39	417,08

Tab. 24: Measurement at f_s = 75 Hz (U_{sd} = 0 V), IM 1640 kW.

Measured input quantities					
M_{load} (N·m)	1000	2079	3036	4067	4969
U_{sq} (V)	1842,59	1830,39	1833,86	1832,27	1830,48
ω_s (rad·s^{-1})	474,42	476,04	477,41	479,10	480,75
I_{sd} (A)	177,85	178,63	183,1	193,2	206,37
I_{sq} (A)	61,37	128,5	187,25	247,15	300,75
ω_m (rad·s^{-1})	473,93	474,92	475,75	476,76	477,73
f_r (Hz)	0,08	0,18	0,26	0,37	0,48
Estimated parameters					
R_r (mΩ)	29,60	31,54	32,09	34,05	35,56
L_m (mH)	21,38	21,64	21,94	21,84	21,55
Values calculated for verification					
R_{rv} (mΩ)	29,60	31,54	32,09	34,05	35,56
I_{sdc} (A)	177,85	178,63	183,10	193,20	206,37
I_{sqc} (A)	61,37	128,50	187,25	247,15	300,75

Tab. 25: Measurement at f_s = 100 Hz (U_{sd} = 0 V), IM 1640 kW.

Measured input quantities				
M_{load} (N·m)	1000	1989	2998	3900
U_{sq} (V)	2506,0	2515,2	2525,6	2536,4
ω_s (rad·s^{-1})	632,64	634,97	637,58	640,31
I_{sd} (A)	155,93	162,63	174,09	188,30
I_{sq} (A)	57,34	115,50	176,39	232,98
ω_m (rad·s^{-1})	632,01	633,66	635,52	637,49
f_r (Hz)	0,10	0,21	0,33	0,45
Estimated parameters				
R_r (mΩ)	41,40	42,77	43,89	45,32
L_m (mH)	24,98	24,48	23,71	22,91
Values calculated for verification				
R_{rv} (mΩ)	41,40	42,77	43,89	45,32
I_{sdc} (A)	155,93	162,63	174,09	188,30
I_{sqc} (A)	57,34	115,50	176,39	232,98

Fig. 71 shows the dependence of R_r to slip frequency f_r, which corresponds with the description in chapter 4.1.9 and 7.1.5. With the rising load torque M_{load} the mechanical speed decreased, which resulted in an increase of slip and therefore the slip frequency f_r. There is also a visible influence of stator frequency f_s. R_r is higher mainly due to skin effect in rotor bars which is more significant the higher the frequencies are.

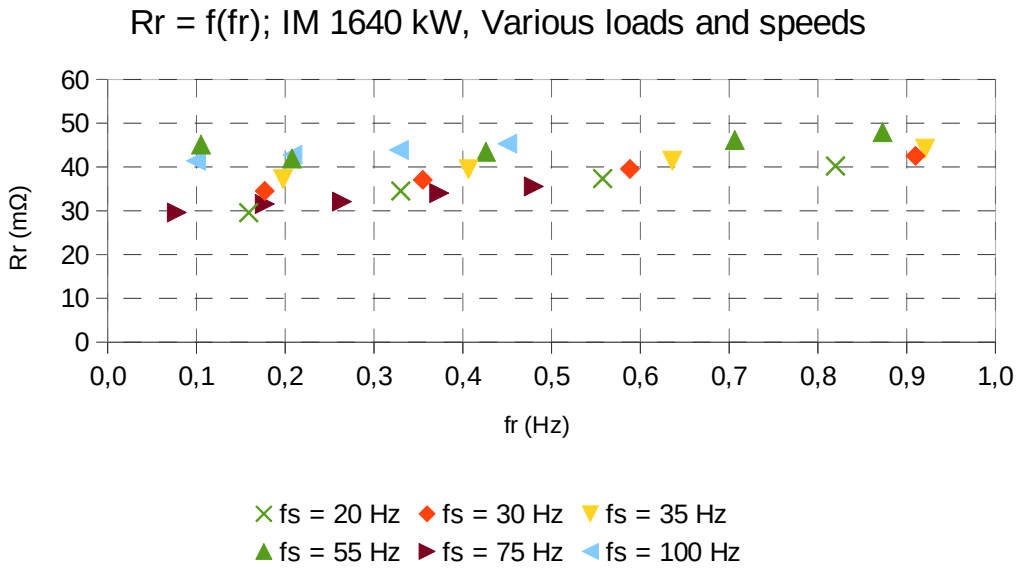

Fig. 71: R_r as a function of slip frequency f_r for different stator frequencies f_s, IM 1640 kW.

Dependence of L_m on the magnetizing component of stator current component I_{sd} (described in chapters 7.1.4 and mainly 4.1.6) is shown in Fig. 51. In this figure, data from all the measurements with different loads and different frequencies are grouped and the trend corresponds with the expected results and findings published elsewhere.

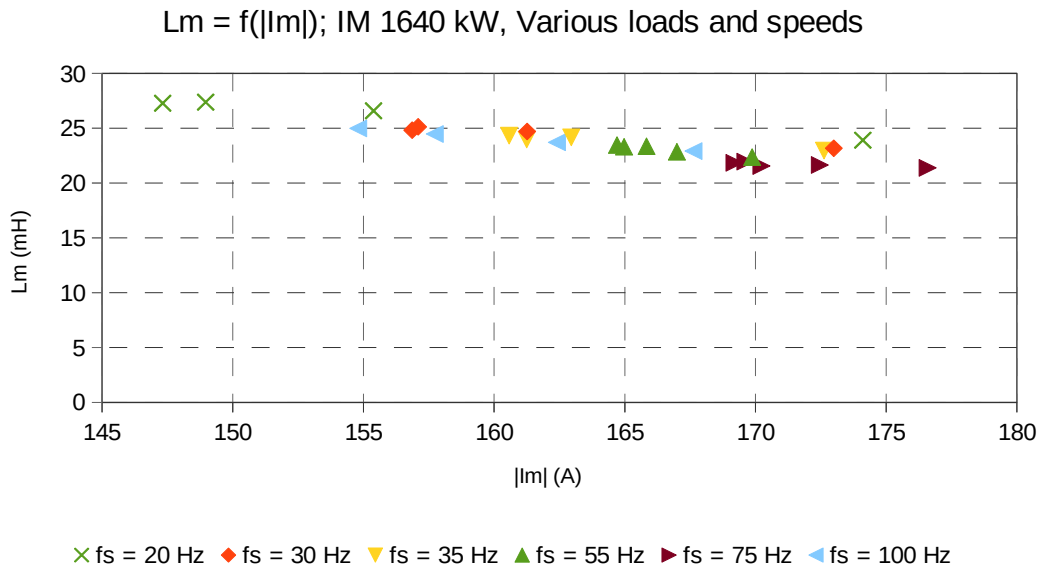

Fig. 72: L_m as a function of stator current component I_{sd} from measurements with different loads and different stator frequencies f_s, IM 1640 kW.

7.6 Discussion

An estimation of the proper value of R_r by the proposed method depends on accuracy of the speed measurement. If the drive is not equipped with a sensor with a suitable number of pulses per revolution, approaches like longer measurement or measurement of period of the pulse can be deployed. Prolonging the speed measurement should not be a problem as the drive should operate in steady-state mode during measurement. Parameters $L_{\sigma s}$, $L_{\sigma r}$ and R_s are assumed to be constant. This simplification can be done without a significant loss of accuracy in the case of $L_{\sigma s}$, $L_{\sigma r}$ as they represent the part of magnetic flux that flows mainly through air. Thus it is not influenced by a change of temperature and the effect of saturation can be also considered negligible. R_s is however influenced by the temperature, but its influence on the calculation is not so significant in most of the operation range. The voltage drop on the $L_{\sigma s}$ is higher than that on the R_s and this difference rises with the rising stator frequency and torque producing stator current component I_{sq}. Moreover, the temperature of the rotor is normally higher than that of the stator [13] which means that change of R_s is smaller than the change of R_r. Frequency should not have any significant effect of the R_s as the stator winding is normally manufactured as parallel filaments to prevent the skin effect.

For example if the R_s increases by 50% by IM 3,5 kW with half of the rated torque (16 Nm) and f_s = 20 Hz (393 min^{-1}), the resulting R_r is 8,8 % higher and L_m 4,2% lower than it should be if the correct value of R_s would be known. With rising torque, the difference in R_r lowers while the difference in L_m rises, which confirms the theory with voltage drop on $L_{\sigma s}$. For M = 30,5 Nm and 50 Hz (967 min^{-1}) R_r is 0,2 % higher and L_m 3,9 % lower than it should be. It must be admitted that if the stator resistance increases two times, than in the worst case (M_{load} = 10 Nm, f_s=20 Hz), the R_r error exceeds 45 %. For rated load, it however decreases to acceptable 4 %. Tab. 26 shows the situation for 50 % increase of R_s that is not known to the controller. Rows "...with R_{sn}" mean the values calculated with firmly set rated value of R_s (R_{sn}), while rows "...with 1,5·R_{sn}" shows results if the algorithm would use the increased stator resistance value.

Tab. 26: Influence of R_s mismatch (1,5 times) to resulting values of R_r and L_m for IM 3,5 kW.

Stator supply frequency f_s = 20 Hz, R_s = 1,5·R_{sn}				
M_{load} (N·m)	9,5	16	23,2	30,5
I_{sq} (A)	3,19	4,66	6,34	8,25
R_r with R_{sn} (Ω)	0,74	0,83	0,89	0,93
R_r with 1,5·R_{sn} (Ω)	0,87	0,90	0,93	0,94
ΔR_r (%)	18,2	8,8	4,4	1,6
L_m with R_{sn} (mH)	99,2	102	104	105
L_m with 1,5·R_{sn} (mH)	96,7	97,5	97,3	95,6
ΔL_m (%)	-2,5	-4,2	-6,1	-11,1
Stator supply frequency f_s = 50 Hz, R_s = 1,5·R_{sn}				

Stator supply frequency f_s = 20 Hz, R_s = 1,5·R_{sn}				
M_{load} (N·m)	9,5	16	23,2	30,5
I_{sq} (A)	2,6	4,1	5,8	7,8
R_r with R_{sn} (Ω)	0,89	0,93	1,0	0,98
R_r with 1,5·R_{sn} (Ω)	0,94	0,95	1,0	0,99
ΔR_r (%)	4,8	2,4	1,1	0,22
L_m with R_{sn} (mH)	107	106	106	101
L_m with 1,5·R_{sn} (mH)	105	104	103	97,3
ΔL_m (%)	-1,2	-1,9	-2,8	-3,9

Both R_r and L_m can be regarded as slowly varying during steady-state operation. In this mode, R_r is mostly influenced by temperature change which rises slowly, as can be seen also for example from Fig. 45. The flux which can influence the value of L_m by saturating the magnetic circuit also does not change quickly during normal operation of IFOC. Therefore the method is enough to be executed within minutes during steady-state operation. In the case of change of a working point of the drive it should be executed after this change as magnetizing current or slip change can result in a sharp change of R_r or L_m. Averaging of multiple measurements of input quantities is advised to prevent variation of results.

8 Conclusions

This thesis proposes a novel, computationally modest on-line parameter identification method for electric drives with induction machines that are equipped with a resource-constrained microcontroller. It is meant for a type of drives which have a part of their working cycle in a steady-state mode and which are equipped with a speed sensor due to technical standards, or for high precision speed or position measurement, but otherwise are equipped with low-cost or older microcontrollers which do not have abundant computational resources. A popular control strategy in these drives is Field Oriented Control, therefore the method simultaneously estimates its two key parameters: magnetizing inductance and rotor resistance. The proposed method does not need any further hardware other than that of an ordinary drive: measurement of stator current of the machine and reconstruction of the stator voltage and its frequency.

Parameters of the machine are changing during its operation due to influences of temperature, saturation of the magnetic circuit and frequency phenomena. With incorrect values of rotor resistance and magnetizing inductance, correct position of the flux cannot be obtained and therefore the performance of control can deteriorate. Hence a large number of so called on-line methods, which are used for parameter identification during operation of a drive, were published so far but most of them are computationally demanding, either on processor time or memory resources.

A summary of main groups of principles of parameter identification methods for induction machines was carried out and presented in this thesis. Among on-line methods, conventional and

off-line methods were covered to give a broader overview of parameter identification. This overview is another contribution of this thesis. Methods based on steady state voltage model were identified to be computationally undemanding and therefore a steady state voltage model was used for the derivation of the proposed method.

Proper knowledge of the mechanisms of parameter changes is necessary for designing an identification method but said knowledge is probably more important for interpreting the obtained results. Hence a detailed overview of the mechanisms of parameter changes is presented in this thesis.

Experimental verification of the proposed method was carried out on four different induction machines with rated power from 3,5 kW to 1,6 MW. Warming tests and measurements with different loads were performed and their results presented. It is however difficult to assess the value of some parameters obtained during the machine operation. With the exception of stator resistance, none of the machine parameters is directly measurable within an induction machine with a squirrel cage rotor. Due to the aforementioned changes of parameters during operation of the drive, the results cannot be compared with values obtained by conventional or off-line methods either. The obtained results are thus compared with theoretical assumptions based on the summarised mechanisms of parameter changes and waveforms published in other sources. The results obtained by the proposed method are in good conformity with these assumptions. Further, an additional method was used to estimate rotor resistance from the measured values and the same resulting values were obtained. To verify the correctness of the mathematical derivation of the method, a verification scheme was carried out. The idea behind this verification is to calculate some measurable quantity from the mathematical model of the machine with the help of estimated parameters and then compare measured and calculated values. This procedure did also show absolute conformity. Therefore it can be stated that the method delivers correct results and its deployment can improve drive performance.

8.1 Suggestions for the Future Work

Within the development of the method, certain simplifications were made to achieve an undemanding algorithm. One of them was the consideration that stator resistance is unchanged. It has been shown that the error caused by this assumption is acceptable, but a modification of the method to respect the change of stator resistance could improve it. Further, the influence of iron loss was neglected, which is common practice in various control strategies or IM problems analysis, but to incorporate its influence into the method could be yet another improvement. During testing the method, it was also discovered that there is an influence of a particular modulation of the stator current to the results, caused by additional saturation due to higher harmonics. This phenomenon, its influence and potential compensation is also deserving of further study.

8.2 Objectives Fulfilment

The stated objectives of this thesis were fulfilled as follows:

1. **Summarize the current state of knowledge on mechanisms that cause changes of the parameters.** Based on the study of research publications, an extensive study of mechanisms that cause parameter changes during operation of the machine was done. This is presented in chapter 4. General mechanisms of influence of different quantities to the parameters as well as particular cases of machine parameter changes are given. The findings stated in this chapter were used for evaluation of the results obtained by the proposed method. There is a good correspondence between the results and the theoretical assumptions.
2. **Summarize the current state of knowledge on parameter identification methods and their principles and evaluate their requirements and effectiveness.** This objective is treated in chapter 5 where a broad summary of various identification methods is given. To describe the area completely, not only on-line methods, which are used for monitoring machine parameters during operation of the drive, but also conventional and off-line methods are presented as they serve as a prerequisite of the on-line methods. Computational requirements and demands on implementation of the methods are also considered in this chapter.
3. **Design an on-line identification method of selected parameters for resource-constrained microcontrollers.** A novel, computationally modest on-line identification method was developed based on steady state voltage model of the machine. It simultaneously estimates the rotor resistance and magnetising inductance of the machine which are two crucial parameters for modern control methods such as FOC. Derivation of this method is presented in chapter 6.
4. **Implement and test the designed method on induction machine drives with various rated power.** The method was tested on machines with rated power of 3,5 kW, 15 kW, 180 kW and 1640 kW. The algorithm of the method was incorporated into the control systems of respective drives. The first two drives were laboratory set-ups while the third (180 kW) was equipped with a traction converter to form a development test bench of an electric multiple unit and the fourth (1640 kW) with components from a railway locomotive. Details of these implementations and tests as well as the results obtained are presented in chapter 7.

Based on that I consider all the objectives of this doctoral thesis fulfilled.

List of Figures

List of Tables

List of Abbreviations

AI Artificial Intelligence

ANN Artificial Neural Network

CSI Current Source Inverter

DTC Direct Torque Control

ELO Extended Luenberger Observer

EKF Extended Kálmán Filter

EMF Electro-Motive Force

EMU Electric Multiple Unit (railway vehicle)

FDTC Fuzzy Direct Torque Control

FEM Finite Element Method (numerical simulation method)

FIFOC Fuzzy Indirect Field Oriented Control

FOC Field Oriented Control

GA Genetic Algorithm

HF High Frequency

IACS International Annealed Copper Standard

IFOC Indirect Field Oriented Control

IGBT Integrated Gate Bipolar Transistor

IM Induction Machine

MMF Magneto-motive Force

MPC Model Predictive Control

PTC Predictive Torque Control

PCC Predictive Current Control

PWM Pulse Width Modulation

RLS Recursive Least Square

RFO Rotor Flux Oriented

TEFC Totally Enclosed Fan Cooled Motor

THD Total Harmonic Distortion

TEFC Totally Enclosed Fan Cooled motor

VSI Voltage Source Inverter

List of Symbols - Nomenclature

b_{v}	Conductor bar width (rotor or stator)
b_{d}	Slot width
$\cos\varphi$	Power factor
f	Frequency (general)
f_{s}	Stator frequency
f_{r}	Slip (rotor) frequency (electrical)
f_{m}	Rotor mechanical frequency
f_{sn}	Rated machine supply frequency
f_{sw}	Stator switching frequency
h_{c}	Conductor bar height (rotor or stator)
j	Imaginary unit
k_{lskin}	Coefficient of inductance lowering due to skin effect
k_{rskin}	Coefficient of resistance increase due to skin effect
k_{wn}	Wave number (skin effect description)
k_{wn}	Winding constant
$I_{\mathrm{s0}}, U_{\mathrm{s0}}, P_{\mathrm{I0}}$	Stator current, voltage and input power during no-load test
$I_{\mathrm{sbr}}, U_{\mathrm{sbr}}, P_{\mathrm{Ibr}}$	Stator current, voltage and input power during locked rotor test
$\hat{I}_{\mathrm{s}}, I_{\mathrm{sd}}, I_{\mathrm{sq}}, I_{\mathrm{s}}$	Stator current vector, its components in dq reference frame and its magnitude
$I_{\mathrm{sdc}}, I_{\mathrm{sqc}}$	Calculated values of stator current components in dq reference fr. (ch. 7.1.1)
$\hat{I}_{\mathrm{r}}, I_{\mathrm{rd}}, I_{\mathrm{rq}}$	Rotor current vector and its components in dq reference frame
$\hat{I}_{\mathrm{m}}, I_{\mathrm{md}}, I_{\mathrm{mq}}$	Magnetizing current vector and its components in dq reference frame
$\hat{I}_{2\Gamma}, \hat{I}_{\mu\Gamma}$	Current vectors in inverse Γ equivalent circuit of induction machine
I_{sn}	Rated machine line current (RMS value)
L_{m}	Magnetizing inductance
L_{mstd}	Magnetizing inductance by conventional methods (laboratory standard tests)
L_{r}	Rotor inductance
L_{s}	Stator inductance
$L_{\mu\Gamma}$	Magnetising inductance in inverse Γ equivalent circuit
$L_{\sigma\mathrm{r}}$	Rotor leakage inductance

$L_{\sigma s}$	Stator leakage inductance
$L_{\sigma I\Gamma}$	Leakage inductance in inverse Γ equivalent circuit
M_{load}	Load torque
M_n	Rated machine torque
M_δ	Torque in the air gap of a machine
n_n	Rated machine speed
n	Rotor (machine) rotational speed
P_{Cu}, P_{Fe}	Copper and iron losses of the machine
P_i	Inner machine power
$P_{mech}, P_{fric}, P_{vent}$	Mechanical, friction and ventilation losses of the machine
P_n	Rated machine power
p, q	Coefficients of the reduced quadratic equation
p_p	Number of pole-pairs of the machine
$2p$	Number of poles of the machine
q_w	Number of slots per pole and phase
R_s, R_{sn}	Stator resistance, rated value
R_r	Rotor resistance
R_{req}	Equivalent rotor resistance defined as $R_{req} = \frac{R_r}{s}$
$R_{SDCtmeas}$	Measured value of the stator resistance during the DC test.
$R_{rI\Gamma}$	Rotor resistance in inverse Γ equivalent circuit
R_{rstd}	Rotor resistance obtained by conventional methods (laboratory standard tests)
R_{rv}	Rotor resistance estimated for verification (see chapter 7.1.2)
R_{br}	Locked rotor resistance
$R_{\vartheta 1}$	Resistance at temperature ϑ_1
$R_{\vartheta 2}$	Resistance at temperature ϑ_2
R_{20}	Resistance recalculated to 20°C
s	Slip
t	Time
$\hat{U}_s, U_{sd}, U_{sq}$	Stator voltage vector and its components in dq reference frame
$\hat{U}_i, U_{id}, U_{iq}$	Back EMF vector (inner voltage) and its components in dq reference frame

$U_\mathrm{i}, \lvert\hat{U}_\mathrm{i}\rvert$	Magnitude of back EMF vector (inner voltage)
U_sn	Rated supply voltage (line to line)
$\hat{U}_{2\Pi\Gamma}$	Voltage vector in inverse Γ equivalent circuit of induction machine
$Z_{\mathrm{s}0}$	Stator impedance of the machine under no-load test
Z_br	Impedance of the machine under locked rotor test
$\alpha_{20}, \alpha_\mathrm{Cu}$	Temperature coefficient, t.c. of 100% IACS copper (α_Cu = 3,92·10^{-3} [K^{-1}/°C^{-1}])
$\alpha_{\rho 1}, \alpha_{\rho 2}$	Linear and quadratic general temperature coefficients
α_skin	Skin effect coefficient describing conductor's shape
γ	Electrical conductivity
δ	Skin depth
ζ	Skin effect coefficient describing conductor's shape
η	Efficiency
$\Delta\vartheta$	Temperature difference
$\vartheta, \vartheta_1, \vartheta_2, \vartheta_{20}$	Temperature – general, measured (all in °C), 20°C
θ_sr	Mutual angle between stator and rotor axes
μ_r, μ_0	Magnetic permeability: relative (of the material), of vacuum
$\Psi_\mathrm{sd}, \Psi_\mathrm{sq}$	Stator flux linkage components in dq reference frame
$\hat{\Psi}_\mathrm{m}, \hat{\Psi}_\mathrm{s}, \hat{\Psi}_\mathrm{r}$	Magnetizing, stator and rotor flux linkage vectors
ρ	Electrical resistivity
σ	Leakage factor
$\tau_\mathrm{t}, \tau_\mathrm{Cu}$	Temperature coefficient, t.c. of 100% IACS copper (τ_Cu = 235 [-]
τ_r	Rotor time constant
ω_s	Angular frequency of the stator supply current
Ω_s	Angular frequency of the stator magnetic field
ω_r	Angular frequency of the rotor current
ω_m	Electrical angular frequency of the rotor
Ω_m	Mechanical angular frequency of the rotor

References

[1] J. Tang, Y. Yang, F. Blaabjerg, J. Chen, L. Diao, and Z. Liu, ‘Parameter Identification of Inverter-Fed Induction Motors: A Review’, *Energies*, vol. 11, no. 9, Art. no. 9, Sep. 2018, doi: 10.3390/en11092194.

[2] A. Keyhani, W. Lu, and B. Proca, *Modeling and Parameter Identification of Electric Machines*. CRC Press - Taylor & Francis Group, 2017, pp. 449–514. doi: 10.1201/9781420028157-25.

[3] ‘IEEE Standard Test Procedure for Polyphase Induction Motors and Generators’, *IEEE Std 112-2017 (Revision of IEEE Std 112-2004)*, pp. 1–115, Feb. 2018, doi: 10.1109/IEEESTD.2018.8291810.

[4] ‘ČSN EN 60034-2-1 (35 0000). Rotating electrical machines - Part 2-1: Standard methods for determining losses and efficiency from tests (excluding machines for traction vehicles). Ed. 2.’ Praha: ÚNMZ, 2008.

[5] H. A. Toliyat, E. Levi, and M. Raina, ‘A review of RFO induction motor parameter estimation techniques’, *IEEE Transactions on Energy Conversion*, vol. 18, no. 2, pp. 271–283, 2003, doi: 10.1109/TEC.2003.811719.

[6] S. Khamehchi, E. Mölsä, and M. Hinkkanen, ‘Comparison of Standstill Parameter Identification Methods for Induction Motors’, in *2018 IEEE 9th International Symposium on Sensorless Control for Electrical Drives (SLED)*, Sep. 2018, pp. 156–161. doi: 10.1109/SLED.2018.8486001.

[7] J. Tang, Y. Yang, L. Diao, J. Chen, Y. Chang, and Z. Liu, ‘Parameter Identification of Induction Motors for Railway Traction Applications’, in *2018 IEEE Energy Conversion Congress and Exposition (ECCE)*, Sep. 2018, pp. 284–288. doi: 10.1109/ECCE.2018.8557866.

[8] L. Stoyanov, V. Lazarov, Z. Zarkov, and E. Popov, ‘Influence of Skin Effect on Stator Windings Resistance of AC Machines for Electric Drives’, in *2019 16th Conference on Electrical Machines, Drives and Power Systems (ELMA)*, Jun. 2019, pp. 1–6. doi: 10.1109/ELMA.2019.8771551.

[9] J. Bašta, *Teorie elektrických strojů*, I. vydání. Praha: Nakladatelství Československé akademie věd, 1957.

[10] J. Chen and J. Huang, ‘Stable Simultaneous Stator and Rotor Resistances Identification for Speed Sensorless IM Drives: Review and New Results’, *IEEE Trans. Power Electron.*, vol. 33, no. 10, pp. 8695–8709, Oct. 2018, doi: 10.1109/TPEL.2017.2785330.

[11] F. Wang, Z. Zhang, X. Mei, J. Rodríguez, and R. Kennel, ‘Advanced Control Strategies of Induction Machine: Field Oriented Control, Direct Torque Control and Model Predictive Control’, *Energies*, vol. 11, no. 1, Art. no. 1, Jan. 2018, doi: 10.3390/en11010120.

[12] F. J. Lin and M. S. Su, ‘A high-performance induction motor drive with on-line rotor time-constant estimation’, *IEEE Transactions on Energy Conversion*, vol. 12, no. 4, pp. 297–303, Dec. 1997, doi: 10.1109/60.638864.

[13] T.-V. Tran and E. Nègre, ‘Efficient Estimator of Rotor Temperature Designing for Electric and Hybrid Powertrain Platform’, *Electronics*, vol. 9, no. 7, Art. no. 7, Jul. 2020, doi: 10.3390/electronics9071096.

[14] J. Li, S. Nie, Q. Meng, and H. Ren, ‘Efficiency optimization of induction motors based on online identification of iron loss equivalent resistance via dual extended Kalman filter’, in *2016 IEEE Region 10 Conference (TENCON)*, Nov. 2016, pp. 3309–3312. doi: 10.1109/TENCON.2016.7848664.

[15] L. Zhao, J. Huang, J. Chen, and M. Ye, ‘A Parallel Speed and Rotor Time Constant Identification Scheme for Indirect Field Oriented Induction Motor Drives’, *IEEE Trans. Power Electron.*, vol. 31, no. 9, pp. 6494–6503, Sep. 2016, doi: 10.1109/TPEL.2015.2504399.

[16] E. Quintero-Manriquez, E. N. Sanchez, R. G. Harley, S. Li, and R. A. Felix, ‘Neural Inverse Optimal Control Implementation for Induction Motors via Rapid Control Prototyping’, *IEEE Trans. Power Electron.*, vol. 34, no. 6, pp. 5981–5992, Jun. 2019, doi: 10.1109/TPEL.2018.2870159.

[17] J. Chen, J. Huang, and Y. Sun, ‘Resistances and Speed Estimation in Sensorless Induction Motor Drives Using a Model With Known Regressors’, *IEEE Trans. Ind. Electron.*, vol. 66, no. 4, pp. 2659–2667, Apr. 2019, doi: 10.1109/TIE.2018.2849964.

[18] Z. Kandoussi, Z. Boulghasoul, A. Elbacha, and A. Tajer, ‘Luenberger observer based sensorless Indirect FOC with stator resistance adaptation’, in *2014 Second World Conference on Complex Systems (WCCS)*, Nov. 2014, pp. 367–373. doi: 10.1109/ICoCS.2014.7060932.

[19] M. S. Zaky, M. M. Khater, S. S. Shokralla, and H. A. Yasin, ‘Wide-Speed-Range Estimation With Online Parameter Identification Schemes of Sensorless Induction Motor Drives’, *IEEE Transactions on Industrial Electronics*, vol. 56, no. 5, pp. 1699–1707, 2009, doi: 10.1109/TIE.2008.2009519.

[20] Y. Liu, ‘Multi-parameter Online Identification Algorithm of Induction Motor for Hybrid Electric Vehicle Applications’, in *2014 Sixth International Symposium on Parallel Architectures, Algorithms and Programming*, Beijing, China, Jul. 2014, pp. 35–39. doi: 10.1109/PAAP.2014.35.

[21] F. Stinga, A. Soimu, and M. Marian, ‘Online estimation and control of an induction motor’, in *2015 19th International Conference on System Theory, Control and Computing (ICSTCC)*, Oct. 2015, pp. 742–746. doi: 10.1109/ICSTCC.2015.7321382.

[22] K. Radhakrishnan, A. Unnikrishnan, and K. Balakrishnan, ‘EM Based Extended Kalman Filter for Estimation of Rotor Time-Constant of Induction Motor’, in *IEEE International Symposium on Industrial Electronics*, 2006 IEEE International Symposium on Industrial Electronics, Jul. 2006, pp. 2434–2438. doi: 10.1109/ISIE.2006.295954.

[23] O. Buchholz, J. Böcker, and J. Bonifacio, ‘Online-Identification of the Induction Machine Parameters Using the Extended Kalman Filter’, in *2018 XIII International Conference on Electrical Machines (ICEM)*, Sep. 2018, pp. 1623–1629. doi: 10.1109/ICELMACH.2018.8506739.

[24] S. Kamankesh and D. A. Khaburi, ‘On-line rotor time constant estimation for induction motor using two new methods, RLS and SDBP algorithms’, in *2009 International Conference on Electrical and Electronics Engineering - ELECO 2009*, Nov. 2009, p. I–184. doi: 10.1109/ELECO.2009.5355327.

[25] D. Telford, M. W. Dunnigan, and B. W. Williams, ‘Online identification of induction machine electrical parameters for vector control loop tuning’, *IEEE Transactions on Industrial Electronics*, vol. 50, no. 2, pp. 253–261, 2003, doi: 10.1109/TIE.2003.809397.

[26] M. Cirrincione, M. Pucci, G. Cirrincione, and G.- Capolino, ‘A new experimental application of least-squares techniques for the estimation of the induction motor parameters’, *IEEE Transactions on Industry Applications*, vol. 39, no. 5, pp. 1247–1256, Sep. 2003, doi: 10.1109/TIA.2003.816565.

[27] D. C. Huynh, M. W. Dunnigan, and S. J. Finney, ‘On-line parameter estimation of an induction machine using a recursive least-squares algorithm with multiple time-varying forgetting factors’, in *2010 IEEE International Conference on Power and Energy*, Nov. 2010, pp. 444–449. doi: 10.1109/PECON.2010.5697624.

[28] L. He, J. Restrepo, S. Cheng, R. G. Harley, and T. G. Habetler, ‘An improved DC-signal-injection method with active torque-ripple mitigation for thermal monitoring of field-oriented-controlled induction motors’, in *2015 IEEE Energy Conversion Congress and Exposition (ECCE)*, Sep. 2015, pp. 4447–4454. doi: 10.1109/ECCE.2015.7310288.

[29] F. Baneira, A. G. Yepes, Ó. López, and J. Doval-Gandoy, ‘Estimation Method of Stator Winding Temperature for Dual Three-Phase Machines Based on DC-Signal Injection’, *IEEE Transactions on Power Electronics*, vol. 31, no. 7, pp. 5141–5148, Jul. 2016, doi: 10.1109/TPEL.2015.2479410.

[30] O. Lipcak, J. Bauer, and M. Chomat, ‘Reactive Power MRAS for Rotor Resistance Estimation Taking Into Account Load-Dependent Saturation of Induction Motor’, in *2019 International Conference on Electrical Drives Power Electronics (EDPE)*, Sep. 2019, pp. 255–260. doi: 10.1109/EDPE.2019.8883887.

[31] J. Zhang, J. Chai, X. Sun, and H. Lu, ‘On-line parameter estimation for indirect field oriented control of induction machine based on steady state voltage model’, in *IECON 2014 - 40th Annual Conference of the IEEE Industrial Electronics Society*, Oct. 2014, pp. 769–773. doi: 10.1109/IECON.2014.7048587.

[32] S. Maiti, C. Chakraborty, Y. Hori, and M. C. Ta, ‘Model Reference Adaptive Controller-Based Rotor Resistance and Speed Estimation Techniques for Vector Controlled Induction Motor Drive Utilizing Reactive Power’, *IEEE Transactions on Industrial Electronics*, vol. 55, no. 2, pp. 594–601, Feb. 2008, doi: 10.1109/TIE.2007.911952.

[33] M. Basic, D. Vukadinovic, I. Grgic, and M. Bubalo, ‘Speed-Sensorless Vector Control of an Induction Generator Including Stray Load and Iron Losses and Online Parameter Tuning’, *IEEE Trans. Energy Convers.*, vol. 35, no. 2, pp. 724–732, Jun. 2020, doi: 10.1109/TEC.2019.2952666.

[34] V. F. Samoseiko, A. V. Saushev, and N. V. Belousova, ‘Asynchronous Motor Control Algorithm with Parameter Identification’, in *2019 International Ural Conference on Electrical Power Engineering (UralCon)*, Oct. 2019, pp. 284–289. doi: 10.1109/URALCON.2019.8877625.

[35] L. Wang, X. Deng, K. Hu, X. Zhang, and K. Wang, ‘A Novel Parameter Identification Method for Induction Motor’, in *2010 International Conference on Measuring Technology and Mechatronics Automation*, Changsha City, China, Mar. 2010, pp. 265–268. doi: 10.1109/ICMTMA.2010.20.

[36] C. Grabner, ‘Control Relevant Equivalent Circuit Parameters of a Squirrel Cage Induction Motor and Their Modern Finite Element Assisted Determination’, in *Electric Machines Drives Conference, 2007. IEMDC ’07. IEEE International*, 2007, vol. 2, pp. 897–903. doi: 10.1109/IEMDC.2007.382793.

[37] B. Mirafzal, G. L. Skibinski, and R. M. Tallam, ‘Determination of Parameters in the Universal Induction Motor Model’, in *Conference Record of the 2007 IEEE Industry Applications Conference, 2007. 42nd IAS Annual Meeting*, 2007, pp. 1207–1216. doi: 10.1109/07IAS.2007.189.

[38] R. K. Ursem and P. Vadstrup, ‘Parameter identification of induction motors using stochastic optimization algorithms’, *Applied Soft Computing*, vol. 4, no. 1, pp. 49–64, nor 2004, doi: 10.1016/j.asoc.2003.08.002.

[39] K. Yamazaki, A. Suzuki, M. Ohto, and T. Takakura, ‘Circuit Parameters Determination Involving Stray Load Loss and Harmonic Torques for High-Speed Induction Motors Fed by Inverters’, *IEEE Transactions on Energy Conversion*, vol. 28, no. 1, pp. 154–163, 2013, doi: 10.1109/TEC.2012.2227058.

[40] L. Peretti and M. Zigliotto, ‘Automatic procedure for induction motor parameter estimation at standstill’, *IET Electric Power Applications*, vol. 6, no. 4, pp. 214–224, 2012, doi: 10.1049/iet-epa.2010.0262.

[41] S. A. Odhano, P. Pescetto, H. A. A. Awan, M. Hinkkanen, G. Pellegrino, and R. Bojoi, ‘Parameter Identification and Self-Commissioning in AC Motor Drives: A Technology Status Review’, *IEEE Transactions on Power Electronics*, vol. 34, no. 4, pp. 3603–3614, Apr. 2019, doi: 10.1109/TPEL.2018.2856589.

[42] E. Mölsä, L. Tiitinen, S. Saarakkala, L. Peretti, and M. Hinkkanen, ‘Standstill Self-Commissioning of an Induction Motor Drive’, in *2020 IEEE Energy Conversion Congress and Exposition (ECCE)*, Oct. 2020, pp. 3044–3050. doi: 10.1109/ECCE44975.2020.9236035.

[43] T. Tuovinen, M. Hinkkanen, and J. Luomi, ‘Modeling of Saturation Due to Main and Leakage Flux Interaction in Induction Machines’, *IEEE Transactions on Industry Applications*, vol. 46, no. 3, pp. 937–945, May 2010, doi: 10.1109/TIA.2010.2045210.

[44] E. Levi, M. Sokola, and S. N. Vukosavic, ‘A method for magnetizing curve identification in rotor flux oriented induction machines’, *IEEE Transactions on Energy Conversion*, vol. 15, no. 2, pp. 157–162, Jun. 2000, doi: 10.1109/60.866993.

[45] H. S. Che, A. S. Abdel-Khalik, O. Dordevic, and E. Levi, ‘Parameter Estimation of Asymmetrical Six-Phase Induction Machines Using Modified Standard Tests’, *IEEE Trans. Ind. Electron.*, vol. 64, no. 8, pp. 6075–6085, Aug. 2017, doi: 10.1109/TIE.2017.2677349.

[46] D. W. Novotny and T. A. Lipo, *Vector control and dynamics of AC drives*. Oxford : New York: Clarendon Press ; Oxford University Press, 1996.

[47] P. Vas, *Vector Control of AC Machines*, vol. 1990. Clarendon Press.

[48] P. Pichlík and J. Bauer, ‘Analysis of the Locomotive Wheel Slip Controller Operation During Low Velocity’, *IEEE Transactions on Intelligent Transportation Systems*, pp. 1–10, 2020, doi: 10.1109/TITS.2020.2971832.

[49] F. Brugnano, C. Concari, E. Imamovic, F. Savi, A. Toscani, and R. Zanichelli, ‘A simple and accurate algorithm for speed measurement in electric drives using incremental encoder’, in *IECON 2017 - 43rd Annual Conference of the IEEE Industrial Electronics Society*, Oct. 2017, pp. 8551–8556. doi: 10.1109/IECON.2017.8217502.

[50] Y. Vázquez-Gutiérrez, D. L. O’Sullivan, and R. C. Kavanagh, ‘Small-Signal Modeling of the Incremental Optical Encoder for Motor Control’, *IEEE Transactions on Industrial Electronics*, vol. 67, no. 5, pp. 3452–3461, May 2020, doi: 10.1109/TIE.2019.2916307.

[51] A. Anuchin, V. Astakhova, D. Shpak, A. Zharkov, and F. Briz, ‘Optimized method for speed estimation using incremental encoder’, in *2017 International Symposium on Power Electronics (Ee)*, Oct. 2017, pp. 1–5. doi: 10.1109/PEE.2017.8171692.

[52] J. Han, J. Xu, G. Zhu, J. Song, and Y. Wang, ‘A Novel Voltage Reconstruction Method for MRAS-Based Sensorless Induction Motor Drives at Low Switching Frequency’, in *2020 IEEE 9th International Power Electronics and Motion Control Conference (IPEMC2020-ECCE Asia)*, Nov. 2020, pp. 336–341. doi: 10.1109/IPEMC-ECCEAsia48364.2020.9367888.

[53] P. Alkorta, O. Barambones, J. A. Cortajarena, I. Martija, and F. J. Maseda, ‘Effective Position Control for a Three-Phase Motor’, *Electronics*, vol. 9, no. 2, Art. no. 2, Feb. 2020, doi: 10.3390/electronics9020241.

[54] M. Basirifar and A. Shoulaie, ‘A comparative study of circulating current free and circulating current cycloconverters’, in *2010 First Power Quality Conferance*, Sep. 2010, pp. 1–4.

[55] A. C. Subrata, T. Sutikno, A. Z. Jidin, and A. Jidin, ‘Review on Adjustable Speed Drive Techniques of Matrix Converter Fed Three-Phase Induction Machine’, in *2018 5th International Conference on Electrical Engineering, Computer Science and Informatics (EECSI)*, Oct. 2018, pp. 350–355. doi: 10.1109/EECSI.2018.8752630.

[56] H. Nikkhajoei and R. Iravani, ‘Application of Matrix Converter for Large Induction Machines’, in *2007 IEEE Power Electronics Specialists Conference*, Jun. 2007, pp. 2535–2540. doi: 10.1109/PESC.2007.4342413.

[57] A. Bento *et al.*, ‘On the Potential Contributions of Matrix Converters for the Future Grid Operation, Sustainable Transportation and Electrical Drives Innovation’, *Applied Sciences*, vol. 11, no. 10, Art. no. 10, Jan. 2021, doi: 10.3390/app11104597.

[58] D. Umadevi and E. G. Shivakumar, ‘Fractional order PID controlled Quadratic-Boost-Converter - Multilevel inverter fed Induction Motor System’, in *2019 IEEE International Conference on Electrical, Computer and Communication Technologies (ICECCT)*, Feb. 2019, pp. 1–6. doi: 10.1109/ICECCT.2019.8869346.

[59] M. Spichartz, C. Heising, V. Staudt, and A. Steimel, ‘State control of MMC-fed ship propulsion induction machine’, in *2013 IEEE Electric Ship Technologies Symposium (ESTS)*, Apr. 2013, pp. 173–177. doi: 10.1109/ESTS.2013.6523730.

[60] A. Benachour, E. M. Berkouk, and M. O. Mahmoudi, ‘DTC-SVM control of induction machine fed by three level NPC matrix converter’, in *2016 8th International Conference on Modelling, Identification and Control (ICMIC)*, Nov. 2016, pp. 628–633. doi: 10.1109/ICMIC.2016.7804188.

[61] B. K. Bose, *Modern Power electronics and AC drives*. The University of Tennessee, Knoxville, USA: Prentice Hall, 2002.

[62] A. Emadi, Ed., *Handbook of automotive power electronics and motor drives*. Boca Raton: Taylor & Francis, 2005.

[63] C. T. Henderson, ‘Electric control for rolling-mill motors’, *Proceedings of the American Institute of Electrical Engineers*, vol. 28, no. 9, pp. 1223–1238, Sep. 1909, doi: 10.1109/PAIEE.1909.6659802.

[64] H. E. White, ‘Automatic motor control’, *Proceedings of the American Institute of Electrical Engineers*, vol. 28, no. 7, pp. 1017–1024, Jul. 1909, doi: 10.1109/PAIEE.1909.6660056.

[65] R. L. Cosgriff, ‘Integral controller for carrier-type servomechanisms’, *Electrical Engineering*, vol. 69, no. 12, pp. 1078–1078, Dec. 1950, doi: 10.1109/EE.1950.6437148.

[66] J. H. Aylor, R. L. Ramey, and G. Cook, ‘Design and Application of a Microprocessor PID Predictor Controller’, *IEEE Transactions on Industrial Electronics and Control Instrumentation*, vol. IECI-27, no. 3, pp. 133–137, Aug. 1980, doi: 10.1109/TIECI.1980.351665.

[67] P. Karlovsky, O. Lipcak, and J. Bauer, ‘Iron Loss Minimization Strategy for Predictive Torque Control of Induction Motor’, *Electronics*, vol. 9, no. 4, Art. no. 4, Apr. 2020, doi: 10.3390/electronics9040566.

[68] L. E. Ortega-García, D. Rodriguez-Sotelo, J. C. Nuñez-Perez, Y. Sandoval-Ibarra, and F. J. Perez-Pinal, ‘DSP-HIL Comparison between IM Drive Control Strategies’, *Electronics*, vol. 10, no. 8, Art. no. 8, Jan. 2021, doi: 10.3390/electronics10080921.

[69] L. Ke, Z. Chenghui, C. Naxin, M. Mingyao, and H. Xiangning, ‘High dynamic response control of induction motor in high-speed region for electric vehicle drive system’, in *2008 IEEE Power Electronics Specialists Conference*, Jun. 2008, pp. 3093–3097. doi: 10.1109/PESC.2008.4592426.

[70] ‘IEC 60034-6:1991. Rotating electrical machines - Part 6: Methods of cooling (IC Code)’. IEC - International Electrotechnical Commission, Geneva, Switzerland, 1991.

[71] ‘IEC 60034-7:2020 - Rotating electrical machines - Part 7: Classification of types of construction, mounting arrangements and terminal box position (IM Code)’. IEC - International Electrotechnical Commission, Geneva, Switzerland, 2020.

[72] M. Srndovic, R. Fišer, and G. Grandi, ‘Analysis of Equivalent Inductance of Three-Phase Induction Motors in the Switching Frequency Range’, *Electronics*, vol. 8, no. 2, Art. no. 2, Feb. 2019, doi: 10.3390/electronics8020120.

[73] X. Sun, B. Zhang, and L. Yang, ‘Design of Motor Observer with Iron Loss and Parameter Identification’, in *2019 8th International Symposium on Next Generation Electronics (ISNE)*, Oct. 2019, pp. 1–3. doi: 10.1109/ISNE.2019.8896543.

[74] A. Accetta, F. Alonge, M. Cirrincione, F. D’Ippolito, M. Pucci, and A. Sferlazza, ‘GA-based off-line parameter estimation of the induction motor model including magnetic saturation and iron losses’, in *2017 IEEE Energy Conversion Congress and Exposition (ECCE)*, Oct. 2017, pp. 2420–2426. doi: 10.1109/ECCE.2017.8096466.

[75] A. Accetta, M. Cirrincione, M. Pucci, and A. Sferlazza, ‘State Space-Vector Model of Linear Induction Motors Including Iron Losses Part I: Theoretical Analysis’, in *2018 IEEE Energy Conversion Congress and Exposition (ECCE)*, Sep. 2018, pp. 3183–3189. doi: 10.1109/ECCE.2018.8558432.

[76] M. Iordache *et al.*, ‘Saturated induction machine steady-state performance assessment through simulations’, in *2014 International Conference on Optimization of Electrical and Electronic Equipment (OPTIM)*, May 2014, pp. 369–374. doi: 10.1109/OPTIM.2014.6850908.

[77] S. Udomsuk, K. Areerak, T. Areerak, and K. Areerak, ‘Power loss identification of three-phase induction motor using adaptive tabu search’, in *2017 International Electrical Engineering Congress (iEECON)*, Mar. 2017, pp. 1–4. doi: 10.1109/IEECON.2017.8075804.

[78] R. S. Kanchan and R. R. Moghaddam, ‘On accuracy of loss models including VSD induced additional harmonic losses for online energy efficient control of induction motor’, in *2017*

IEEE 12th International Conference on Power Electronics and Drive Systems (PEDS), Dec. 2017, p. 1,178-1,183. doi: 10.1109/PEDS.2017.8289110.

[79] E. Mölsä, S. E. Saarakkala, M. Hinkkanen, A. Arkkio, and M. Routimo, 'A Dynamic Model for Saturated Induction Machines With Closed Rotor Slots and Deep Bars', *IEEE Transactions on Energy Conversion*, vol. 35, no. 1, pp. 157–165, Mar. 2020, doi: 10.1109/TEC.2019.2950810.

[80] H. V. Khang, W. Pawlus, and K. G. Robbersmyr, 'Identification of parameters and harmonic losses of a deep-bar induction motor', in *2017 Seventh International Conference on Information Science and Technology (ICIST)*, Apr. 2017, pp. 194–199. doi: 10.1109/ICIST.2017.7926756.

[81] S. Musuroi, M. Svoboda, C. Sorandaru, T. Koblara, and N. Olarescu, 'Deep bar effects produced by PWM power supplies in induction machines: Application to rotor parameters determination', in *2011 IEEE EUROCON - International Conference on Computer as a Tool (EUROCON)*, 2011, pp. 1–4. doi: 10.1109/EUROCON.2011.5929282.

[82] R. Běloušek and M. Patočka, 'Analysis of the induction machine substituting circuit', in *Proceedings of the 16th International Conference on Mechatronics - Mechatronika 2014*, Dec. 2014, pp. 612–618. doi: 10.1109/MECHATRONIKA.2014.7018329.

[83] A. M. Alturas, S. Gadoue, M. A. Elgendy, B. Zahawi, and A. S. Abdel-Khalik, 'Structural Identifiability Analysis of Steady-State Induction Machine Models', in *2015 4th International Conference on Electric Power and Energy Conversion Systems (EPECS)*, Nov. 2015, pp. 1–6. doi: 10.1109/EPECS.2015.7368508.

[84] P. Vas, *Parameter Estimation, Condition Monitoring, and Diagnosis of Electrical Machines*. Clarendon Press, 1993.

[85] J. Pavelka, J. Zděnek, České vysoké učení technické v Praze, and Elektrotechnická fakulta, *Elektrické pohony a jejich řízení*. V Praze: České vysoké učení technické, 2010.

[86] T. Kost'al, 'Reducing electrical energy consumption of AHU fans through parameter identification of the drive', in *2018 3rd International Conference on Intelligent Green Building and Smart Grid (IGBSG)*, Yi-Lan, Apr. 2018, pp. 1–4. doi: 10.1109/IGBSG.2018.8393529.

[87] J. Lipták and J. Sedláček, *Úvod do elektrotechnických materiálů*, 1. Praha, 2005.

[88] W. H. Hayt, *Engineering electromagnetics*, 4th ed. New York: McGraw-Hill Book Co, 1981.

[89] F. M. H. Khater, R. D. Lorenz, D. W. Novotny, and K. Tang, 'Selection of Flux Level in Field-Oriented Induction Machine Controllers with Consideration of Magnetic Saturation Effects', *IEEE Transactions on Industry Applications*, vol. IA-23, no. 2, pp. 276–282, Mar. 1987, doi: 10.1109/TIA.1987.4504903.

[90] A. F. Almarshoud, M. A. Abdel-halim, and A. I. Alolah, 'Including effects of cross-saturation and leakage path saturation together in the generalized model of three phase induction machine', in *Canadian Conference on Electrical and Computer Engineering 2001. Conference Proceedings (Cat. No.01TH8555)*, May 2001, vol. 1, pp. 195–200 vol.1. doi: 10.1109/CCECE.2001.933682.

[91] M. AKBABA and S. Q. FAKHRO, 'Saturation Effects in Three-Phase Induction Motors', *Electric Machines & Power Systems*, vol. 12, no. 3, pp. 179–193, Jan. 1987, doi: 10.1080/07313568708960102.

[92] M. Akbaba, ‘Modeling of the Saturated Leakage Reactance of Induction Motors as a Time Varying Parameter for Transient Computations’, *Electric Machines & Power Systems*, vol. 20, no. 5, pp. 539–548, Sep. 1992, doi: 10.1080/07313569208909616.

[93] D. G. Watterson, W. Prescott, M. Bradford, M. Lockwood, and S. Bagk, ‘MMF and permeance harmonic torques and losses in cage induction motors-the effects of skew, bar-to-bar impedance and saturation’, in *1989 Fourth International Conference on Electrical Machines and Drives Conf. Publ. No. ??)*, Sep. 1989, pp. 275–281.

[94] K. L. V. Iyer, V. Ramakrishnan, and N. C. Kar, ‘Significance of incorporating proximity effect in aluminum- and copper-rotor SEIGS for wind power application’, in *2011 IEEE International Electric Machines Drives Conference (IEMDC)*, May 2011, pp. 300–305. doi: 10.1109/IEMDC.2011.5994864.

[95] J. Gyselinck, P. Dular, N. Sadowski, P. Kuo-Peng, and R. V. Sabariego, ‘Homogenization of Form-Wound Windings in Frequency and Time Domain Finite-Element Modeling of Electrical Machines’, *IEEE Transactions on Magnetics*, vol. 46, no. 8, pp. 2852–2855, Aug. 2010, doi: 10.1109/TMAG.2010.2043515.

[96] H. L. Kwok, *Electronic materials*. Trans Tech Pub., 2010.

[97] J. Košťál, ‘Teplotní závislost odporu kovových vodičů. Elektro, časopis pro elektrotechniku’, vol. 18, no. 1, pp. 22–23, 2008.

[98] J. B. Watkins, *Modern Electronic Materials*. Elsevier, 2016.

[99] G. Elert, ‘Electric Resistance’, *The Physics Hypertextbook*. https://physics.info/electric-resistance/ (accessed Jun. 29, 2021).

[100] R. Krishnan, *Electric motor drives: modeling, analysis, and control*. Upper Saddle River, N.J: Prentice Hall, 2001.

[101] J. Talla, V. Q. Leu, V. Šmídl, and Z. Peroutka, ‘Adaptive Speed Control of Induction Motor Drive With Inaccurate Model’, *IEEE Transactions on Industrial Electronics*, vol. 65, no. 11, pp. 8532–8542, Nov. 2018, doi: 10.1109/TIE.2018.2811362.

[102] P. Castaldi and A. Tilli, ‘Parameter estimation of induction motor at standstill with magnetic flux monitoring’, *IEEE Transactions on Control Systems Technology*, vol. 13, no. 3, pp. 386–400, 2005, doi: 10.1109/TCST.2004.841643.

[103] W. Xuhui, G. Jianhua, and H. Yang, ‘The influence for field orient of rotor resistance in induction motor’, in *Sixth International Conference on Electrical Machines and Systems, 2003. ICEMS 2003.*, Nov. 2003, vol. 2, pp. 581–584 vol.2.

[104] ‘IEC 60085:2007 - Electrical insulation – Thermal evaluation and designation.’ 2007.

[105] W. Michalik, ‘Parameter estimation methods at three-phase induction machines’, in *2005 European Conference on Power Electronics and Applications*, 2005, p. 10 pp.-P.10. doi: 10.1109/EPE.2005.219603.

[106] W. Michalik, *Anwendung moderner Verfahren zur Parameterbestimmung an Asynchronmaschinen*. 2003. [Online]. Available: https://books.google.cz/books?id=gMjbtgAACAAJ

[107] ‘How Online Estimation Differs from Offline Estimation, Mathworks Documentation’. [Online]. Available: ttp://www.mathworks.com/help/ident/ug/how-online-estimation-differs-from-offline-estimation.html?requestedDomain=www.mathworks.com

[108] H. Schierling, ‘Self-commissioning – A novel feature of modern inverter-fed induction motor drives’, in *Proceedings of Third International Conference on Power Electronics and Variable-Speed Drives,* London, Jul. 1988, vol. 3, pp. 287–290.

[109] S. Peresada, S. Kovbasa, D. Prystupa, and S. E. Lyshevski, ‘Identification of induction motor parameters for self-commissioning procedure: A new algorithm and experimental verification’, in *2014 IEEE 23rd International Symposium on Industrial Electronics (ISIE)*, Istanbul, Turkey, Jun. 2014, pp. 818–823. doi: 10.1109/ISIE.2014.6864717.

[110] ‘NEMA MG-1: Motors and Generators.’ Rosslyn, VA, USA: National Electric Manufacturers Association, 2009.

[111]A. Boglietti, P. Ferraris, M. Lazzari, and F. Profumo, ‘Induction motor equivalent circuit parameters determination from standard tests made with inverter supply’, in *Electrical Machines and Drives, 1993. Sixth International Conference on (Conf. Publ. No. 376)*, 1993, pp. 271–276. Accessed: Sep. 08, 2013. [Online]. Available: http://ieeexplore.ieee.org/xpls/abs_all.jsp?arnumber=253527

[112] M. H. Haque, ‘Determination of NEMA Design Induction Motor Parameters From Manufacturer Data’, *IEEE Transactions on Energy Conversion*, vol. 23, no. 4, pp. 997–1004, Dec. 2008, doi: 10.1109/TEC.2008.2001451.

[113] M. Gomez-Gonzalez, F. Jurado, and I. Pérez, ‘Shuffled frog-leaping algorithm for parameter estimation of a double-cage asynchronous machine’, *IET Electric Power Applications*, vol. 6, no. 8, pp. 484–490, Sep. 2012, doi: 10.1049/iet-epa.2011.0262.

[114] A. Boglietti, A. Cavagnino, and M. Lazzari, ‘Computational Algorithms for Induction Motor Equivalent Circuit Parameter Determination—Part II: Skin Effect and Magnetizing Characteristics’, *IEEE Transactions on Industrial Electronics*, vol. 58, no. 9, pp. 3734–3740, Sep. 2011, doi: 10.1109/TIE.2010.2084975.

[115] A. Boglietti, A. Cavagnino, and M. Lazzari, ‘Computational Algorithms for Induction-Motor Equivalent Circuit Parameter Determination—Part I: Resistances and Leakage Reactances’, *IEEE Transactions on Industrial Electronics*, vol. 58, no. 9, pp. 3723–3733, Sep. 2011, doi: 10.1109/TIE.2010.2084974.

[116] K. Wang, W. Yao, B. Chen, G. Shen, K. Lee, and Z. Lu, ‘Magnetizing Curve Identification for Induction Motors at Standstill Without Assumption of Analytical Curve Functions’, *IEEE Transactions on Industrial Electronics*, vol. 62, no. 4, pp. 2144–2155, Apr. 2015, doi: 10.1109/TIE.2014.2354012.

[117] T. Košťál, ‘Induction machine parameters identification method suitable for self-commissioning’, in *2017 XXVI International Scientific Conference Electronics (ET)*, Sozopol, Bulgaria, Sep. 2017, pp. 1–4. doi: 10.1109/ET.2017.8124357.

[118] Y.-S. Kwon, J.-H. Lee, S.-H. Moon, B.-K. Kwon, C.-H. Choi, and J.-K. Seok, ‘Standstill Parameter Identification of Vector-Controlled Induction Motors Using the Frequency Characteristics of Rotor Bars’, *IEEE Transactions on Industry Applications*, vol. 45, no. 5, pp. 1610–1618, 2009, doi: 10.1109/TIA.2009.2027164.

[119] R. J. Kerkman, J. D. Thunes, T. M. Rowan, and D. W. Schlegel, ‘A frequency-based determination of transient inductance and rotor resistance for field commissioning purposes’, *IEEE Transactions on Industry Applications*, vol. 32, no. 3, pp. 577–584, May 1996, doi: 10.1109/28.502169.

[120] A. Bunte and H. Grotstollen, ‘Parameter identification of an inverter-fed induction motor at standstill with a correlation method’, in *1993 Fifth European Conference on Power Electronics and Applications*, Sep. 1993, pp. 97–102 vol.5.

[121] L. Monjo, H. Kojooyan-Jafari, F. Córcoles, and J. Pedra, ‘Squirrel-Cage Induction Motor Parameter Estimation Using a Variable Frequency Test’, *IEEE Transactions on Energy Conversion*, vol. 30, no. 2, pp. 550–557, Jun. 2015, doi: 10.1109/TEC.2014.2362964.

[122] Y. He, Y. Wang, Y. Feng, and Z. Wang, ‘Parameter Identification of an Induction Machine at Standstill Using the Vector Constructing Method’, *IEEE Transactions on Power Electronics*, vol. 27, no. 2, pp. 905–915, 2012, doi: 10.1109/TPEL.2010.2089699.

[123] J. Ruan and S. Wang, ‘A Prediction Error Method-Based Self-Commissioning Scheme for Parameter Identification of Induction Motors in Sensorless Drives’, *IEEE Transactions on Energy Conversion*, vol. 30, no. 1, pp. 384–393, Mar. 2015, doi: 10.1109/TEC.2014.2346198.

[124] J.-K. Seok, S.-I. Moon, and S.-K. Sul, ‘Induction machine parameter identification using PWM inverter at standstill’, *IEEE Transactions on Energy Conversion*, vol. 12, no. 2, pp. 127–132, Jun. 1997, doi: 10.1109/60.629694.

[125] A. Gastli, ‘Identification of induction motor equivalent circuit parameters using the single-phase test’, *IEEE Transactions on Energy Conversion*, vol. 14, no. 1, pp. 51–56, 1999, doi: 10.1109/60.749147.

[126] N. R. Klaes, ‘Parameter identification of an induction machine with regard to dependencies on saturation’, *IEEE Transactions on Industry Applications*, vol. 29, no. 6, pp. 1135–1140, 1993, doi: 10.1109/28.259724.

[127] F. Alonge, F. D’Ippolito, G. Ferrante, and F. M. Raimondi, ‘Parameter identification of induction motor model using genetic algorithms’, *Control Theory and Applications, IEE Proceedings* -, vol. 145, no. 6, pp. 587–593, 1998, doi: 10.1049/ip-cta:19982408.

[128] R. F. F. Koning, C. T. Chou, M. H. G. Verhaegen, J. Ben Klaassens, and J. R. Uittenbogaart, ‘A novel approach on parameter identification for inverter driven induction machines’, *IEEE Transactions on Control Systems Technology*, vol. 8, no. 6, pp. 873–882, 2000, doi: 10.1109/87.880588.

[129] T. M. Wolbank, M. A. Vogelsberger, R. Stumberger, S. Mohagheghi, T. G. Habetler, and R. G. Harley, ‘Autonomous Self-Commissioning Method for Speed-Sensorless-Controlled Induction Machines’, *IEEE Transactions on Industry Applications*, vol. 46, no. 3, pp. 946–954, May 2010, doi: 10.1109/TIA.2010.2046288.

[130] P. J. Chrzan and H. Klaassen, ‘Parameter identification of vector-controlled induction machines’, *Electrical Engineering*, vol. 79, no. 1, pp. 39–46, Jan. 1996, doi: 10.1007/BF01840706.

[131] S. Moonl and A. Keyhani, ‘Estimation of Induction Machine Parameters from Standstill Time-Domain Data’, *IEEE Transactions on Industry Applications*, vol. 30, no. 6, pp. 1609-, Nov. 1994, doi: 10.1109/TIA.1994.350316.

[132] R. D. Lorenz, ‘Tuning of Field-Oriented Induction Motor Controllers for High-Performance Applications’, *IEEE Transactions on Industry Applications*, vol. IA-22, no. 2, pp. 293–297, Mar. 1986, doi: 10.1109/TIA.1986.4504717.

[133] M. Sumner and G. M. Asher, ‘Self-commissioning for voltage-referenced voltage fed vector controlled induction motor drives’, in *PESC ’92 Record. 23rd Annual IEEE Power Electronics Specialists Conference*, Jun. 1992, pp. 139–144 vol.1. doi: 10.1109/PESC.1992.254703.

[134] D. D. Reigosa, J. M. Guerrero, A. B. Diez, and F. Briz, ‘Rotor Temperature Estimation in Doubly-Fed Induction Machines Using Rotating High-Frequency Signal Injection’, *IEEE Trans. on Ind. Applicat.*, vol. 53, no. 4, pp. 3652–3662, Jul. 2017, doi: 10.1109/TIA.2017.2684742.

[135] H. Sugimoto and S. Tamai, ‘Secondary Resistance Identification of an Induction-Motor Applied Model Reference Adaptive System and Its Characteristics’, *IEEE Transactions on Industry Applications*, vol. IA-23, no. 2, pp. 296–303, Mar. 1987, doi: 10.1109/TIA.1987.4504905.

[136] H. A. Toliyat and A. A. Gh. Hosseiny, ‘Parameter estimation algorithm using spectral analysis for vector controlled induction motor drives’, in *ISIE ’93 - Budapest: IEEE International Symposium on Industrial Electronics Conference Proceedings*, Jun. 1993, pp. 90–95. doi: 10.1109/ISIE.1993.268809.

[137] P. R. Matić, M. A. Gecić, D. M. Lekić, and D. P. Marčetić, ‘Thermal Protection of Vector-Controlled IM Drive Based on DC Current Injection’, *IEEE Transactions on Industrial Electronics*, vol. 62, no. 4, pp. 2082–2089, Apr. 2015, doi: 10.1109/TIE.2014.2354015.

[138] S. Cheng, Y. Du, J. A. Restrepo, P. Zhang, and T. G. Habetler, ‘A Nonintrusive Thermal Monitoring Method for Induction Motors Fed by Closed-Loop Inverter Drives’, *IEEE Transactions on Power Electronics*, vol. 27, no. 9, pp. 4122–4131, Sep. 2012, doi: 10.1109/TPEL.2012.2188045.

[139] O. Wallscheid, M. Schenke, and J. Böcker, ‘A Combined Approach to Identify Induction Machine Parameters and to Design an Extended Kalman Filter for Speed and Torque Estimation’, in *2018 IEEE 18th International Power Electronics and Motion Control Conference (PEMC)*, Aug. 2018, pp. 793–799. doi: 10.1109/EPEPEMC.2018.8522008.

[140] M. Barut, S. Bogosyan, and M. Gokasan, ‘Experimental Evaluation of Braided EKF for Sensorless Control of Induction Motors’, *IEEE Transactions on Industrial Electronics*, vol. 55, no. 2, pp. 620–632, Feb. 2008, doi: 10.1109/TIE.2007.911956.

[141] F. L. Mapelli, A. Bezzolato, and D. Tarsitano, ‘A rotor resistance MRAS estimator for induction motor traction drive for electrical vehicles’, in *2012 XXth International Conference on Electrical Machines*, Sep. 2012, pp. 823–829. doi: 10.1109/ICElMach.2012.6349972.

[142] T. M. Rowan, R. J. Kerkman, and D. Leggate, ‘A simple on-line adaption for indirect field orientation of an induction machine’, *IEEE Transactions on Industry Applications*, vol. 27, no. 4, pp. 720–727, Jul. 1991, doi: 10.1109/28.85488.

[143] H. Madadi Kojabadi, ‘Active power and MRAS based rotor resistance identification of an IM drive’, *Simulation Modelling Practice and Theory*, vol. 17, no. 2, pp. 376–389, Feb. 2009, doi: 10.1016/j.simpat.2008.09.014.

[144] M. Munshi and S. G. Choudhuri, ‘Model Reference Adaptive System using Rotor Flux and Back Emf techniques for speed estimation of an Induction Motor operated in Vector Control mode: A comparative study’, in *2016 IEEE Uttar Pradesh Section International Conference on Electrical, Computer and Electronics Engineering (UPCON)*, Dec. 2016, pp. 44–49. doi: 10.1109/UPCON.2016.7894622.

[145] X. Yu, M. W. Dunnigan, and B. W. Williams, ‘A novel rotor resistance identification method for an indirect rotor flux-orientated controlled induction machine system’, *IEEE Transactions on Power Electronics*, vol. 17, no. 3, pp. 353–364, May 2002, doi: 10.1109/TPEL.2002.1004243.

[146] M. Koyama, M. Yano, I. Kamiyama, and S. Yano, ‘Microprocessor-Based Vector Control System for Induction Motor Drives with Rotor Time Constant Identification Function’, *IEEE Transactions on Industry Applications*, vol. IA-22, no. 3, pp. 453–459, May 1986, doi: 10.1109/TIA.1986.4504742.

[147] M. Rashed and A. F. Stronach, ‘A stable back-EMF MRAS-based sensorless low-speed induction motor drive insensitive to stator resistance variation’, *IEE Proceedings - Electric Power Applications*, vol. 151, no. 6, pp. 685–693, Nov. 2004, doi: 10.1049/ip-epa:20040609.

[148] H. Li, W. Xuhui, and C. Guilan, ‘New General MRAS Adaptive Scheme to Estimate Stator and Rotor Resistance of Induction Motors’, in *Conference Record of the 2006 IEEE Industry Applications Conference Forty-First IAS Annual Meeting*, Oct. 2006, vol. 4, pp. 1775–1780. doi: 10.1109/IAS.2006.256775.

[149] J. Stephan, M. Bodson, and J. Chiasson, ‘Real-time estimation of the parameters and fluxes of induction motors’, in *Conference Record of the 1992 IEEE Industry Applications Society Annual Meeting*, Oct. 1992, pp. 578–585 vol.1. doi: 10.1109/IAS.1992.244343.

[150] M. Cirrincione and M. Pucci, ‘Experimental verification of a technique for the real-time identification of induction motors based on the recursive least-squares’, in *7th International Workshop on Advanced Motion Control. Proceedings (Cat. No.02TH8623)*, Jul. 2002, pp. 326–334. doi: 10.1109/AMC.2002.1026940.

[151] L. A. de Souza Ribeiro, C. B. Jacobina, A. M. N. Lima, and A. C. Oliveira, ‘Real-time estimation of the electric parameters of an induction machine using sinusoidal PWM voltage waveforms’, *IEEE Transactions on Industry Applications*, vol. 36, no. 3, pp. 743–754, May 2000, doi: 10.1109/28.845049.

[152] F. Alonge, F. D’Ippolito, S. La Barbera, and F. M. Raimondi, ‘Parameter identification of a mathematical model of induction motors via least squares techniques’, in *Proceedings of the 1998 IEEE International Conference on Control Applications (Cat. No.98CH36104)*, Sep. 1998, vol. 1, pp. 491–496 vol.1. doi: 10.1109/CCA.1998.728497.

[153] D. Fodor, G. Griva, and F. Profumo, ‘Compensation of parameters variations in induction motor drives using a neural network’, in *Proceedings of PESC ’95 - Power Electronics Specialist Conference*, Jun. 1995, vol. 2, pp. 1307–1311 vol.2. doi: 10.1109/PESC.1995.474983.

[154] M. Wlas, Z. Krzemiński, and H. A. Toliyat, ‘Neural-Network-Based Parameter Estimations of Induction Motors’, *IEEE Transactions on Industrial Electronics*, vol. 55, no. 4, pp. 1783–1794, 2008, doi: 10.1109/TIE.2008.918615.

[155] B. Karanayil, M. F. Rahman, and C. Grantham, ‘Induction motor parameter determination technique using artificial neural networks’, in *International Conference on Electrical Machines and Systems, 2008. ICEMS 2008*, 2008, pp. 793–798.

[156] J. Campbell and M. Sumner, ‘Practical sensorless induction motor drive employing an artificial neural network for online parameter adaptation’, *IEE Proceedings - Electric Power Applications*, vol. 149, no. 4, pp. 255–260, Jul. 2002, doi: 10.1049/ip-epa:20020289.

[157] A. Charette, J. Xu, A. Ba-Razzouk, P. Pillay, and V. Rajagopalan, ‘The use of the genetic algorithm for in-situ efficiency measurement of an induction motor’, in *IEEE Power Engineering Society Winter Meeting, 2000*, 2000, vol. 1, pp. 392–397 vol.1. doi: 10.1109/PESW.2000.849996.

[158] V. P. Sakthivel, R. Bhuvaneswari, and S. Subramanian, ‘Multi-objective parameter estimation of induction motor using particle swarm optimization’, *Engineering Applications of Artificial Intelligence*, vol. 23, no. 3, pp. 302–312, Apr. 2010, doi: 10.1016/j.engappai.2009.06.004.

[159] J. A. Riveros, D. G. Reina, F. Barrero, S. L. Toral, and M. J. Durán, ‘Five-phase induction machine parameter identification using PSO and standstill techniques’, in *IECON 2015 - 41st Annual Conference of the IEEE Industrial Electronics Society*, Nov. 2015, pp. 000613–000618. doi: 10.1109/IECON.2015.7392167.

[160] A. R. Noei and H. A. Kholerdi, ‘Practical intelligent modeling of three-phase induction machine’, in *2015 7th Conference on Information and Knowledge Technology (IKT)*, May 2015, pp. 1–6. doi: 10.1109/IKT.2015.7288670.

[161] W. Pawlus, J. T. Birkeland, H. Van Khang, and M. R. Hansen, ‘Identification and Experimental Validation of an Induction Motor Thermal Model for Improved Drivetrain Design’, *IEEE Trans. on Ind. Applicat.*, vol. 53, no. 5, pp. 4288–4297, Sep. 2017, doi: 10.1109/TIA.2017.2700283.

[162] S. D. Sudhoff, D. C. Aliprantis, B. T. Kuhn, and P. L. Chapman, ‘Experimental characterization procedure for use with an advanced induction machine model’, *IEEE Transactions on Energy Conversion*, vol. 18, no. 1, pp. 48–56, Mar. 2003, doi: 10.1109/TEC.2002.808333.

List of Author’s Publications

All authors hold an equal share in the joint publications, otherwise stated.

List of Author’s Publications Related to the Thesis

Publications in Journals with Impact Factor

- T. Košťál, P. Kobrle, ‘Induction Machine On-line Parameter Identification for Resource-constrained Microcontrollers based on Steady-State Voltage Model’, *Electronics*, ISSN 2079-9292, vol. 10, no. 16, a. 1981, p. 19. IF: 2.397 (2020). doi: 10.3390/electronics10161981.

Publications Excerpted in Web of Science

- T. Košťál, ‘Reducing electrical energy consumption of AHU fans through parameter identification of the drive’, in *2018 3rd International Conference on Intelligent Green Building and Smart Grid (IGBSG)*, Yi-Lan, Apr. 2018, pp. 1–4. doi: 10.1109/IGBSG.2018.8393529.

- T. Košťál, 'Induction machine parameters identification method suitable for self-commissioning', in *2017 XXVI International Scientific Conference Electronics (ET)*, Sep. 2017, pp. 1–4. doi: 10.1109/ET.2017.8124357.
- T. Košťál, 'Offline induction machine parameters identification suitable for self-commissioning', in *2017 International Conference on Applied Electronics (AE)*, Pilsen, Czech Republic, Sep. 2017, pp. 1–4. doi: 10.23919/AE.2017.8053587.

Other Publications

- T. Košťál, 'Identification of Parameters of a 15 kW Induction Machine Implemented in FPGA - Processor System-On-Chip', in *Recenzovaný sborník příspěvků mezinárodní vědecké konference Mezinárodní Masarykova konference pro doktorandy a mladé vědecké pracovníky 2019*, Hradec Králové, Česká republika, Dec. 2019, vol. 2019, pp. 1376–1384.
- T. Košťál, 'Optimisation of Power Consumption of Electric Drive With Induction Machine Through Online Parameter Identification', in *Proceedings | Research Track of the 8th Biannual CER Comparative European Research Conference*, London, United Kingdom of Great Britain and Northern Ireland, Oct. 2017, vol. 8, pp. 139–142.
- T. Košťál, 'Influence of the Rotor Resistance Change to Control Performance of an Induction Machine', in *Proceedings of the International Student Scientific Conference Poster – 21/2017*, Prague, Czech Republic, May 2017, vol. 21, p. 6. [Online]. Available: http://poseidon2.feld.cvut.cz/conf/poster/
- T. Košťál, 'Offline Parameter Identification of an Induction Machine Supplied by Impressed Stator Voltages', in *Proceedings of the 20th International Scientific Student Conferenece POSTER 2016*, Prague, Czech Republic, May 2016, vol. 20. [Online]. Available: http://poseidon2.feld.cvut.cz/conf/poster/

Research Reports

- Pavelka, J.; Künzel, K.; Kobrle, P.; Brejcha, M.; Košťál, T.; Hájek, J., Research Report JC2015-0066, Joint Research Center CRRC – CTU, 2015. CTU Project identifier: 130028C000 K13114 CNR (CZECH) sp.lab.JC., RIV identier: RIV/68407700:21230/15:00237365.
- Pavelka, J.; Janoušek, J.; Pivoňka, P.; Künzel, K.; Kobrle, P.; Brejcha, M.; Košťál, T.; Hájek, J., Research Report JC2014-0062, Joint Research Center CRRC – CTU, 2014. CTU Project identifier: 130028C000 K13114 CNR (CZECH) sp.lab.JC., RIV identier: RIV/68407700:21230/14:00225966.
- Pavelka, J.; Brejcha, M.; Košťál, T., Research Report JC2014-0053, Joint Research Center CRRC – CTU, 2014. CTU Project identifier: 130028C000 K13114 CNR (CZECH) sp.lab.JC., RIV identier: RIV/68407700:21230/14:00225965.

- Pavelka, J.; Kobrle, P.; Brejcha, M.; Košťál, T., Research Report JC2014-0052, Joint Research Center CRRC – CTU, 2014. CTU Project identifier: 130028C000 K13114 CNR (CZECH) sp.lab.JC., RIV identier: RIV/68407700:21230/14:00225964.
- Pavelka, J.; Künzel, K.; Brejcha, M.; Hájek, J.; Košťál, T., Research Report JC2014-0050, Joint Research Center CRRC – CTU, 2014. CTU Project identifier: 130028C000 K13114 CNR (CZECH) sp.lab.JC., RIV identier: RIV/68407700:21230/14:00225959.
- Pavelka, J.; Kobrle, P.; Košťál, T.; Brejcha, M.; Hájek, J., Research Report JC2014-0046, Joint Research Center CRRC – CTU, 2014. CTU Project identifier: 130028C000 K13114 CNR (CZECH) sp.lab.JC., RIV identier: RIV/68407700:21230/14:00225955.
- Pavelka, J.; Košťál, T., Research Report JC2014-0045, Joint Research Center CRRC – CTU, 2014. CTU Project identifier: 130028C000 K13114 CNR (CZECH) sp.lab.JC., RIV identier: RIV/68407700:21230/14:00225954.
- Pavelka, J.; Janoušek, J.; Pivoňka, P.; Kobrle, P.; Košťál, T.; Wang, R.; Wang, X., Research Report JC2014-0033, Joint Research Center CRRC – CTU, 2014. CTU Project identifier: 130028C000 K13114 CNR (CZECH) sp.lab.JC., RIV identier:
- Pavelka, J.; Janoušek, J.; Künzel, K.; Kobrle, P.; Košťál, T., Research Report JC2014-0032, Joint Research Center CRRC – CTU, 2014. CTU Project identifier: 130028C000 K13114 CNR (CZECH) sp.lab.JC., RIV identier:
- Pavelka, J.; Brejcha, M.; Hájek, J.; Košťál, T., Research Report JC2014-0030, Joint Research Center CRRC – CTU, 2014. CTU Project identifier: 130028C000 K13114 CNR (CZECH) sp.lab.JC., RIV identier: RIV/68407700:21230/14:00225773.
- Pavelka, J.; Kobrle, P.; Košťál, T., Research Report JC2014-0019, Joint Research Center CRRC – CTU, 2014. CTU Project identifier: 130028C000 K13114 CNR (CZECH) sp.lab.JC., RIV identier: IV/68407700:21230/14:00225760.
- Pavelka, J.; Kobrle, P.; Košťál, T., Research Report JC2014-0018, Joint Research Center CRRC – CTU, 2014. CTU Project identifier: 130028C000 K13114 CNR (CZECH) sp.lab.JC., RIV identier: RIV/68407700:21230/14:00225758.
- Pavelka, J.; Kobrle, P.; Košťál, T., Research Report JC2014-0015, Joint Research Center CRRC – CTU, 2014. CTU Project identifier: 130028C000 K13114 CNR (CZECH) sp.lab.JC., RIV identier: RIV/68407700:21230/14:00225757.
- Pavelka, J.; Kobrle, P.; Košťál, T., Research Report JC2013-0011, Joint Research Center CRRC – CTU, 2013. CTU Project identifier: 130028C000 K13114 CNR (CZECH) sp.lab.JC., RIV identier: RIV/68407700:21230/13:00225755.

List of Author’s Other Publications

Publications in Reviewed Journals

- J. Pavelka, P. Kobrle, T. Košťál, and J. Zedník, ‘Řízení výkonu v solid state transformátoru – budoucí možné náhradě distribučního transformátoru | Power Flow Control in Solid State Transformer – the Future Replacement of the Distribution Transformer’, *Energetika*, vol. 70, no. 2, pp. 118–127, 2020.
- J. Pavelka, P. Kobrle, T. Košťál, and J. Zedník, ‘Energy router a jeho úloha v inteligentní síti (Energy Router and its Task in the Intelligent Network)’, *ELEKTRO*, vol. 28, pp. 6–11, May 2018.

Publications Excerpted in Web of Science

- T. Kostal and P. Kobrle, ‘FPGA based modulator for five level flying capacitor inverter’, in *2018 International Conference on Applied Electronics (AE)*, Pilsen, Sep. 2018, pp. 1–4. doi: 10.23919/AE.2018.8501417.
    - Cited, Conference Proceedings Citation Index:
        - G.-K. Wu, K.-S. Su, and J.-F. Chen, ‘Electrolytic Capacitor-Less Multilevel Inverter with AC-DC Energy Conversion’, in *2019 IEEE 4th International Future Energy Electronics Conference (IFEEC)*, Nov. 2019, pp. 1–7. doi: 10.1109/IFEEC47410.2019.9015039.
- P. Kobrle, T. Kostal, J. Zednik, J. Pavelka, and X. Yang, ‘Task of Energy Router in Smart Grids’, in *2018 10th International Conference on Electronics, Computers and Artificial Intelligence (ECAI)*, Iasi, Romania, Jun. 2018, pp. 1–6. doi: 10.1109/ECAI.2018.8679057.
    - Cited, Conference Proceedings Citation Index:
        - S. Li, Z. Li, P. Li, Y. Zhang, and D. Xie, ‘Energy flow analysis of the multi-energy energy router’, *IOP Conf. Ser.: Earth Environ. Sci.*, vol. 467, p. 012026, Apr. 2020, doi: 10.1088/1755-1315/467/1/012026.
    - Cited, Science Citation Index Expanded:
        - G. Gong *et al.*, ‘Electric Power System Operation Mechanism with Energy Routers Based on QoS Index under Blockchain Architecture’, *Energies*, vol. 13, no. 2, Art. no. 2, Jan. 2020, doi: 10.3390/en13020418.

Publications Excerpted in Scopus

- T. Košťál, P. Kobrle, J. Zedník, J. Pavelka, and X. Yang, 'Comparison of SST Topologies Suitable for Energy Applications', in *AETA 2019 - Recent Advances in Electrical Engineering and Related Sciences: Theory and Application*, vol. 685, D. F. Cortes Tobar, V. Hoang Duy, and T. Trong Dao, Eds. Cham: Springer International Publishing, 2021, pp. 252–261. doi: 10.1007/978-3-030-53021-1_26.

Other Publications

- J. Zedník and T. Košťál, 'Determination of MMC Submodule Capacitor Value', in *Proceedings of the International Student Scientific Conference Poster – 23/2019*, Prague, Czech Republic, May 2019, vol. 23. [Online]. Available: http://poseidon2.feld.cvut.cz/conf/poster/
- J. Zedník, P. Kobrle, T. Košťál, and J. Pavelka, 'Návrh velikosti kapacity submodulu MMC (Determination of MMC Submodule Capacitor Value)', in *XXXVI. CELOSTÁTNÍ KONFERENCE O ELEKTRICKÝCH POHONECH*, Plzeň, Czech Republic, Jun. 2019, vol. 36.
- T. Košť'ál and M. Košťál, 'Modular approach to FPGA based modulator for power inverters', in *Proceedings of the International Student Scientific Conference Poster – 22/2018*, Prague, Czech Republic, May 2018, vol. 22.
- T. Košťál and M. Košťál, 'Comparison of two Approaches to FPGA Based Sinusoidal PWM Generators for Electric Power Frequency Converters', in *Recenzovaný sborník Mezinárodní Masarykova konference pro doktorandy a mladé vědecké pracovníky 2017*, Hradec Králové, Czech Republic, vol. 8, pp. 1079–1086.
- T. Košťál, 'Užití víceúrovňových měničů v systémech s obnovitelnými zdroji energie (Usage of Multilevel Inverters in Renewable Energy Systems)', in *International Masaryk Conference for Ph.D. Students and Young Researchers 2015*, Hradec Králové, Česká republika, Dec. 2015, pp. 2075–2083.
- T. Košťál and P. Kobrle, 'Analýza spínání při balancování napětí plovoucích kondenzátorů pětiúrovňového měniče', in *Sborník XXXIV. celostátní konferenci elektrické pohony*, Plzeň, Czech Republic, Jun. 2015, vol. 34.
- T. Košťál and M. Košťál, 'Comparison and Verification of Propagation Models Accuracy for Specific Urban Area', in *Poster 2015*, Prague, Czech Republic, May 2015, vol. 19. [Online]. Available: http://poseidon2.feld.cvut.cz/conf/poster/
- T. Košťál, 'Realization of modulator for three-level inverter with FPGA and Microblaze processor system', in *POSTER 2014 - 18th International Student Conference on Electrical Engineering*, Prague, Czech Republic, May 2014, vol. 18. [Online]. Available: http://poseidon2.feld.cvut.cz/conf/poster/

- T. Košťál and M. Kozelka, 'Archive of Antonín Svoboda at Laboratory for History of Electrotechnics (K 13116) at FEE CTU in PragueConverters', in *POSTER 2013 - 17th International Student Conference on Electrical Engineering*, Prague, Czech Republic, May 2013, vol. 17.
  Contribution: 75 %
- T. Košťál and P. Kobrle, 'From the Mercury-Arc to Multilevel Converters', in *POSTER 2013 - 17th International Student Conference on Electrical Engineering*, Prague, Czech Republic, May 2013, vol. 17.
- P. Kobrle and T. Košťál, 'Evolution of the Semiconductor Devices and Multilevel Converter Topologies', in *XX. International Symposium on Electric Machinery In Prague*, Prague, Czech Republic, Sep. 2013, vol. 20.
- T. Košťál, 'Practical Problems with DC-Motor Control', in *POSTER 2012 - 16th International Student Conference on Electrical Engineering*, Prague, Czech Republic, May 2012, vol. 16. [Online]. Available: http://poseidon2.feld.cvut.cz/conf/poster/

Research Reports

- Zoubek, O.; Kobrle, P.; Košťál, T.; Musil, T.; Mňuk, P.; Zděnek, J., Research Report JC2016-TCU-0023, Joint Research Center CRRC – CTU, 2017. CTU Project identifier: 130028C000 K13114 CNR (CZECH) sp.lab.JC.
- Musil, T.; Künzel, K.; Košťál, T.; Zděnek, J.; Kobrle, P., Research Report JC2017-TCU-0026, Joint Research Center CRRC – CTU, 2017. CTU Project identifier: 130028C000 K13114 CNR (CZECH) sp.lab.JC.
- Kobrle, P.; Košťál, T.; Musil, T., Research Report JC2017-TCU-0031, Joint Research Center CRRC – CTU, 2017. CTU Project identifier: 130028C000 K13114 CNR (CZECH) sp.lab.JC.
- Zoubek, O.; Kobrle, P.; Musil, T.; Košťál, T.; Zděnek, J., Research Report JC2017-TCU-0035, Joint Research Center CRRC – CTU, 2017. CTU Project identifier: 130028C000 K13114 CNR (CZECH) sp.lab.JC.
- Pavelka, J.; Kobrle, P.; Müller, Z.; Košťál, T.; Zedník, J., Assessing the feasibility of energy routers topologies. Praha, Ministerstvo školství, mládeže a tělovýchovy ČR, 2017. Report no. VZ469/K13114/17.
- Musil, T.; Zděnek, J.; Košťál, T., Research Report JC2016-TCU-0025, Joint Research Center CRRC – CTU, 2016. CTU Project identifier: 130028C000 K13114 CNR (CZECH) sp.lab.JC, RIV identifier: RIV/68407700:21230/16:00307261.
- Košťál, T.; Brejcha, M.; Künzel, K.; Zděnek, J., Research Report JC2016-TCU-0018, Joint Research Center CRRC – CTU, 2016. CTU Project identifier: 130028C000 K13114 CNR (CZECH) sp.lab.JC, RIV identifier: RIV/68407700:21230/16:00307259.

- Zděnek, J.; Brejcha, M.; Hájek, J.; Kobrle, P.; Košťál, T.; Künzel, K.; Mňuk, P.; Musil, T. et al., Research Report JC2015-CRRC-0001, Joint Research Center CRRC – CTU, 2015. CTU Project identifier: 130028C000 K13114 CNR (CZECH) sp.lab.JC, RIV identifier: RIV/68407700:21230/15:00237454.
- Zděnek, J.; Brejcha, M.; Hájek, J.; Kobrle, P.; Košťál, T.; Künzel, K.; Mňuk, P.; Musil, T. et al., Research Report JC2015-CNR-0009, Joint Research Center CRRC – CTU, 2015. CTU Project identifier: 130028C000 K13114 CNR (CZECH) sp.lab.JC, RIV identifier: RIV/68407700:21230/15:00237453.
- Zděnek, J.; Brejcha, M.; Hájek, J.; Kobrle, P.; Košťál, T.; Künzel, K.; Mňuk, P.; Musil, T. et al., Research Report JC2015-CNR-0008, Joint Research Center CRRC – CTU, 2015. CTU Project identifier: 130028C000 K13114 CNR (CZECH) sp.lab.JC, RIV identifier: RIV/68407700:21230/15:00237452.
- Zděnek, J.; Brejcha, M.; Hájek, J.; Kobrle, P.; Košťál, T.; Künzel, K.; Mňuk, P.; Musil, T. et al., Research Report JC2015-CNR-0007, Joint Research Center CRRC – CTU, 2015. CTU Project identifier: 130028C000 K13114 CNR (CZECH) sp.lab.JC, RIV identifier: RIV/68407700:21230/15:00237450.
- Zděnek, J.; Brejcha, M.; Hájek, J.; Kobrle, P.; Košťál, T.; Künzel, K.; Mňuk, P.; Musil, T. et al., Research Report JC2015-CNR-0006, Joint Research Center CRRC – CTU, 2015. CTU Project identifier: 130028C000 K13114 CNR (CZECH) sp.lab.JC, RIV identifier: RIV/68407700:21230/15:00237449.
- Zděnek, J.; Brejcha, M.; Hájek, J.; Kobrle, P.; Košťál, T.; Künzel, K.; Mňuk, P.; Musil, T. et al., Research Report JC2015-CNR-0005, Joint Research Center CRRC – CTU, 2015. CTU Project identifier: 130028C000 K13114 CNR (CZECH) sp.lab.JC, RIV identifier: RIV/68407700:21230/15:00237448.
- Zděnek, J.; Brejcha, M.; Hájek, J.; Kobrle, P.; Košťál, T.; Mňuk, P.; Musil, T.; Zoubek, O. et al., Research Report JC2015-CNR-0004, Joint Research Center CRRC – CTU, 2015. CTU Project identifier: 130028C000 K13114 CNR (CZECH) sp.lab.JC, RIV identifier: RIV/68407700:21230/15:00237447.
- Zděnek, J.; Brejcha, M.; Hájek, J.; Kobrle, P.; Košťál, T.; Künzel, K.; Mňuk, P.; Musil, T. et al., Research Report JC2015-CNR-0003, Joint Research Center CRRC – CTU, 2015. CTU Project identifier: 130028C000 K13114 CNR (CZECH) sp.lab.JC, RIV identifier: RIV/68407700:21230/15:00237445.
- Musil, T.; Košťál, T., Research Report JC2015-TCU-0010, Joint Research Center CRRC – CTU, 2015. CTU Project identifier: 130028C000 K13114 CNR (CZECH) sp.lab.JC, RIV identifier: RIV/68407700:21230/15:00237383.
- Zděnek, J.; Zoubek, O.; Košťál, T., Research Report JC2015-TCU-0009, Joint Research Center CRRC – CTU, 2015. CTU Project identifier: 130028C000 K13114 CNR (CZECH) sp.lab.JC, RIV identifier: RIV/68407700:21230/15:00237453.